

University of Kentucky

UKnowledge

Theses and Dissertations--Plant Pathology

Plant Pathology

2019

STRAIN-SPECIFIC PROTEIN INTERACTION AND LOCALIZATION OF TWO STRAINS OF POTATO YELLOW DWARF VIRUS AND FUNCTIONAL DOMAINS OF THEIR MATRIX PROTEIN

Chanyong Jang

University of Kentucky, chanyong.947@uky.edu

Digital Object Identifier: <https://doi.org/10.13023/etd.2019.008>

[Right click to open a feedback form in a new tab to let us know how this document benefits you.](#)

Recommended Citation

Jang, Chanyong, "STRAIN-SPECIFIC PROTEIN INTERACTION AND LOCALIZATION OF TWO STRAINS OF POTATO YELLOW DWARF VIRUS AND FUNCTIONAL DOMAINS OF THEIR MATRIX PROTEIN" (2019).

Theses and Dissertations--Plant Pathology. 25.

https://uknowledge.uky.edu/plantpath_etds/25

This Doctoral Dissertation is brought to you for free and open access by the Plant Pathology at UKnowledge. It has been accepted for inclusion in Theses and Dissertations--Plant Pathology by an authorized administrator of UKnowledge. For more information, please contact UKnowledge@lsv.uky.edu.

STUDENT AGREEMENT:

I represent that my thesis or dissertation and abstract are my original work. Proper attribution has been given to all outside sources. I understand that I am solely responsible for obtaining any needed copyright permissions. I have obtained needed written permission statement(s) from the owner(s) of each third-party copyrighted matter to be included in my work, allowing electronic distribution (if such use is not permitted by the fair use doctrine) which will be submitted to UKnowledge as Additional File.

I hereby grant to The University of Kentucky and its agents the irrevocable, non-exclusive, and royalty-free license to archive and make accessible my work in whole or in part in all forms of media, now or hereafter known. I agree that the document mentioned above may be made available immediately for worldwide access unless an embargo applies.

I retain all other ownership rights to the copyright of my work. I also retain the right to use in future works (such as articles or books) all or part of my work. I understand that I am free to register the copyright to my work.

REVIEW, APPROVAL AND ACCEPTANCE

The document mentioned above has been reviewed and accepted by the student's advisor, on behalf of the advisory committee, and by the Director of Graduate Studies (DGS), on behalf of the program; we verify that this is the final, approved version of the student's thesis including all changes required by the advisory committee. The undersigned agree to abide by the statements above.

Chanyong Jang, Student

Dr. Michael M. Goodin, Major Professor

Dr. Rick Bennett, Director of Graduate Studies

STRAIN-SPECIFIC PROTEIN INTERACTION AND LOCALIZATION OF
TWO STRAINS OF POTATO YELLOW DWARF VIRUS AND
FUNCTIONAL DOMAINS OF THEIR MATRIX PROTEIN

DISSERTATION

A dissertation submitted in partial fulfillment of the
Requirements for the Degree of Doctor of Philosophy in the
College of Agriculture, Food and Environment
At the University of Kentucky

By

Chanyong Jang

Lexington, Kentucky

Director: Dr. Michael M. Goodin, Professor of Plant Pathology

Lexington, Kentucky

2018

Copyright © Chanyong Jang 2018

ABSTRACT OF DISSERTATION

STRAIN-SPECIFIC PROTEIN INTERACTION AND LOCALIZATION OF TWO STRAINS OF POTATO YELLOW DWARF VIRUS AND FUNCTIONAL DOMAINS OF THEIR MATRIX PROTEIN

Potato yellow dwarf virus (PYDV) is the type species of the genus nucleorhabdovirus which is typified by its nucleotropic characters of the members. The virus accomplishes its replication and morphogenesis in the nuclei of infected cells. Two strains, *Constricta* strain (CYDV) and *Sanguinolenta* strain (SYDV) have been described at the level of vector-specificity. CYDV is vectored by *Agallia constricta* and SYDV is transmitted by *Aceratagllia sanguinolenta*. The full-length genome of CYDV was sequenced. The 12,792 nt antisense genome encodes seven open reading frames in the order of, nucleocapsid protein (N), unknown protein (X), phosphoprotein (P), movement protein (Y), matrix protein (M), glycoprotein (G), and large polymerase protein (L). The features of each protein including a nuclear localization signal, isoelectric point, and transmembrane domain, were determined by predictive algorithms. The gene coding region was flanked by leader and trailer, and each ORF was separated by a conserved intergenic junction. In the intergenic junctions, the highly conserved cis-regulatory elements, polyadenylation signal, gene spacer, and transcription start site, were identified. The similarities of amino acid sequences between each cognate protein of SYDV and CYDV were higher than 80% except for X and P proteins. The protein localization and interaction assays of each CYDV protein identified strain-specific associations in comparison with those of SYDV and generated unique protein interaction and localization map compared to SYDV. Phylogenetic analysis using L protein identified that CYDV forms a clade with other leafhopper-transmitted rhabdoviruses. Protein sequence comparisons revealed that CYDV X has greater similarity to the cognate protein of *Eggplant mottle disease virus* than to SYDV X. The localization patterns of CYDV-N and -Y were different compared the cognate proteins of SYDV. The functional nuclear export domain of SYDV M was identified using c-terminal fragments of the M^{wt}(aa 211-243), M^{LL223AA}(aa 211-243), and M^{KR225AA}(aa 211-243). Based on the data, the functional domains M mediating membrane association, nuclear import and export were mapped for both strains and suggested a model whereby M mediates intra- and intercellular movement of PYDV nucleocapsid.

KEYWORDS: rhabdovirus, protein localization and interaction map, nuclear localization signal, nuclear export signal

Chanyong Jang

1/21/2019

Date

STRAIN-SPECIFIC PROTEIN INTERACTION AND LOCALIZATION OF
TWO STRAINS OF POTATO YELLOW DWARF VIRUS AND
FUNCTIONAL DOMAINS OF THEIR MATRIX PROTEIN

By
Chanyong Jang

Dr. Michael M. Goodin
Director of Dissertation

Dr. Rick Bennett
Director of Graduate Studies

(Date) 1/21/2019

TABLE OF CONTENTS

List of Tables.....iv

List of Figures.....v

Chapter 1..... 1

A comprehensive literature reviews

 Rhabdovirus.....1

 Plant-adapted Rhabdoviruses.....7

 Potato yellow dwarf virus.....9

 Nuclear transport.....11

 1)Nuclear pore complex.....11

 2)Nuclear transport receptors.....14

 3)Nuclear import.....15

 4)Nuclear export.....18

 NLSs and NESs in plant nucleorhabdoviruses.....19

Chapter 2.....32

Genome sequence variation in the constricta strain dramatically alters the protein interaction and localization map of *Potato yellow dwarf virus*.....32

 Methods.....34

 Results.....37

 Discussion.....42

Chapter 3.....59

Validation of nuclear export function of the 3' terminal leucine-rich domain of PYDV matrix protein.....59

 Methods.....61

 Results.....63

 Discussion.....64

Chapter 4.....71

Future studies71

Attempt to establish the reverse genetic system for plant-adapted negative-strand RNA viruses.71

 Methods.....74

 Results.....80

 Discussion.....87

 Overall discussion and future direction.....92

References.....129

Vita.....148

LIST OF TABLES

| | |
|--|-----|
| Chapter 1 | |
| Table 1, Genera of Rhabdoviridae..... | 24 |
| Chapter 2 | |
| Table 2, Features of PYDV proteins determined by predictive algorithms..... | 50 |
| Chapter 4 | |
| Table 3, Number of the nuclei classified according to the shape at each temperature..... | 119 |

LIST OF FIGURES

Chapter 1

| | |
|--|----|
| Figure 1.1. The genome organization of selected plant negative-strand RNA viruses..... | 25 |
| Figure 1.2. Insect vectors and serotype-specific detection of the CYDV and SYDV strains of PYDV..... | 26 |
| Figure 1.3. Structure of nuclear pore complexes in human, yeast, and plant..... | 27 |
| Figure 1.4. Generalized diagram of nuclear transport..... | 29 |
| Figure 1.5. Comparison of life cycle between nucleo- and cytorhabdoviruses in the host cell..... | 31 |

Chapter 2

| | |
|--|----|
| Figure 2.1. Comparison of CYDV and SYDV genomes and proteins..... | 46 |
| Figure 2.2. L protein derived phylogeny..... | 47 |
| Figure 2.3. Complementarity in the leader (3') and trailer (5') regions of selected rhabdoviruses..... | 48 |
| Figure 2.4. Comparison of the intergenic junction sequences of rhabdoviruses..... | 49 |
| Figure 2.5. Subcellular localization of CYDV proteins..... | 51 |
| Figure 2.6. The different localization pattern of CYDV-N and -Y compared to their cognate proteins of SYDV..... | 52 |
| Figure 2.7. BiFC assay for all pairwise combinations of CYDV-encoded proteins, except L..... | 53 |
| Figure 2.8. Comparison of integrated protein interaction and localization maps..... | 56 |
| Figure 2.9. The localization pattern of CYDV-encoded proteins in the context of the virus-infected plant cell..... | 57 |
| Figure 2.10. Localization pattern of SYDV-encoded proteins in the context of the virus-infected plant cell..... | 58 |

Chapter 3

| | |
|--|----|
| Figure 3.1. Confocal micrograph of the cellular localization of GFP tagged fragments of SYDV M ^{wt} (aa 211-243), M ^{LL223AA} (aa 211-243), and M ^{KR225AA} (aa 211-243)..... | 68 |
| Figure 3.2. Functional domain map of amino acids 211-253 residue of M protein of SYDV and CYD..... | 69 |
| Figure 3.3. "Catch and release" model of SYDV-M nuclear transport..... | 70 |

Chapter 4

| | |
|---|-----|
| Figure 4.1. Common strategy for recovery of negative-strand RNA virus..... | 98 |
| Figure 4.2. Map of pCass4HDV..... | 99 |
| Figure 4.3. Schematic diagram for construction of full-length antigenomic sequence in the pGEM-T easy vector..... | 100 |
| Figure 4.4. Schematic diagram for construction of pCass4HDV_R1 and pCass4HDV_R2..... | 102 |
| Figure 4.5. Schematic diagram of pCass4HDVagSYDV construction..... | 103 |
| Figure 4.6. Construction of N, P, and L expression vectors for CoRSV and SYDV..... | 105 |

| | |
|--|-----|
| Figure 4.7. Construction of full-length antigenome and L of SYDV using yeast mediated homologous recombination..... | 107 |
| Figure 4.8. Expression of agCoRSV RNA1 and RNA2 from pCass4HDV..... | 108 |
| Figure 4.9. Expression of FLAG-fusion of CoRSV-N, -P, and -L..... | 109 |
| Figure 4.10. Expression of CoRSV-N and -P protein from pTRBO vector..... | 110 |
| Figure 4.11. Formation of viroplasm-like structure (VpLS) by CoRSV-N and -P in RFP-H2b <i>N. benthamiana</i> | 111 |
| Figure 4.12. GFP-ER signal accumulation in the subnuclear space by CoRSV-P expression..... | 112 |
| Figure 4.13. Inhibited DAPI staining of nuclei in GFP-ER <i>N. benthamiana</i> with simultaneous expression of CoRSV agRNA1, agRNA2, N, P, and L..... | 114 |
| Figure 4.14. Size-depend inhibition of DAPI staining under simultaneous expression of viral RNAs, and N, P, and L in RFP H2b <i>N. benthamiana</i> | 115 |
| Figure 4.15. The alteration of VpLS pattern according to temperature in infiltrated plant..... | 118 |
| Figure 4.16. Effect of temperature change on ER localization pattern and the size of nuclei in the agroinfiltrated plants..... | 120 |
| Figure 4.17. Test for recovery of infectious virus from the infiltrated plants..... | 122 |
| Figure 4.18. leader and trailer sequence specific inhibition of GFP from minigenome by CoRSV-N and -P co-expression..... | 124 |
| Figure 4.19. Expression of agSYDV, SYDV-N, -P, an -L in <i>N. benthamiana</i> | 127 |

CHAPTER 1

A Comprehensive literature reviews

Rhabdovirus

The Rhabdoviridae are a family in the order Mononegavirales, whose members infect a wide range of hosts including vertebrates, arthropods, and plants (Dietzgen *et al.*, 2017, Walker *et al.*, 2015). Many of them (i.e., rabies virus, viral hemorrhagic septicemia virus, maize mosaic virus) are pathogens that significantly affect public health and agricultural industries (Bohle *et al.*, 2011; Jackson *et al.*, 1997; Reed *et al.*, 2005). Currently, rhabdoviruses are taxonomically classified into eighteen genera and one unassigned species (Table 1) (Walker *et al.*, 2018).

The majority of rhabdoviruses are transmitted by arthropod vectors, such as aphids, planthoppers, leafhoppers, blackflies, and mosquitoes (Franck, 1973; Jackson *et al.*, 2005; Walker *et al.*, 2015). Metagenomic studies have found rhabdovirus-like endogenous viral elements from arthropod genomes, and these data suggest that the vectors were subjected to repeated rhabdovirus infection during their evolutionary history and the integrated sequences are engaged actively in the vector evolution. (Geisler *et al.*, 2016; Longdon *et al.*, 2015; Fort *et al.*, 2012). While the other 13 genera of rhabdoviruses are transmitted by insect vectors, lyssaviruses, novirhabdoviruses, perhabdoviruses, spriviviruses, and tupaviruses are circulated among vertebrate hosts without a biological vector (Table 1) (Dietzgen *et al.*, 2017; Walker *et al.*, 2018).

All rhabdovirus genomes are about 11 to 16 kb in size and include at least five common genes encoding nucleoprotein (N), phosphoprotein (P), matrix protein (M), glycoprotein (G) and RNA-dependent RNA polymerase (L) (Fig. 1.1) (Dietzgen *et al.*, 2017; Walker *et al.*, 2015). These genes are flanked by leader and trailer sequences which are untranslated and partially complementary (Bejerman *et al.*, 2015; Heaton *et al.*, 1989; Jackson *et al.*, 2005). Each gene is separated by a conserved intergenic junction region (Bejerman *et al.*, 2015; Heaton *et al.*, 1989). These intergenic junctions have three highly-conserved *cis*-regulatory elements, namely the

polyadenylation signal, the intergenic spacer, and the transcription start site (Follett *et al.*, 1974; Banerjee *et al.*, 1987; Ivanov *et al.*, 2011; Liu *et al.*, 2018). Some rhabdovirus genomes encode accessory genes in addition to the five major structural protein coding genes (Fig 1.1). These accessory proteins are likely to confer virus-specific biological properties such as host specificity, and pathogenicity (Walker *et al.*, 2015).

The five canonical proteins, N, P, M, G, and L are common across all members of Rhabdoviridae, and they serve as structural components of the virion (Luo *et al.*, 2007; Ryu *et al.*, 2017; Jackson *et al.*, 2005). Nucleoprotein (N) is a major component of the nucleocapsid. This RNA-binding protein encapsidates the virus genome RNA and actively interacts with the L and P proteins to form the minimal infectious unit, the ribonucleoprotein (RNP) complex (Green *et al.*, 2009). Rhabdovirus N proteins are comprised of two main domains, the N-terminal domain (N_{NTD}) and the C-terminal domain (N_{CTD}). Two other sub-domains, the N_{NT}-arm and N_{CT}-loop, are extended from N_{NTD} and C_{CTD}, respectively. The RNA binding cavity locates at the interface between N_{NTD} and N_{CTD}, and the viral RNA is tightly bound to the cavity. One nucleoprotein interacts with nine ribonucleotides of viral genome (Iseni *et al.*, 1998). The basic residues of N form multiple salt-bridges with the sugar-phosphate groups of RNA and these electrostatic interactions stabilize the N-RNA complex. This N-RNA complex is highly protected against degradation by nuclease (Iseni *et al.*, 1998). The exchange of the N_{NT}-arm and N_{CT}-loop in opposite directions between adjacent N protomers mediates N polymerization to encapsidate the entire virus genomic RNA (R. Assenberg *et al.*, 2010; Ivanov *et al.*, 2011, Luo *et al.*, 2007). While RNA encapsidation by N is selective to its compatible virus genomic- and antigenomic RNA, the viral- and host- mRNAs do not interact with N proteins (Ivanov *et al.*, 2011, Luo *et al.*, 2007). The concentration of N⁰-P (0 represents absence of RNA) plays a role in switching the mode of replicase (L) from transcription to replication (Arnheiter *et al.*, 1985; Gupta *et al.*, 1997).

Phosphoprotein (P) plays multifunctional roles during the transcription and replication processes (R. Assenberg *et al.*, 2010; Leyrat *et al.*, 2011). P is an essential non-catalytic cofactor of the large polymerase (L) that mediates the attachment of L to the N-RNA template and stabilizes the interaction between L and nucleocapsid during RNA synthesis (Leyrat *et al.*, 2011). P also chaperones N during the assembly of new nucleocapsids. P binds to nascent N and produces N⁰-P complex, and this interaction prevents self-aggregation and non-selective binding to host RNAs (Ivanov *et al.*, 2011; Chenik *et al.*, 1998). The nascent N proteins are transferred from the soluble N⁰-P complex to encapsidate newly synthesized viral genome- and anti-genome (Leyrat *et al.*, 2011). P protein has a modular structure with three structured domains that are concatenated by two intrinsically disordered regions (IDRs) in order N⁰-binding MoRE (molecular recognition element)-IDR_{NT}-P_{CED} (central oligomerization domain)-IDR_{CT}-P_{CTD} (C-terminal N-RNA binding domain) (R. Assenberg *et al.*, 2010; Leyrat *et al.*, 2011). The N⁰-binding MoRE interacts with nascent N proteins. The IDR_{NT} contains phosphorylation sites that may be involved in the modulation of transcription. N⁰-binding MoRE, IDR_{NT}, and N-partial P_{CED} together form a highly acidic N-terminal region and mediate P-L interaction. P_{CED} mediates the self-assembly of P. The IDR_{CT} has been known as the interaction domain for cellular partners (e.g., dynein). The P_{CTD} interacts with N-RNA complexes (Ivanov *et al.*, 2011; R. Assenberg *et al.*, 2010; Leyrat *et al.*, 2011). P protein was shown to possess multiple binding sites for host factors and viral proteins (i.e., NES, NLS, N-, N-RNA-, L- binding domains). In infected cells P occurs in several truncated forms in different phosphorylation states (R. Assenberg *et al.*, 2010; Leyrat *et al.*, 2011). These data indicate that the P protein plays multiple roles as a component of multi-molecular complexes.

Matrix protein (M) is a structural component that related to maturation of rhabdovirus virion: it condenses ribonucleocapsid into the core and produces the M protein layer between the condensed RNP and the viral envelope containing glycoproteins. In addition to the structural role, M has been implicated in regulating the host immune response by suppressing the related gene

expression (Connor *et al.*, 2002, Finke *et al.*, 2003). In 2005, Faria *et al.* (2005). reported that the interaction of M with host Rae1 inhibits nuclear export of host mRNA. The tertiary structures of rhabdovirus M proteins are similar between distantly related rhabdoviruses despite the dissimilar amino acid sequence (Graham *et al.*, 2008). The detailed functional domains of the matrix proteins of rhabdoviruses are still not clear. However, the role of the basic N-terminus domain of the protein for self-aggregation and membrane association has been well characterized in the protein structure level (Gaudier *et al.*, 2001, Gaudier *et al.*, 2002 Graham *et al.*, 2008). The late domain (PPPY motif) in the matrix protein is essential for virus budding via interaction with specific cellular proteins containing WW domains (i.e., NEDD4, a ubiquitin ligase that interacts with the vesicle formation and cargo sorting ESCRT complexes) (Harty *et al.*, 1999, Craven *et al.*, 1999).

Glycoprotein (G) is an N-glycosylated type I transmembrane protein. G proteins are assembled into trimer complexes to form the spikes on the virion surface (Goder *et al.*, 2001, Walker *et al.*, 1999, Coll *et al.*, 1995). Although G proteins of the rhabdovirus members from different genera share a low level of amino acid sequence identity, the sequence alignment results have revealed that they have 12-16 highly conserved cysteine residues, 2-6 potential glycosylation sites, an amino-terminal hydrophobic signal peptide, and a carboxy-terminal hydrophobic transmembrane domain (Goder *et al.*, 2001, Walker *et al.*, 1999, Coll *et al.*, 1995). The disulfide bridges formed by the most highly conserved six cysteines produce the core of the G protein structure and define the common discontinuous antigenic sites (Walker *et al.*, 1999). In the early stage of virus infection, the G protein spikes mediate the attachment of the virion to host cell receptors and induce virus mediated-endocytosis (Albertini *et al.*, 2012). During the endocytosis, the pH-dependent conformational change of the G protein into trimer induces virus membrane fusion with endosomal membranes and releases the virus nucleocapsid into the cytoplasm (Regan *et al.*, 2013; Johannsdottir *et al.*, 2009; Albertini *et al.*, 2012). In the early studies about rhabdovirus maturation and budding, the glycoproteins were found to be one of the major determinants for the

virus budding process (Simons *et al.*, 1980, Weiss *et al.*, 1980). However, electron microscopy studies using the VSV and RV lacking the G protein gene demonstrated that the G protein is not necessary for the release of the virus particle, but it contributed to the efficiency of virus budding (Mebatsion *et al.*, 1996; Robison *et al.*, 2000). According to Mebatsion *et al.*, the budding efficiency of ΔG rabies viruses was 30-fold less than that observed for the wild type virus.

The rhabdovirus large (L) proteins are an approximately 250 kDa multi-enzymatic proteins that catalyzing genome RNA transcription and replication in association with viral ribonucleoprotein as a template (Baltimore *et al.*, 1970). In addition to the RdRP (RNA-dependent RNA polymerase) activity, the protein catalyzes viral mRNA capping, methylation, and polyadenylation. The L protein sequence is well conserved among all rhabdoviruses and electron cryomicroscopic data identified the five conserved functional domains and two structural domains in the L protein that represent their enzymatic functions: polymerase (RdRP)-, capping (Cap)-, linker-1, connector (CD)-, linker-2, methyltransferase (MT)-, and C-terminal (CDT)- domains in order (Liang *et al.*, 2015). In transcription, the L protein mediated-mRNA capping mechanism is different from that of their eukaryote hosts (Ivanov *et al.*, 2011). While eukaryotes transfer GMP to the terminal diphosphate of RNA, the GDP is preferentially transferred to a 5' monophosphate RNA by the capping domain of the rhabdovirus L protein. After that, the cap is methylated at ribose 2'-O and guanine-N-7 positions by the MT domain (Ivanov *et al.*, 2011; Liang *et al.*, 2015). The poly-adenylation of mRNA is catalyzed by the C-terminal region of the RdRP domain, and the poly-A tail is synthesized by slippage of L protein on a U-track region in the intergenic junction region (Barr *et al.*, 1997). During replication and transcription, L protein does not directly bind to the N-RNA template, but L requires the viral phosphoprotein (P) as a cofactor, which serves as a bridge between L and the N-RNA complex (Wu *et al.*, 2002; Banerjee *et al.*, 1987, Whelan *et al.*, 2002). The structural conformation and enzymatic activity of L is controlled by phosphoprotein (Das *et al.*, 1997, Pattnaik *et al.*, 1997)

Rhabdoviruses have a characteristic bullet-shaped or bacilliform enveloped virion. The size of virions ranges from 100 to 430 x 45 to 100 nm (Bandyopadhyay *et al.*, 2010; Burrell *et al.*, 2017; Higgins *et al.*, 2016; Jackson *et al.*, 2005; Ryu *et al.*, 2017). In general, the chemical composition of rhabdovirus is 0.7 % to 5 % RNA, 20 to 25 % lipid, 60 to 70 % protein, and 3 to 13 % carbohydrate (Ahmed *et al.*, 1964; Bishop *et al.*, 2018). In the virus particle, the negative-sense single-strand RNA genome is encapsidated along its entire length by the N protein. The polymerase complexes which consist of L and P proteins are associated with the N-RNA complex and form ribonucleoprotein (Luo *et al.*, 2007; Ruigrok *et al.*, 2011; Yang *et al.*, 1999; Ye *et al.*, 2006). This complex represents the minimum infectious unit of rhabdovirus (Ganesan *et al.*, 2013; WalPita *et al.*, 2005). The nucleocapsid is condensed into the core structure by the M protein layer (Raux *et al.*, 2010; Solon *et al.*, 2005). The core particle is surrounded by lipid bilayer containing transmembrane G proteins that constitutes the spikes exposed on the surface of the virion (Bejerman *et al.*, 2015; Burrell *et al.*, 2017; Mann *et al.*, 2014; Regan *et al.*, 2013).

The replication mechanism is almost universal across all members of the family except the genus *Nucleorhabdovirus*, due to the plant cell environment and formation of a replication factory in the nucleus by the genus members (Jackson *et al.*, 2005; Redinbaugh *et al.*, 2005, Burrell *et al.*, 2017; Ryu *et al.*, 2017). The rhabdoviruses replication cycle follows: 1) cell entry, 2) uncoating and releasing the nucleocapsid to the cytoplasm, 3) transcription and translation, 4) genome replication and encapsidation, and 5) assembly and budding (Hull *et al.*, 2014; Ivanov *et al.*, 2011; Albertini *et al.*, 2012; Ammar *et al.*, 2008; Burrell *et al.*, 2017; Mann *et al.*, 2014; Regan *et al.*, 2013).

While the entry of rhabdoviruses is mediated by receptor binding and endocytosis (Sun *et al.*, 2005; Sun *et al.*, 2010), that of plant-adapted rhabdoviruses is mediated by insect vectors (Albertini *et al.*, 2012; Johannsdottir *et al.*, 2009; Regan *et al.*, 2013). In the entry of animal rhabdoviruses, the viral envelope fuses to the endosomal lipid bilayer by the pH-dependent conformational change of the G protein trimer (Coll *et al.*, 1995; Albariño *et al.*, 2011, Kim *et al.*,

2017). Subsequently, the matrix protein layer of the core is dissociated from ribonucleocapsid, followed by the liberation of the infectious unit to host cytoplasm. After the uncoating process, the liberated RNPs form characteristic cytoplasmic inclusions where the viral transcription and replication occurs (Albertini *et al.*, 2012; Dietzgen *et al.*, 2017; Kim *et al.*, 2017). The transcription mechanism of rhabdoviruses is called the stop-start mechanism. (Abraham *et al.*, 1976; Ball *et al.*, 1976; Ivanov *et al.*, 2011, Whelan *et al.*, 2002). In this mechanism, the viral polymerase binds to the single-entry point of 3' terminal of ribonucleocapsid and produces first the leader RNA (not capped nor polyadenylated) (Kurilla *et al.*, 1983; Abraham *et al.*, 1976) and reinitiates the transcription of the downstream genes, i.e., the nucleoprotein gene (Abraham *et al.*, 1976; Ball *et al.*, 1976). The polyadenylation of mRNA of the upstream gene and the re-initiation of the downstream gene expression is regulated by the regulatory elements encoded in the gene junction regions (Barr *et al.*, 1997; Ivanov *et al.*, 2011; Iverson *et al.*, 1981). One of features of the stop-and-start mechanism is transcriptional attenuation at gene borders, which results in a transcript gradient due to the detachment of polymerase from each gene junction (Abraham *et al.*, 1976; Ball *et al.*, 1976; Whelan *et al.*, 1999). The genome replication is initiated after the polymerase function switches to replication by N protein accumulation. In the replicative mode, the polymerase complex ignores the regulatory sequence and synthesizes the full-length genome and anti-genome (Mann *et al.*, 2014). Nucleocapsids are assembled during RNA replication. Matrix proteins are recruited to condense the new RNPs at the host plasma membrane from where virions will bud (Graham *et al.*, 2008; Raux *et al.*, 2010; Solon *et al.*, 2005). Glycoproteins are incorporated during budding into virion, and the matured- and enveloped progeny particles are produced (Chen *et al.*, 2008; Jayakar *et al.*, 2004).

Plant-adapted Rhabdoviruses

Plant rhabdoviruses infect a wide variety of plants including agriculturally important crops such as lettuce, potatoes, tomatoes, maize, barley, and rice (Jackson *et al.*, 2005; Mann *et al.*, 2014;

Redinbaugh *et al.*, 2005; Dietzgen *et al.*, 2017, Walker *et al.*, 2015). More than 90 plant rhabdoviruses have been identified (Jackson *et al.*, 2005; Mann *et al.*, 2014). Currently, The complete genome sequences of fifteen plant-adapted rhabdoviruses are available: *Alfalfa dwarf virus* (Bejerman *et al.*, 2015), *Barley yellow striate mosaic virus* (Yan *et al.*, 2015), *Colocasia bobone disease-associated virus* (Higgins *et al.*, 2016), *Lettuce necrotic yellows virus* (Dietzgen *et al.*, 2006), *Lettuce yellow mottle virus* (Heim *et al.*, 2008), *Northern cereal mosaic virus* (Tanno *et al.*, 2000), *Datura yellow vein virus* (Dietzgen *et al.*, 2015), *Eggplant mottled dwarf virus* (Zhai, unpublished, Genbank: KJ080287.1), *Maize Iranian mosaic virus* (Ghorbani *et al.*, 2018), *Maize fine streak virus* (Tsai *et al.*, 2005), *Potato yellow dwarf virus* (Bandyopadhyay *et al.*, 2010) *Rice yellow stunt virus* (Huang *et al.*, 2003), *Sonchus yellow net virus* (Heaton *et al.*, 1989), *Taro vein chlorosis virus* (Revill *et al.*, 2005). Plant-adapted rhabdoviruses are taxonomically divided into four genera, *Cytorhabdovirus*, *Nucleorhabdovirus*, *Varicosavirus* and *Dichorhavirus*. The virions of plant-adapted rhabdoviruses are typically bacilliform in shape except *Varicosavirus* (rod shape). Cyto-, nucleo- rhabdovirus and dichoravirus are transmitted by arthropod vectors such as aphids, leafhoppers, planthoppers, and mites in the persistent manner (Kuzmin *et al.*, 2009; Lvov *et al.*, 2015; Jackson *et al.*, 2005). Otherwise, *Varicosavirus* is transmissible by fungi (Hartwrite *et al.*, 2010). The members of *Cytorhabdovirus* and *Varicosavirus* replicate in the cytoplasm of infected host cells. The maturation and budding of virions are associated with the endoplasmic reticulum membrane (Mann *et al.*, 2014). Currently, eleven species cytorhaboviruses are identified and of which *Lettuce necrotic yellows virus* is the type species (Jackson *et al.*, 2005). The type species is “a virus chosen for each genus to serve as an example of a well characterized virus species among the members of the genus” (ICTV master species lists, 2016). Nucleorhabdoviruses and dichoraviruses replicate in the nuclei of infected plant cells. The viruses do their replication and morphogenesis in the infected host nuclei (Bejerman *et al.*, 2015; Jackson *et al.*, 2005; Mann *et al.*, 2014). The genus has ten species, and *Potato yellow dwarf virus* is the type species. (Bandyopadhyay *et al.*, 2010; Lamprecht *et al.*, 2009; Liu *et al.*, 2018; Martin *et al.*, 2012). All

plant-adapted rhabdovirus genomes encode the accessory movement protein (MP) that mediates cell-to-cell movement and induces systemic infection. The MP gene is located between P and M genes, and the movement proteins are thought to be related to the microtubules and plasmodesmata in the plant cell (Bejerman *et al.*, 2015; Heaton *et al.*, 1989; Jackson *et al.*, 2005; Redinbaugh *et al.*, 2005; Walker *et al.*, 2011).

Potato yellow dwarf virus

Potato yellow dwarf virus (PYDV) is the type species of genus *Nucleorhabdovirus*. Black (1941) described the two strains of PYDV at the vector-specificity level (Black *et al.*, 1941). According to the data, the leafhopper, *Agallia constricta* (Fig. 1.2a) that transmits the New Jersey strain of PYDV did not transmit the New York strain, which is vectored by *Aceratagallia sanguinolenta* (Fig. 1.2b) (Black *et al.*, 1941). The New Jersey strain and the New York strain of PYDV were later renamed as *Constricta yellow dwarf virus* (CYDV) and *Sanguinolenta yellow dwarf virus* (SYDV). The two strains are also serologically distinct. Except for G protein, CYDV antigens do not interact with the SYDV antibody (Black *et al.*, 1941) (Fig. 1.2d). The same result was obtained from SYDV antigens with the CYDV antibody (Fig. 1.2c). Development of the method for inoculation of *Potato yellow dwarf virus* on the vector cell monolayers allowed more detailed studies to explain the biological distinction between the two PYDV strains in the vector specificity (Black *et al.*, 1941, Hsu *et al.*, 1973). The optimal pH for the *Sanguinolenta* strain of PYDV inoculation to the leafhopper cell was 5.9, while the optimal inoculation pH for the *Constricta* strain was 5.3 (Hsu *et al.*, 1973). The data indicated that the surface proteins of the virus particle are involved in the functional role during the inoculation of insect vector cells (Falk *et al.*, 1983; Hsu *et al.*, 1984). Hsu *et al.* used two-dimensional protein gel electrophoresis to determine the isoelectric point (pI) of SYDV-G and CYDV-G proteins and identified their pI as 4.8 and 4.3, respectively (Hsu *et al.*, 1984). The infectivity neutralization tests by Hsu *et al.* (1984) revealed that SYDV-G specific-antibody significantly reduced the number of CYDV-infected AS-2 cells.

Infection of the cell by CYDV was inhibited by the SYDV-G specific antibody as well, but the sensitivity was tenfold less than that of SYDV (Hsu *et al.*, 1984).

Among the two strains, the full-length genome sequence and protein localization and interaction map of the SYDV were determined (Bandyopadhyay *et al.*, 2010). The SYDV genome consists of 12,881 nucleotides that have two more ORFs of X and Y proteins in addition to the five common canonical protein genes that are shared by all rhabdoviruses (Bandyopadhyay *et al.*, 2010). ORF X is located between the N and P genes, and ORF Y is located between the P gene and the M gene (Fig. 1.1b, PYDV). The gene coding region is flanked by the leader and trailer sequences. The overall genome structure is 3' leader-N-X-P-Y-M-G-L-trailer 5' (Bandyopadhyay *et al.*, 2010). The functional role of SYDV-X is unclear, but a BLASTp search using the X protein amino acid sequence suggested that SYDV-X is similar to the MFSV-ORF3 protein (Bandyopadhyay *et al.*, 2010). The amino acid sequence similarity of SYDV-Y to SYN-SC4, which has been identified as a movement protein, suggests its cell-to-cell movement function (Heaton *et al.*, 1989; Anderson *et al.*, 2014; Huang *et al.*, 2005). The GFP-tagged Y protein localized on the cell periphery region, and this localization aspect was similar to the SYN SC4 (Bandyopadhyay *et al.*, 2010; Min *et al.*, 2010). The function of N, P, M, G, and L of SYDV was proposed based upon amino acid similarity with the cognate proteins of SYN which was previously characterized (Bandyopadhyay *et al.*, 2010; Heaton *et al.*, 1989). N, P, and M proteins were localized on the nucleus (Bandyopadhyay *et al.*, 2010). Bandyopadhyay *et al.* (2010) showed the rearrangement of the inner nuclear membrane by SYDV-M without the context of virus infection, which was not observed from the SYN-M expression. The SYDV-G protein was localized on the nuclear membrane (Bandyopadhyay *et al.*, 2010; Anderson *et al.*, 2014). In addition to the accumulation of the PYDV particle in the perinuclear space (Knudson *et al.*, 1973), these interactions and localization patterns of the viral proteins in the plant cell explain the nucleotropic life cycle of PYDV in more detail (Bandyopadhyay *et al.*, 2010; Anderson *et al.*, 2014).

Nuclear transport

Molecular transport between the cytoplasm and nucleoplasm is essential for many physiological and cytopathological processes, such as gene expression, cell signaling, pathogen infection, and immune response in cells (Raikhel *et al.*, 1992; Moore *et al.*, 1996; Sanderfoot *et al.*, 1996; Whittaker *et al.*, 1998). The cytoplasm and nucleoplasm are separated by the nuclear envelope (NE), which consists of the inner nuclear membrane (INM) and outer nuclear membrane (ONM). The ONM is continuous with the membrane of the endoplasmic reticulum. The space between the INM and ONM is termed the perinuclear space, and this space is connected to the lumen of the ER (Fig. 1.3a). The only channels through which molecular transport can take place are the selectively permeable channels called nuclear pore complexes (NPCs) (Naim *et al.*, 2007; Wang *et al.*, 2007; Wentz *et al.*, 2010; Kabachinski *et al.*, 2015). Cargo proteins travel between the cytoplasm and the nucleus in association with nuclear transport receptors (Kabachinski *et al.*, 2015).

1) Nuclear Pore Complex

The general structure of the NPC is an octagonal cylindrical opening that is embedded within nuclear envelope. Each NPC consists of eight symmetrical spokes that surround a central channel. The spokes are attached to a nuclear ring and cytoplasmic ring (Fig. 1.3a). The cytoplasmic filaments extend from the cytoplasmic ring toward the cytoplasm, while the nuclear filaments emanate from the nuclear ring and conjoin distally to form a nuclear basket. The central channel connects the cytoplasmic space to the nucleoplasm and contains selectively permeable barrier that is formed by FG rich domains extended from central nucleoporins (D'Angelo *et al.*, 2008, Onischenko *et al.*, 2011; Alber *et al.*, 2007) (Fig. 1. 3a, b). These substructures of the NPC consist of multiple copies of about 30 different nucleoporins (Ibarra *et al.*, 2015; Tamura *et al.*, 2013). Comprehensive proteomic studies of NPC in *Saccharomyces cerevisiae* determined 29 different nucleoporins (Rout *et al.*, 2000). Rout *et al.*, (2000), characterized the localization of each nucleoporin in NPC and their functions (Rout *et al.*, 2000). Two years after this study, the first vertebrate NPC proteomics data reported that there are 29 nucleoporins in rat liver nuclei

(Cronshaw *et al.*, 2002). In addition to yeast and vertebrates nucleoporins, thirty putative nucleoporins were reported from *Arabidopsis thaliana* in 2010 by Tamura *et al.* (2010). Their data revealed that plant nucleoporins have higher sequence homology to vertebrate nucleoporins than to those of yeast (Tamura *et al.*, 2010). Despite the low primary sequence similarity, the basic NPC structure is conserved in plants, yeast, and vertebrates (Tamura *et al.*, 2010; Eckardt *et al.*, 2010). The nucleoporins in vertebrates, yeast, and plants are listed in Figure 1.3b.

The nucleoporins can be broadly grouped into three categories based on their functional properties and localization in the NPC: (1) membrane nucleoporins, (2) scaffold nucleoporins, and (3) barrier nucleoporins (Fig. 1.3b) (Onischenko *et al.*, 2011; Tamura *et al.*, 2013; Alber *et al.*, 2007; Parry *et al.*, 2014). The membrane nucleoporins are thought to anchor the NPC to the nuclear envelope. In plants, the membrane nucleoporins, GP210 (homology of yeast pom152)(Gerace *et al.*, 1982; Greber *et al.*, 1990) and NDC1(Wonzniak *et al.*, 1994) form an outer transmembrane ring of NPC. Yeast and vertebrates possess additional nucleoporins, Pom 34 and Pom 121, respectively. The scaffold nucleoporins bridge the membrane nucleoporins to the barrier nuclear porins. The scaffold nucleoporin group is comprised of 19 members in plants. These nucleoporins constitute the outer ring, inner ring, and linker in the NPC. These substructures are thought to play a key role to maintain the stable connection between the NPC and the nuclear envelope. In plants, the outer ring is composed of 12 nucleoporin members: Nup160, Nup133, Nup107, Nup96, Nup75, Nup43, SEH1, SEC13, ALADIN, GLE1, RAE1, and Elys. The inner ring is located in the central part of the main channel and consists of 4 nucleoporin members (Nup205, Nup188, Nup155, Nup35). The linker nups (Nup93 and Nup88) connects the outer ring and inner ring. The barrier nucleoporins are categorized into three groups: cytoplasmic FG-Nups, Central FG-Nups, and Nuclear-FG Nups based on their orientation in NPC. FG-Nups have phenylalanine-glycine repeats, the large intrinsically-disordered domains. The two cytoplasmic FG-nups, Nup214 and CG1 are the constituents of cytoplasmic filaments in plants and vertebrates. In plants, the Nup1/136, Nup50,

and NUA (Nup153, Nup50, and Tpr in vertebrate) form the nuclear basket. These structures play a role in interaction transport receptors and serve as docking sites for nuclear import and export. Hutton *et al.*, (2009) reported that Nup358, a cytoplasmic filament component, interacts with RanGAP (RanGTPase-activating protein) to facilitate the nuclear transport receptor-dependent nuclear import (Hutton *et al.*, 2019). Nup358 is absent in plants, but plant RanGAPs have a conserved WPP domain which interacts with the WPP domain-interacting proteins (WIPs) that direct RanGAP to NE (Zhao *et al.*, 2008). The nuclear basket components, Nup136 and NUA, are involved in mRNA export (Xu *et al.*, 2010) and plant developments (Tamura *et al.*, 2010). The overexpression of the nuclear basket components induced dramatic accumulation of poly-A RNA in nucleus, and gene silencing of Nup 153 induced a dwarf phenotype of *A. thaliana*. Nup153 (Nup136 homolog) interacts with lamin B, which supports the nuclear structure. The association of plant Nup136 with the nuclear lamina has also been suggested (Tamura *et al.*, 2013). The central FG Nups have FG-rich repeats forming a selective barrier regulating nucleocytoplasmic transport in the central channel of NPC. The unfolded structure allows low-affinity and high-specific interactions with the transport factors (Strawn *et al.*, 2004). Five FG nups (Nup98, Nup58, Nup54, and Nup35) have been identified from plants (Zhao *et al.*, 2011). Ryan *et al.* (2010) showed that all FG nucleoporins could interact with at least one transport receptor (Ryan *et al.*, 2010). As briefly stated above, the central channel of the NPC is filled with these highly flexible, natively unfolded- and fiber-like FG repeats that extended from FG-Nups located in NPC center (Jovanovic-Talisman *et al.*, 2017). The meshwork of FG-Nup filaments forms the permeable barrier in the central channel of NPCs and directly mediates nucleocytoplasmic transport via interaction with nuclear transport receptors (NTR). (Freitas *et al.*, 2009; Naim *et al.*, 2007; Wentz *et al.*, 2010). The NTRs bind to cargo and the transport complexes gain access the central channel through the intrinsic weak affinities between NTRs and FG-repeats. The weak and transient interaction prevents the transport complex from getting stuck in the mesh structure and allow it moves rapidly in the pore (Boche *et al.*, 1997; Fung *et al.*, 2017).

2) Nuclear transport receptors

There are two types of passage through the central barrier of the NPC. Small molecules below 40 kDa or 5nm in diameter move through NPC rapidly by free diffusion (Alberts B *et al.*, 2002). Although the passive diffusion of the proteins larger than 40 kDa has been reported (Wang *et al.*, 2007, Popken *et al.*, 2015), the diffusion efficiency was much lower than the small molecules (Timney *et al.*, 2016; Wang *et al.*, 2007). The transport of most proteins larger than the diffusion limit is mediated by nuclear transport receptors (NTR) (Timney *et al.*, 2016; Naim *et al.*, 2007; Wang *et al.*, 2007). The NTRs are collectively referred to as karyopherins with those involved in import and export termed importins and exportins, respectively (Lusk *et al.*, 2002). The importin- β superfamily proteins are major nuclear transport receptors that interact with Ran small GTPase and transport of cargo proteins (Merke *et al.*, 2011). Goldfarb *et al.* (2004) classified the 14 importin- β s in the yeast genome, 18 of these proteins in human genome. Eighteen importin- β proteins were identified from the *Arabidopsis thaliana* genome (Tamura *et al.*, 2014). In the classical nuclear import model, the interaction between cargo and importin- β is mediated by adapter proteins called importin- α s. The adapter protein recognizes two classes of NLS, known as classical NLSs: monopartite and bipartite NLSs (Kosugi *et al.*, 2008). Several structural studies revealed that importin- α is composed of an N-terminal importin- β -binding (IBB) domain, ten armadillo (Arm) repeats, and conserved short acidic amino acids clusters in the C-terminal region (Kobe *et al.*, 1999; Lott *et al.*, 2011; Lange *et al.*, 2007). The IBB domain has the autoinhibitory sequence, KRR residue, which regulates the binding affinity of both types of cNLS, preventing re-binding and mediating the release of cargo in the nucleoplasm (Lott *et al.*, 2011; Lange *et al.*, 2007). The Arm repeats produce two binding domains, major groove and minor groove, that interact with the cargo NLSs (Lange *et al.*, 2007). Although many cargo proteins can be imported in importin- α -independent manners, cNLS-mediated nuclear import has been assumed as the most prevalent pathway due to the surfeit of known cNLS containing proteins (Goldfarb *et al.*, 2004). The global

analysis of protein localization in yeast revealed that 45% of the 5850 yeast proteins in the GenBank™ set have the potential to be imported by the cNLS (Huh *et al.*, 2003).

The karyopherins which mediate nuclear export of cargo proteins are called exportins. The chromosome regions maintenance 1/exportin1/Exp1/XPO1 (CRM1) has been reported as the major transport receptor for the export of proteins from the nucleoplasm to the cytoplasm (Thakar *et al.*, 2013). CRM1 recognizes the leucine-rich nuclear export signals of cargo proteins. O'Reilly *et al.*, (2011) classified nine exportin gene families, XPO 1-7, XPOT, and TNPO from human and mice karyopherins. Plant genomes encodes PLATKAP instead of XPO6 gene (O'Reilly *et al.*, 2011; Tamura *et al.*, 2014). These exportins are functionally diverse. XPOT and XPO1 export tRNAs and proteins containing leucine-rich NESs. XPO5 exports eEF1A, tRNA, and 60S ribosomal subunits. XPO6 exports actin (O'Reilly *et al.*, 2011).

3) Nuclear import

The NLSs are typically a stretch of 7-20 amino acids within karyophilic proteins. Various classes of NLSs have been reported from different organisms (Cooper *et al.*, 2000; Krichevsky *et al.*, 2006; Whittaker *et al.*, 1998). The first NLS to be identified, at the molecular level, was the large T antigen NLS of the simian virus 40 (SV40) (Kalderon *et al.*, 1984). The viral NLS was found to consist of the seven basic amino acids, PKKKRKV. Kalderon *et al.* demonstrated that this sequence was sufficient to import the heterologous cytoplasmic proteins, namely B-galactosidase and pyruvate kinase (Kalderon *et al.*, 1984). Four years later, Dingwall *et al.* identified the amino acid structure of another type of cNLS, the bipartite signal (underlined), from *Xenopus* nucleoplasmin which consists of sixteen residues, KRPAATKKAGQAKDKK (Dingwall *et al.*, 1988). They found that two clusters of basic residues (underlined) are necessary for nuclear targeting of the protein (Dingwall *et al.*, 1988). These two NLSs are considered as the prototypes of the classical nuclear localization signals (cNLS) (Rihs *et al.*, 1991). Although the prototypical sequence of the cNLSs have been defined and may be the most common, there are still many

different NLSs that do not match the consensus rule (Kosugi *et al.*, 2009). Kosugi *et al.* classified NLSs binding to importin- α into six classes, based on their binding modes and amino acid sequence similarities. In their study, the monopartite NLSs that bind to the major groove of importin- α were designated to Class 1 and Class 2 based on its consensus sequence. Class 1 NLSs have monopartite and consecutive basic amino acid residues with a consensus sequence of KR(K/R)R or K(K/R)RK. The prototype monopartite NLS of SV40 (PKKKRKV) is an example of Class 1 NLS. Class 2 has (P/R)XXKR(^DE)(KR) as its consensus sequence. The NLS of human c-myc (PAAKRVKLD/RQRRNELKRSF) is an example of Class 2 NLSs. Amino acid replacement analysis revealed that the activity of Class 2 NLS is affected by flanking residues (Kosugi *et al.*, 2009). The NLSs of Class 3 and Class 4 bind to the minor groove of importin- α (Kosugi *et al.*, 2009). They are also monopartite NLSs but differ from Class 1 and Class 2, in that they have only two or three consecutive basic amino acids. Class 3 has a consensus sequence KRX(W/F/Y)XXAF (Kosugi *et al.*, 2009). This sequence was identified in the C terminus of nucleolar RNA helicase II/Gu(Ddx21) in mice (Kosugi *et al.*, 2009). The consensus sequence of Class 4 NLS was determined to be (R/P)XXKR(^DE) (Kosugi *et al.*, 2009). Class 5 NLSs are also monopartite and importin- α minor groove binding signals but differ from other NLS subgroups in their specific binding activity to plant importin- α . The consensus sequence of the NLS subgroup is LGKR(K/R)(W/K/Y) (Kosugi *et al.*, 2009). The prototype bipartite NLS of nucleoplasmin and its homologs are designated Class 6. These cNLSs interact with the heterodimeric import receptor, Importin- α/β complex. These NLSs have two clusters of basic amino acids separated by a linker domain which consists of 10-12 amino acids. The consensus amino acid sequence of Class 6 NLS has been defined as (K/R)(K/R)X₁₀₋₁₂(K/R)_{3/5}. (K/R)_{3/5} represents at least three of either lysine or arginine of five consecutive amino acids. The bipartite NLS binds to both the major groove and minor groove of importin- α . While the N terminal basic stretches (K/R)(K/R) bind to the minor groove, the C-terminal basic stretches bind to the major groove (Kosugi *et al.*, 2009).

The cargo proteins bearing cNLSs interact with a heterodimeric complex which consists of importin- α and - β . The importin- α in the complex specifically recognizes the NLS in the cargoes. The trimeric complex (importin α/β -cargo) binds to the cytoplasmic side of the NPC (Whittaker *et al.*, 1998; Natalia *et al.*, 2009; Miyamoto *et al.*, 2016). Translocation of the trimeric complex into the nucleus is mediated by the interaction between importin- β and FG-Nups. (Kalab *et al.*, 2008; Lui *et al.*, 2009). The cargo complex is driven by the progressively increasing binding affinity of importin- β for Nup358, Nup62, and Nup 153, which are in the cytoplasmic, central, and nucleoplasmic regions of the NPC, respectively (Fig. 1.3b-c) (Ben-Efraim *et al.*, 2001). The liberation of the cargo from the nuclear import complex is mediated by Ran (Ras-related nuclear protein) protein which is also known as GTP-binding nuclear protein Ran in nucleus. The protein is one of major components directing nucleocytoplasmic trafficking. While Ran proteins are distributed in a GDP-binding state in the cytoplasm, the GTP-binding form predominates in the nucleus. The cytoplasmic Ran-GDPs are imported by NTF2 (nuclear transport factor 2) and converted into Ran-GTP by Ran nucleotide exchange factor, a regulator of chromosome condensation 1 (RCC1) (Lui *et al.*, 2009; Renault *et al.*, 2001). Once the nuclear import complexes arrive inside the nucleus, Ran-GTP binds to the importin- β , followed by the release of cargo from the complex (Alberts B *et al.*, 2002; Askjaer *et al.*, 1999; Lui *et al.*, 2009). After cargo release, the importins and Ran-GTPs are exported to the cytoplasm for recycling. The importin β /Ran-GTP complexes are exported through the NPCs, and, the free importin- α proteins bind to the export factor CAS (Cellular apoptosis susceptibility protein) which interacts with Ran-GTP to be exported (Cressman *et al.*, 2001; Freitas *et al.*, 2009; Kobayashi *et al.*, 2013; Miyamoto *et al.*, 2016). At the cytoplasmic surface of NPC, Ran-GTP is hydrolyzed by the Ran-GTPase activation protein (RanGAP). At this time, Ran-binding proteins (e.g., RanBP1) in cytoplasmic space enhance the GTPase activity of Ran to recycle the protein for the next round of nuclear import cycle (Fig.1. 4a) (Boche *et al.*, 1997).

In addition to the classical import pathway, some cargo proteins are imported into the nucleus without the interaction between cargoes and adapter proteins. The importin α -independent nuclear import pathways for Human Immunodeficiency Virus (HIV) Rev and Tat (Traut *et al.*, 1999), ribosomal proteins (Rout *et al.*, 1997), cAMP-response element binding protein (CREB) (Forwood *et al.*, 200), the human-T-cell leukemia virus type 1 (HTLV-1) protein Rex (Palmeri *et al.*, 1999), Cyclin B1 (Takizawa *et al.*, 1999) have been defined. These NLSs bind directly to importin- β . The proline-tyrosine localization signals (PY-NLSs) are also recognized by importin- β 2 or transportin-1. The PY-NLSs are structures disordered in free cargoes. The transportin-binding domain composed of a hydrophobic N-terminal, a central arginine residue and a C-terminal RX₂-₅PY sequence (Soniati *et al.*, 2016). The import of the cargoes including phosphorylated Arg-Ser (RS) repeats is mediated by transportin3 (Trn3) (Maertens *et al.*, 2014). About 32% of cargoes that bind to Trn3 have the RS repeat. Other Trn3 cargoes use the Arg-Glu (RE) motif or Arg-Asp (RN) motif. The NLS of Mat- α 2 type protein contains a mix of hydrophobic and basic amino acids (Raikhel *et al.*, 1992).

4) Nuclear export

Transport of cargo from the nucleoplasm to the cytoplasm is mediated by the specific receptors, called exportins (Moore *et al.*, 1996). The chromosome region maintenance 1 (CRM1) protein (also known as exportin-1 or XPO1) binds various nuclear export signals (NESs) in hundreds of different cargoes (Fung *et al.*, 2017). Currently, 265 experimentally identified protein cargoes are recorded in NES databases (Xu *et al.*, 2012; Fu *et al.*, 2018, <http://prodata.swmed.edu>), and over 1000 putative CRM1 cargoes were identified in a recent proteomics study (Fu *et al.*, 2018). The first characterized NES was HIV-1 Rev, and the transcription factor, TFIIA, from *Xenopus* (Askjaer *et al.*, 1998, Moore *et al.*, 1996). Sequence-wise, NESs are hydrophobic sequences of 10-14 amino acids, often rich in leucine residues. For example, the C-terminal of HIV1 Rev, LQLPPLERLTL, is essential in the trafficking of the protein from the nucleus to the cytoplasm (Alberts B *et al.*, 2002; Moore *et al.*, 1996). In plant viruses, one of the well-described NES is the

Squash leaf curl virus (SLCV: Geminivirus) BR1 movement protein that functions as a nuclear shuttle protein (NSP) (Sanderfoot *et al.*, 1996, Ward *et al.*, 1999). The *Xenopus* TFIIA NES can functionally substitute the SLCV NSP NES in both nuclear protein export and virus infectivity. This data suggested that the basic nuclear export machinery is highly conserved between animals and plants (Ward *et al.*, 1999).

Several nuclear export receptors such as CRM1/exportin (XPO 1) and cellular apoptosis susceptibility proteins (CAS), were identified in various eukaryotic organisms (Fornerod *et al.*, 1997; Stade *et al.*, 1997; Kutay *et al.*, 1997). During protein export, the trimeric export complexes, which consists of cargo, CRM1, and Ran-GTP, are translocated through the central channel of NPC and bind to Ran-binding protein 1 (RanBP1). RanBP1 releases CRM1 from Ran GTP, which is followed by the dissociation of the complex. The de-phosphorylation of RanGTP is mediated by RanBP1-associated RanGAP. Once the exported molecules are released into the cytoplasm, CRM1 is recycled back to the nucleus, and Ran-GDP is directed to the nuclear import cycle (Fig. 1. 4b) (Seewald *et al.*, 2003, Askjaer *et al.*, 1999, Kehlenbach *et al.*, 1999).

NLSs and NESs in plant nucleorhabdoviruses

Nucleorhabdoviruses, such as SYNV, PYDV, MFSV, and RYSV have a nucleotropic life cycle. The accumulation of viral genomes and structural proteins in the host nucleus (especially in the viroplasm) is characteristic of the cytopathology of a nucleorhabdovirus infection. The newly assembled virions are found in the perinuclear spaces (Fig. 1.5) (Krichevsky *et al.*, 2006). These data indicate that the viruses accomplish transcription, replication, and morphogenesis using the host nuclear machinery, and must be shuttled using the nuclear transport machinery to gain access to the replication factory (Claudia *et al.*, 1998; Follett *et al.*, 1974, Ghosh *et al.*, 2008; Goodin *et al.*, 2001; Revill *et al.*, 2005; Chambers *et al.*, 1965). The nuclear-cytoplasmic transports of the viral components can be mediated by the NLSs and NESs on the viral proteins or those of their interaction partners (Min *et al.*, 2010).

Goodin *et al.*, determined the NLSs of N and P proteins of SYNV in 2001 (Goodin *et al.*, 2001). The site-specific mutagenesis and deletion analyses demonstrated that the SYNV-N protein contains a bipartite NLS in its C-terminus between amino acids 465 and 481 (Goodin *et al.*, 2001). The functional NLS domain of P was identified from the N-terminal between amino acids 40 and 124 (Goodin *et al.*, 2001). However, the nuclear import of P was not mediated by importins- α which binds to cNLS. This data suggests that P use an alternative pathway for nuclear import. Also, a putative NES was suggested to be located in the C-terminus of the P protein (Goodin *et al.*, 2001). Co-expression of N and P affected their cellular localization pattern and nuclear structure as well (Goodin *et al.*, 2001). Considering that N and P are essential nucleocapsid core components in all rhabdoviruses, the functional NLSs on the two proteins suggest that nuclear transport of the SYNV ribonucleoprotein complex is most probably associated with the core components (Goodin *et al.*, 2001; Min *et al.*, 2010; Krichevsky *et al.*, 2006). A model for the nuclear exportation of the SYNV ribonucleocapsid was suggested by Min in 2010 (Min *et al.*, 2010). The model suggests that the unbudded ribonucleocapsids of SYNV serve as a cell-to-cell movement complex via the RNPs interaction with the host factors Ni67, Mi7, sc4i17 and sc4i21 (Min *et al.*, 2010). The Ni67 and Mi7 are the ER-associated transcription activator and transcription factor respectively. Sc4i17 and sc4i21 are microtubules associated host factors, a microtubule-anchored transcription activator and motor-kinesin, respectively. The N/Ni67 and M/Mi7 interactions take place in the nucleus, and the two host factors have NESs. The interaction between the RNPs and the host factors could mediate the export of the minimal infectious units to the cytoplasm. Sc4 and glycoprotein interact with the RNPs to establish the cell-to-cell movement complex with the sc4i17 and sc4i21. The interaction pattern of sc4/sc4i17 on the nuclear periphery and filamentous complexes that radiated from the nucleus suggest that the movement protein-related host factors could guide the RNPs to the plasmodesmata (Min *et al.*, 2010).

The nuclear localization of PYDV proteins (Bandyopadhyay *et al.*, 2010) and the functional NLSs on N, P, and M have been identified (Anderson *et al.*, 2014; Anderson *et al.*, 2018). PYDV-N is localized exclusively on the nucleus when expressed as a GFP fusion in the plant cell (Anderson *et al.*, 2014). Alanine-scanning mutagenesis identified the two amino acid motifs, ⁴¹⁹QKR⁴²¹ and ⁴³²KR⁴³³, in the N protein. The two motifs were essential for nuclear import and interaction with importin- α . The three amino acid regions ⁶ISPSRKLDR¹⁵, ¹⁸SK¹⁹, ³⁵KK³⁷ of the phosphoprotein were identified as functional NLSs. The mutagenesis on these regions altered the nuclear localization pattern (Anderson *et al.*, 2014). SYDV-P did not interact with NbIMP- α but interacted with importin- $\alpha 7$ and $-\alpha 9$ of the non-host plant *Arabidopsis thaliana* (Anderson *et al.*, 2014). The protein functional domain predictive program, PSORT identified a possible bipartite NLS between amino acids 213-229 of PYDV-M (Anderson *et al.*, 2014; Anderson *et al.*, 2018). Alanine scanning analysis revealed that the individual amino acids K225 and R226 are required for the NLS function of the protein. The existence of an NES of PYDV-M was suggested by the exclusive cytoplasmic localization of the M fragment spanning amino acid residues 211-253. An NES was predicted by NetNES algorithm on the C-terminal of M, between amino acid 241-251 of M. The M and XPOI interaction were confirmed by BiFC assay (Anderson *et al.*, 2018).

Despite the long history of Potato yellow dwarf virus as a research subject for the studies of fine-structure of virion (MacLeod *et al.*, 1966), structural proteins (Adam *et al.*, 1944; Knudson *et al.*, 1972), cytological effects of the virus infection in host plant cells (Goodin *et al.*, 2005; Ghosh *et al.*, 2008; MacLeod *et al.*, 1966; Lin *et al.*, 1987), and the vector specificity (Chiu *et al.*, 1970; Gaedigk *et al.*, 1986) of plant-adapted rhabdoviruses, little has been known about the molecular determinants of its interaction with plant hosts or insect vectors. Until now, at least seven strains of PYDV have been described based on their biological properties including vector-specificity and symptom severity on model plants (Black *et al.*, 1940). Of which, the two strains of PYDV, Constricta- and Sanguinolenta- potato yellow dwarf virus, which are distinguished by the two

different leafhopper vector transmissions, *Agallia constricta* and *Aceratagallia sanguinolenta*, respectively, became the predominant research strains to study the strain-specific differences of the virus structural proteins and cytopathology on the vector (leafhopper) cells (Black *et al.*, 1941; Chiu *et al.*, 1970; Lin *et al.*, 1987). However, no attempt has been made to study genotypic differences between the two strains that may affect their remarkably different biological properties including pathogenesis and vector specificity.

Regarding viral proteins commonly have various functional domains that mediate interactions of the viral proteins with multiple factors of hosts and vectors (Verdaguer *et al.*, 2014; Subramani *et al.*, 2018) and these interactions are critical determinants of host range and vector specificity of the virus (Wintermantel *et al.*, 2016; Mendez-Rios *et al.*, 2010), the sequence variations between the two very closely related virus subspecies, CYDV and SYDV, will have profound effects on their virus-host and virus-vector protein interactions which would be directly linked to their differential symptom development in the host plant (Ghosh *et al.*, 2008) and distinct vector specificity (Black *et al.*, 1941). Furthermore, the impact of sequence variation between the two strains will be resulted in as unique subcellular interaction and localization patterns of the virus proteins for each virus in the host cell. Therefore, determining full-length genome sequence, analyzing genomic structure, prediction of functional domains for viral genome and proteins, and determining subcellular localization and interaction of viral proteins for the two viruses will provide a clue to find out the molecular determinants that make the two viruses have different biological characteristics.

The purpose of this research is determining the full-length genome sequence of CYDV to allow comparative genomic analysis of two PYDV subspecies, CYDV and SYDV, and characterization of protein interaction and localization patterns of the viruses *in-vivo* to provide linkage between the sequence information and subcellular functions of the proteins. The SYDV genome sequence was already fully sequenced by Bandyopadhyay (2010) in our previous research.

Their genomic information including cis-regulatory elements, amino-acids similarities, predicted functional domains of proteins of each virus can be used to explain the distinct spatial patterns of protein localizations and interactions between the two viruses at subcellular level. Further, this research also focuses on highly conserved functional regions of CYDV and SYDV proteins to predict commonly pivotal function of the proteins for the nucleotropic biology of nucleorhabdovirus.

To achieve the purpose of this research, each ORF of the CYDV, except L protein, was cloned into GFP fusion expression vector and bimolecular fluorescence complementary assay vector to define the subcellular localization and binary interaction of the viral proteins. The resulted information was integrated into protein interaction and localization map (PILM). The subcellular localization, interaction patterns and PILM of CYDV were compared to those of SYDV to elucidate the protein functions and phenotypic uniqueness of them. In-silico prediction for features of viral proteins supported the in-vivo results. These in-vivo and in-silico results were used for mapping of the functional domains of viral proteins that related to the inter- and intracellular movement of PYDV. Ultimately, these comparative analysis results of two strains of PYDV will provide a link between the molecular features of rhabdovirus strains and their differential interactions with host and vector species.

Table 1. Genera of Rhabdoviridae

| Genus | No. of Species | Type species |
|--------------------------|----------------|--|
| <i>Almendravirus</i> | 5 | <i>Puerto Almendras almenravirus</i> |
| <i>Curiovirus</i> | 4 | <i>Curionopolis curiovirus</i> |
| <i>Cytorhabdovirus</i> | 11 | <i>Lettuce necrotic yellows cytorhabdovirus</i> |
| <i>Dichorhavirus</i> | 2 | <i>Orchid fleck dichorhavirus</i> |
| <i>Ephemerovirus</i> | 8 | <i>Bovine fever ephemerovirus</i> |
| <i>Hapavirus</i> | 15 | <i>Flanders hapavirus</i> |
| <i>Ledantevirus</i> | 15 | <i>Le Dantec ledantevirus</i> |
| <i>Lyssavirus</i> | 16 | <i>Rabies lyssavirus</i> |
| <i>Novirhabdovirus</i> | 4 | <i>Salmonid novirhabdovirus</i> |
| <i>Nucleorhabdovirus</i> | 10 | <i>Potato yellow dwarf nucleorhabdovirus</i> |
| <i>Perhabdovirus</i> | 3 | <i>Perch perhabdovirus</i> |
| <i>Sigmavirus</i> | 7 | <i>Drosophila melanogaster sigmavirus</i> |
| <i>Sprivivirus</i> | 2 | <i>Carp sprivivirus</i> |
| <i>Sripuvirus</i> | 5 | <i>Niakha sripuvirus</i> |
| <i>Tibrovirus</i> | 7 | <i>Tibrogargan tibrovirus</i> |
| <i>Tupavirus</i> | 3 | <i>Durham tupavirus</i> |
| <i>Varicosavirus</i> | 1 | <i>Lettuce big-vein associated varicosavirus</i> |
| <i>Vesiculovirus</i> | 16 | <i>Indiana vesiculovirus</i> |
| <i>Unassigned</i> | 1 | <i>Moussa virus</i> |

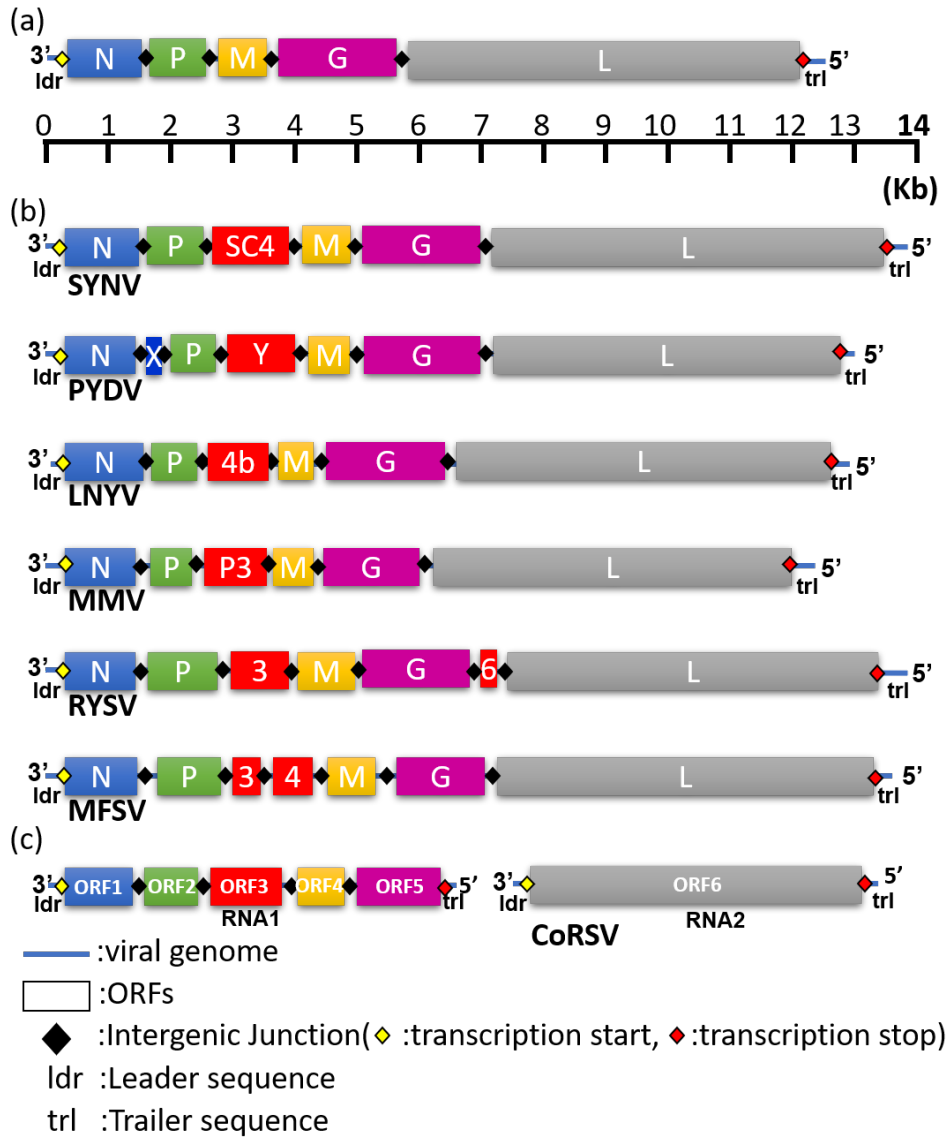


Figure 1.1. The genome organizations of selected plant negative-strand RNA viruses. (a) Common genomic structure of rhabdovirus. All members of the Rhabdoviridae family have the five canonical proteins the order, Nucleoprotein (N), Phosphoprotein (P), Matrix protein (M), Glycoprotein (G), RNA-dependent RNA polymerase (L). The ORFs are distinguished by intergenic junctions (diamond). (b) Genome organization of plant rhabdoviruses. The accessory genes are shown as red boxes in the genomes.

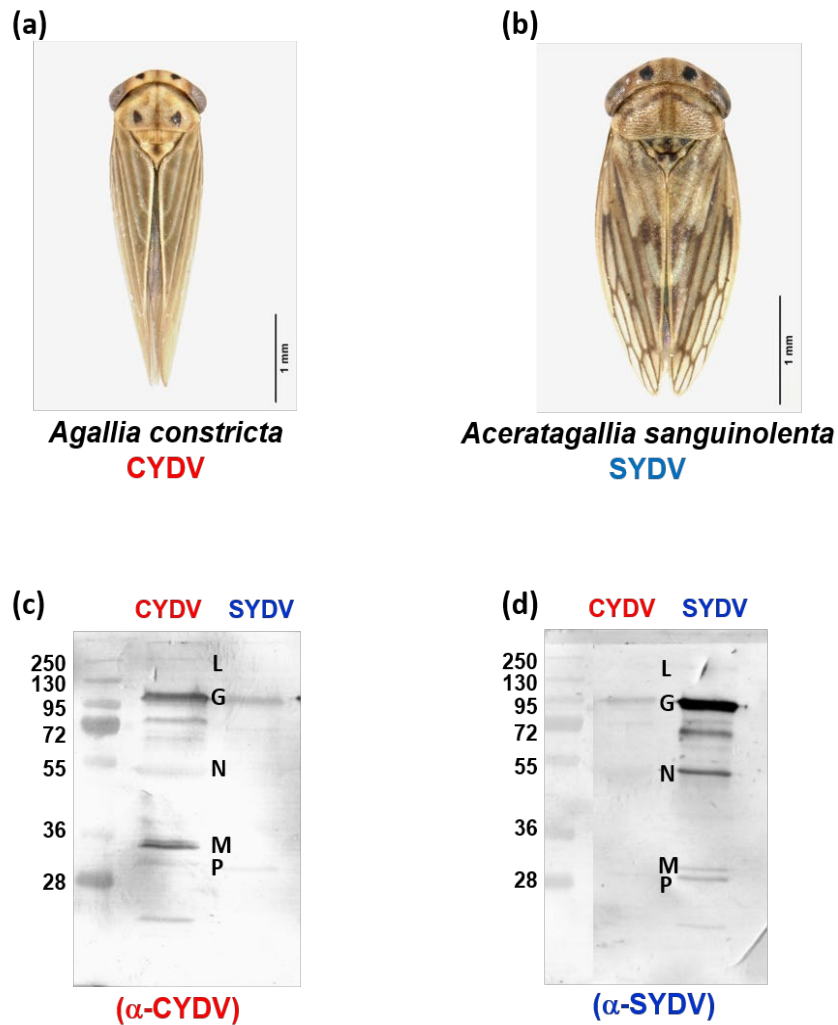


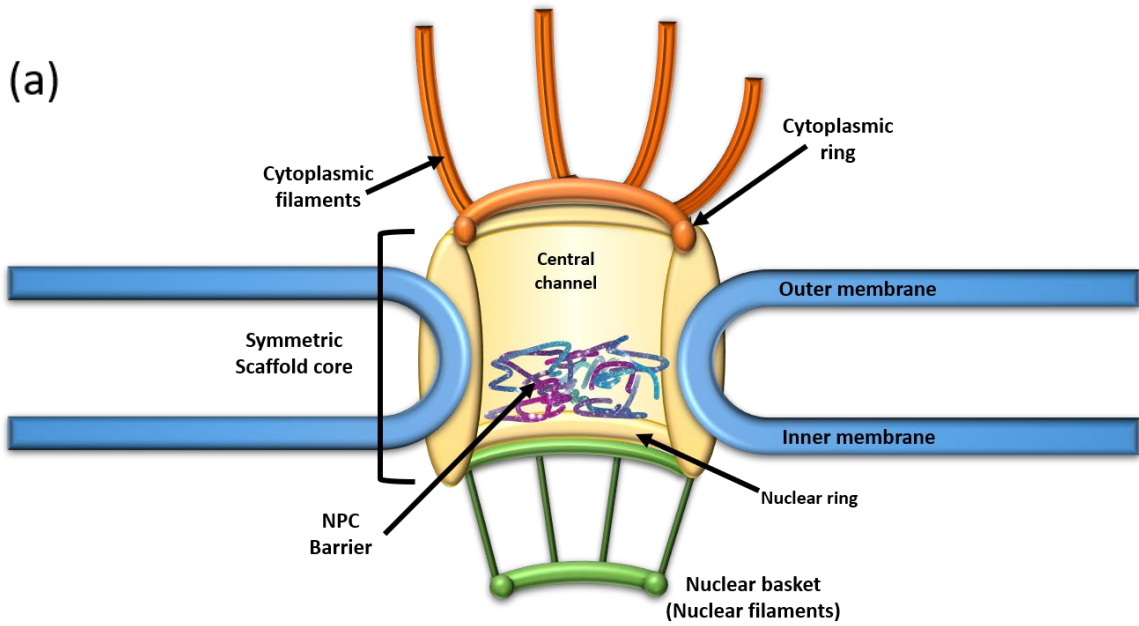
Figure 1.2. Insect vectors and serotype-specific detection of the CYDV and SYDV strains of PYDV.

(a) *Agallia constricta*, the vector of CYDV (b) *Aceratagallia sanguinolenta*, the vector of SYDV.

(C-D) Serological difference between CYDV and SYDV.

(Picture courtesy: National Museum Wales. *Agallia constricta*: NMW image No. i14071,

Aceratagallia sanguinolenta: NMW image No. i14089)



(b)

| Membrane Nups | | | Scaffold Nups | | | Barrier Nups | | |
|---------------|--------|-------------|---------------|---------|-------------|--------------|------------|------------|
| Plant | Yeast | Vertebrates | Plant | Yeast | Vertebrates | Plant | Yeast | Vertebrate |
| Ndc1 | Ndc1 | Ndc1 | Nup133 | Nup133 | Nup133 | - | - | Nup358 |
| - | Pom34 | - | Nup96 | Nup145C | Nup96 | Nup214 | Nup159 | Nup214 |
| - | Pom152 | - | Sec13 | Sec13 | Sec13 | Gle1 | Gle1 | Gle1 |
| ? | Pom33 | ? | Nup107 | Nup84 | Nup107 | Nup88 | Nup82 | Nup88 |
| Gp210 | - | Gp210 | Nup75 | Nup85 | Nup85 | Nup42 | Nup42 | NLP1 |
| Pom121 | - | Pom121 | Seh1 | Seh1 | Seh1 | Nup98 | Nup100 | Nup98 |
| Nup35 | Nup53 | Nup35 | Nup160 | Nup120 | Nup160 | Nup98 | Nup116 | Nup98 |
| - | Nup59 | - | - | - | Nup37 | Gle2(Rae1) | Gle2(Rae1) | Gle2(Rae1) |
| | | | Nup43 | - | Nup43 | Nup58 | Nup49 | Nup58/45 |
| | | | ALADIN | - | ALADIN | Nup62 | Nsp1 | Nup62 |
| | | | Nup93 | Nic96 | Nup93 | Nup54 | Nup57 | Nup54 |
| | | | Nup188 | Nup188 | Nup188 | Nup98 | Nup145(N) | Nup98 |
| | | | Nup205 | Nup192 | Nup205 | - | Nup60 | - |
| | | | Nup155 | Nup157 | Nup155 | Nup1/136 | Nup1 | Nup153 |
| | | | - | Nup170 | - | Nup50 | Nup2 | Nup50 |
| | | | | | | NUA | Mlp1/2 | Tpr |

(c)

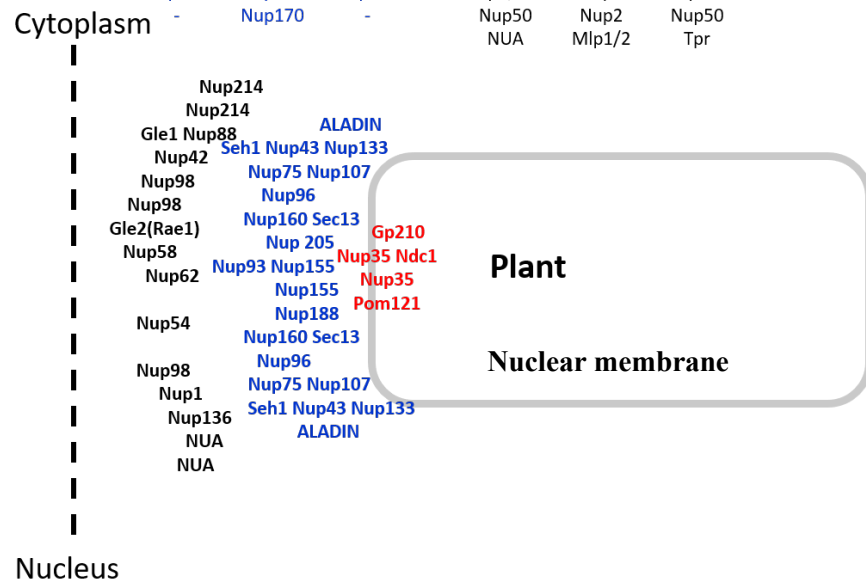


Figure 1.3. Structure of nuclear pore complexes in human, yeast, and plant. (a) Schematic image of NPC. (b) Nucleoporins of plant, yeast, and vertebrates. (c) The distribution and approximate location of nucleoporins in Plant.

(a)

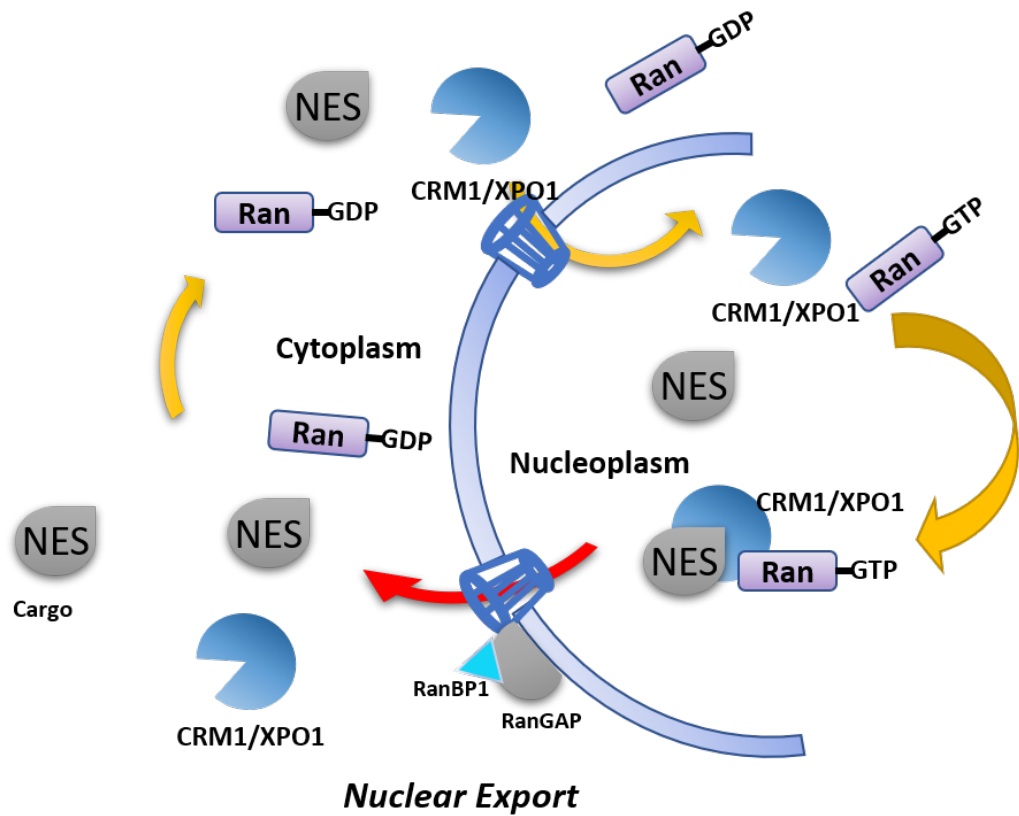
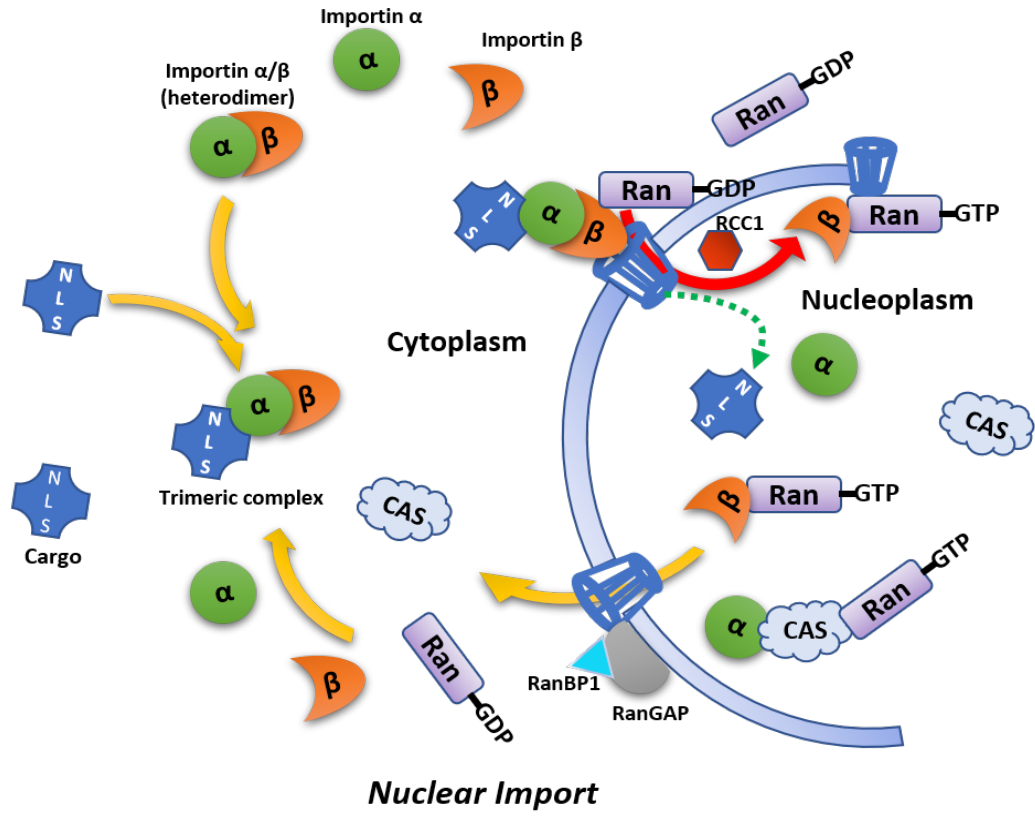


Figure 1.4. Generalized diagram of nuclear transport. (a) Nuclear import. The nuclear import begins with the dimeric complex formation between importin α and importin- β . The importin- α of the heterodimer binds to the import cargo which has cNLS domain. The trimeric complex is imported to the nucleoplasm through NPC. The imported Ran-GDP is phosphorylated by RCC1 and interacts with importin- β , followed by cargo and importin- α dissociation from the complex. After cargo releasing, the import complex components are exported through NPC and recycled for next round of nuclear import. (b) Nuclear export. The substrates in the nucleus which has NES motif are shuttled out of nucleus using exportin (CRM1/XPO1). The export receptor binds to Ran-GTP and recognize the NES cargo. The interaction generates the trimeric export complex NES cargo/CRM1/Ran-GTP. The complex translocated via the NPC channel. The complex is dissociated by dephosphorylation of Ran-GTP to release the cargo into cytoplasm.

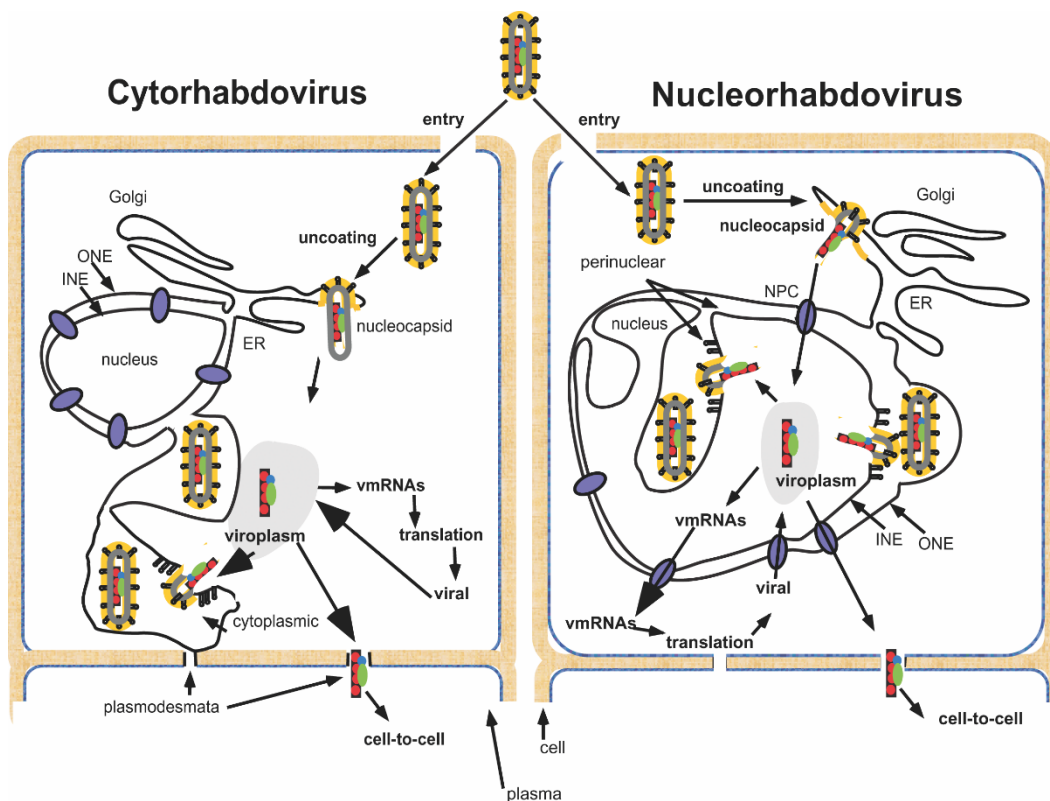


Figure 1.5. Comparison of life cycle between nucleo- and cytorhabdoviruses in the host cell. In the early stage of infection, the viruses are introduced into the host cell by the feeding behavior of the vector. The uncoating of virion take places through the cytoplasmic membrane, mostly ER, association of the virion. The RNP complex is released into cytoplasmic space. The members of *Cytorhabdovirus* induce the formation of inclusion bodies in the cytoplasm. The transcription, replication, and morphogenesis occur in the cytoplasmic inclusion body. Otherwise, nucleorhabdoviruses transport their RNP core into nucleus and induce nuclear viroplasm. The transcription of viral mRNA and replication, production of progeny particles takes place in the nucleus. [INE: Inner Nuclear Membrane, ONE: Outer Nuclear Membrane]

(Picture courtesy: *Biology of plant rhabdoviruses. Annu Rev Phytopathol (2005) 43:623-60*)

Chapter 2¹

Genome sequence variation in the constricta strain dramatically alters the protein interaction and localization map of Potato yellow dwarf virus

Although the coding capacity of viral genomes is low, it is common for each encoded protein to interact with multiple target factors, often located in different subcellular loci (Nagy *et al.*, 2016; Min *et al.*, 2010; Martínez *et al.*, 2016). Additionally, sequence divergence among viral strains can have profound effects on virulence, symptom development or adaptation to new hosts and vectors (Sánchez *et al.*, 2015; Pita *et al.*, 2015). As such, determination of the subcellular localization of viral proteins and mapping their interacting partners is fundamental to understanding virus-host interactions (Dietzgen *et al.*, 2017; Ramalho *et al.*, 2014; Martin *et al.*, 2012; Dietzgen *et al.*, 2012). Of particular interest in this regard are viruses that are able to replicate in diverse cell types, as proteins encoded by these viruses must contain domains that mediate interaction with factors in evolutionarily divergent hosts.

Rhabdoviruses infect a broad range of hosts, and members of this group includes viruses that infect humans, terrestrial animals/vertebrates, fish, arthropods and plants (Dietzgen *et al.*, 2017; Jackson *et al.*, 2005). Currently, the plant-adapted rhabdoviruses are assigned to two genera, *Cytorhabdovirus* and *Nucleorhabdovirus*, and two more recently described genera, *Dichoravirus* and *Varicosavirus*, contain members with bi-segmented genomes that also infect plants (Dietzgen *et al.*, 2017; Dietzgen *et al.*, 2014, Kormelink *et al.*, 2011). The genus *Cytorhabdovirus*, for which the type species is *Lettuce necrotic yellows virus*, contains those plant rhabdoviruses that replicate and undergo morphogenesis in the cytoplasm of infected cells (Fig. 1.5) (Dietzgen *et al.*, 2006). *Potato yellow dwarf virus* (PYDV) is the type species of the genus *Nucleorhabdovirus*, while *Orchid fleck virus* is the type species of the genus *Dichoravirus*. Both of these genera are typified

¹ This chapter was originally published as: Jang, C., Wang, R., Wells, J., Leon, F., Farman, M., Hammond, J., and Goodin, M (2017). Genome sequence variation in the constricta strain dramatically alters the protein interaction and localization map of *Potato yellow dwarf virus*. *Journal of general virology*. 98(6),: 1526-1536. All experiments were conducted by Chanyong Jang.

by the nucleotrophic character of the member viruses (Fig. 1.5) (Dietzgen *et al.*, 2017; Dietzgen *et al.*, 2014; Kondo *et al.*, 2006; Bandyopadhyay *et al.*, 2010).

PYDV was first reported as a highly destructive pathogen of potato (*Solanum tuberosum*), and early research of this virus contributed significantly in the arena of virus-insect interactions (Hsu *et al.*, 1973; Black *et al.* 1943). At least seven strains of PYDV have been described at the level of vector-specificity and biological variation in symptom severity (Black *et al.*, 1941; Black *et al.*, 1943). Of these, two strains distinguished by their differential transmission by leafhopper vectors, *Aceratagallia sanguinolenta* and *Agallia constricta*, referred to hereafter as sanguinolent yellow dwarf virus (SYDV; also called PYDV-New York) and constricta yellow dwarf virus (CYDV; also called PYDV-New Jersey), respectively, became the predominant research strains that served as early models for defining the ultrastructure and cytopathology of plant-adapted rhabdoviruses (Black *et al.* 1965; MacLeod *et al.*, 1966; Reeder *et al.*, 1972) and development of sucrose-gradient centrifugation (Brakke *et al.*, 1970) as an analytical method. Symptom severity of SYDV is greater than CYDV in *Nicotiana benthamiana*, and, in our hands, is easier to purify given its higher titre in that host (Bandyopadhyay *et al.*, 2010; Ghosh *et al.*, 2008; Brakke *et al.*, 1970).

The genome of SYDV was characterized previously (Bandyopadhyay *et al.*, 2010) and, since then, those of several segmented and non-segmented plant rhabdoviruses have been described (Min *et al.*, 2010; Dietzgen *et al.*, 2017; Ramalho *et al.*, 2014; Martin *et al.*, 2012; Deitzgen *et al.*, 2012). Collectively, the pattern that has emerged is that the protein interaction and localization maps (PILMs) for each virus are unique (Dietzgen *et al.*, 2017; Ramalho *et al.*, 2014; Martin *et al.*, 2012). Much of this variation is attributable to highly divergent genomic sequences among the viral species. In light of this, we sought to determine if lesser variation in genome sequence could profoundly affect PILMs at the level of viral strains, instead of between viruses. As such, we developed a PILM for the CYDV strain of PYDV and compared it to that of SYDV (Bandyopadhyay *et al.*, 2010). It is clear from our studies that even modest changes in sequence

variation can affect the topology of PILMs. These studies provide a link between the molecular features of rhabdovirus strains and their differential interactions with host and vector species.

Methods

Virus maintenance and purification

Potato yellow dwarf virus strain CYDV (American Type Culture collections accession PV-233) was maintained by serial passage in *N. benthamiana* and *N. rustica*. Plants housed in insect-proof cages. Field isolates of CYDV were collected from infected tomato (*Solanum lycopersicum*) in 2010, and black nightshade (*Solanum nigrum*) and pepper plants (*Capsicum annuum*) in the fall of 2016 in Beltsville, MD (Hammond, unpublished data). This isolate will hereafter be referred to as CYDV^{MD}. *Potato yellow dwarf virus* strain CYDV (American Type Culture collections accession PV-233) was maintained by serial passage in *N. benthamiana* and *N. rustica*. *N. benthamiana* lines expressing autofluorescent proteins fused to histone 2B, a nuclear marker, or RFP-HDEL (endomembrane marker), were maintained in the greenhouse for virus infection under conditions reported previously (Goodin *et al.*, 2007). Plants housed in insect-proof cages. As reported for SYDV, CYDV was purified on sucrose density gradients, as described previously (Ghosh *et al.*, 2008).

Isolation of total RNA, RT-PCR

Total RNA was extracted from plant tissues using the Qiagen RNeasy Plant minikit. Except where noted, first-strand cDNA synthesis and PCRs were carried out using Superscript reverse transcriptase IV (Thermo Fisher Scientific) and Phusion high-fidelity DNA polymerase (Finnzymes), respectively.

ION Torrent sequencing

Poly(A)⁺-RNA was purified from total RNA isolated from CYDV-infected leaves of *N. rustica* at 30 days post inoculation using a Dynabeads mRNA Purification Kit according to the manufacturer's instructions. The genomic sequence of CYDV was determined using the same ION

Torrent sequencing pipeline utilized for determination of the CoRSV genome (Ramalho *et al.*, 2014). All library construction and sequencing steps were performed by staff of the Advanced Genetic Technology Center (University of Kentucky). Template cDNA was prepared using an IonPGM Template OT (One-Touch) 200 Kit. Sequencing was performed with an Ion PGM sequencing 200 Kit and the Ion 316 chip. Contigs were assembled from the high-quality read data using the Trinity assembler package (Haas *et al.*, 2013).

5' and 3' RACE

5'- and 3'-RACE were performed with the BD-SMART RACE cDNA Amplification kit according to the manufacturer's instructions (Thermo-Scientific). For these analyses, cDNA was synthesized using MMLV reverse transcriptase, and PCRs were conducted with Advantage-II DNA polymerase (Clontech).

DNA sequence analysis

Homology searches were used to compare CYDV sequences to the genomes of other rhabdoviruses using the various BLAST tools provided on the National Center for Biotechnology Information (NCBI) server. ORFs were identified using the ORF finder search tool (Wheeler *et al.*, 2007). The primary structures of proteins encoded by CYDV were analyzed using a variety of algorithms provided by the ExPASy proteomics server: <https://www.expasy.org/> (Gasteiger *et al.*, 2003), including Compute pI/MW (Bjellqvist *et al.*, 1993), PSORT for prediction of protein localization (Nakai *et al.*, 1991), signal P for prediction of signal peptide cleavage sites (Bendtsen *et al.*, 2004) and NetNGlyc for prediction of N-glycosylation sites (Blom *et al.*, 2004).

Phylogenetic analysis

All L-protein sequences used in the sequence alignment study were obtained from data deposited in the NCBI database. In addition to that for CYDV, L-gene sequences utilized in phylogenetic analyses include the following: *coffee ringspot virus*-Larvas strain (CoRSV; KF812526), *Eggplant mottled dwarf virus* (EMDV;NC_025389), *Lettuce necrotic yellows virus*

(LNYV; AJ867584), *Maize mosaic virus* (MMV; AY618418.1), *Sonchus yellow net virus* (SYNV; L32603.1), *Maize fine streak virus* (MFSV; AY618417.1), *Potato yellow dwarf virus* (PYDV; NC_016136.1), *Maize Iranian mosaic virus* (MIMV; DQ186554), *Northern cereal mosaic virus* (NCMV; NC_00225.1), *Orchid fleck virus* (OFV; NC_009609), *Rice yellow stunt virus* (RYSV; NC_003746.1), *Taro vein chlorosis virus* (TaVVCV; NC_006942.1) and *Vesicular Stomatitis Indiana virus* (VSIV; NC_001560.1).

Sequence alignment and phylogenetic trees, generated using the neighbor-joining method with a bootstrap test with 1000 replicates, were conducted using the phylogeny.fr suite of online tools, as described previously (Dereeper *et al.*, 2008; Ramalho *et al.*, 2016).

A partial sequence of the L gene from CYDV^{MD} (isolated from tomato) was recovered by PCR using generic plant rhabdovirus primers (Lamprecht *et al.*, 2009). This sequence had a 99% nucleotide sequence identity to CYDV and was deposited in GenBank as accession (No. JQ405264).

Protein expression in plant cells

Sequence-validated clones in vector pDONR221 (Invitrogen) of all CYDV ORFs, except L, were recombined into the appropriate binary vectors for localization of fluorescent protein fusions in plant cells (Goodin *et al.*, 2007; Chakrabarty *et al.*, 2007). Tests for protein interactions were conducted using BiFC assays as described previously (Ramalho *et al.*, 2014; Anderson *et al.*, 2018, Jang *et al.*, 2017). Importantly, the conversion of the pSAT-based vectors to allow Gateway recombination-based cloning entirely eliminate the high background when ‘empty’ vectors expressing the two halves of YFP were co-expressed. As such, we have determined that false positives are less likely to occur when using the pSITE-BiFC vectors (Min *et al.*, 2010; Martin *et al.*, 2009). Therefore, the vectors employed in this study were pSITE-2CA (GFP fusions) and localization experiments, and the pSITE-BiFC-nEYFP and pSITE-BiFC-cEYFP vectors for BiFC assays. Recombinant vectors were transformed into *Agrobacterium tumefaciens* strain LBA4404.

Agroinfiltration for expression of protein fusion in plant cells was conducted essentially as described previously (Goodin *et al.*, 2007).

Laser scanning confocal microscopy

Microscopy for this study was conducted using an Olympus FV1000 laser-scanning confocal microscope as described previously (Goodin *et al.*, 2007).

Results

Genome sequence of CYDV

The complete 12 792 nt genome of CYDV deposited in GenBank as accession KY549567, was determined. The antigenomic sequence has the coding capacity for ORFs, encoding proteins greater than 100 aa each (Fig. 2.1). The L gene shares 99% nucleotide sequence identity with a partial L-gene sequence of a rhabdovirus isolated from Maryland, here identified as CYDV^{MD} (GenBank JQ405264.1). Overall, the genome of CYDV shares 69% sequence identity with SYDV at the nucleotide level. This variation is distributed more or less evenly across the genome, with the N genes sharing 71 % identity, and the X, P, Y, M, G and L genes sharing 22, 52, 74, 72, 69 and 72 %, respectively. The relationship between CYDV and SYDV is closer if the comparisons are relaxed and similar aa substitutions are considered, i.e., isoleucine and leucine at the same position being considered as functional equivalent, according to default settings on the blast server. In this scenario, the N, X, P, Y, M, G and L relationships are 83, 43, 73, 88, 83, 88 and 81% aa similarity, respectively. Interestingly, the CYDV X gene shares greater sequence relatedness (90% identity) with the cognate protein of *Eggplant mottled dwarf virus* (EMDV). At 52%, the phosphoproteins of CYDV and SYDV share the lowest aa identity of any cognate pair within the genomes of these viruses.

Phylogenetics of CYDV based on L-protein sequence comparisons

The phylogenetic relationship of the SYDV strain of PYDV to that of other rhabdoviruses has been established previously (Dietzgen *et al.*, 2016; Bandyopadhyay *et al.*, 2010). Based on a

similar analysis using the primary structure of L proteins, we show that CYDV is most closely related to other leafhopper-transmitted rhabdoviruses, with EMDV being the next most closely related species after SYDV (Fig. 2.2) (Pappi *et al.*, 2013). The aphid-transmitted SYNV, as well as the *Brevipalpus* mite-transmitted dichoraviruses, OFV and CoRSV, form clades that are well separated from the leafhopper-transmitted viruses (Fig. 2.2). Likewise, the planthopper-transmitted viruses and TaVCV form a separate clade.

Terminal sequences and gene junctions in the CYDV genome

Regarding SYDV reported previously, the leader and trailer terminal sequences of CYDV have a complete base complementarity over only a very short region, namely the terminal nine bases of the genome (Fig. 2.3) (Bandyopadhyay *et al.*, 2010).

A conserved gene junction with the consensus 3'-AAUUAUUUUUGGGUUG-5' (Fig. 2.4a) was located between each of the ORFs in the CYDV genome, as well as the leader (ldr)/N gene junction. This junction differs from that for SYDV only with respect to the position of the adenine in the poly-U track (Fig. 2.4b). Overall, the CYDV junctions share a similar tripartite organization with that of other plant-adapted rhabdoviruses. Region 1, consisting of a poly-U track that serves as a template for poly-adenylation of nascent mRNA transcripts; region 2, consists of triple guanine residues; and region 3, the transcriptional start site, consisting of UUG. As is typical for rhabdoviruses, each individual gene junction differs slightly from the consensus sequence. Most notably for CYDV, the intergenic spacer in the N/X and G/L junctions contained an additional guanosine residue (Fig. 2.4a).

Predict features of PYDV proteins

Generally, the predicted sizes of CYDV-encoded proteins are the same as, or slightly smaller, than their SYDV cognates. The N, X and G proteins are approximately 1, 1 and 3 kDa smaller than their SYDV counterparts, respectively, whereas the P, Y, M and L proteins are of equivalent sizes for both viruses.

Various protein localization prediction algorithms were used to identify potentially biologically relevant motifs in the CYDV-encoded proteins. A subset of this information is provided in table 1. Regarding its SYDV cognate, protein localization prediction algorithms failed to identify a nuclear localization signal (NLS) in the CYDV nucleocapsid protein. Furthermore, the primary structure of CYDV-N does not contain the mapped QKRANEEAPPAAQKR bipartite NLS found in SYDV-N (Anderson *et al.*, 2012). Algorithm-predicted NLSs were identified in the phosphoprotein, matrix protein and polymerase protein. Both CYDV and SYDV N proteins have a predicted isoelectric point (pI) of 7.62. The X protein of CYDV has a predicted pI of 3.87, slightly more acidic than the pI 4.5 of its SYDV cognate. Similar to CYDV-X, the P protein at pI 6.23 is slightly more acidic than the 7.72 of its SYDV cognate. The putative movement protein, CYDV-Y has a pI of 6.6 while that of SYDV is 7.0, both matrix proteins sharing a pI close to 9.0. Both CYDV and SYDV glycoproteins have a pI around 4.6. However, consistent with other proteins, the CYDV-L at pI 6.75 is greater than one log more acidic than its SYDV cognate (pI 7.99) (Table 2).

Although the CYDV-G ORF predicts a smaller protein than its cognate, the relative molecular weight based on the electrophoretic mobility of CYDV-G was reported to be greater than that for SYDV-G (92 kDa versus 85 kDa) (Falk *et al.*, 1983). The CYDV-G and SYDV-G proteins are predicted to have seven N-linked glycosylation sites each, and six and nine, respectively, O-linked glycosylation sites. The actual degree of glycosylation has not been mapped physically, and therefore the reason for the difference in electrophoretic mobility of these proteins remains equivocal.

Localization of CYDV protein fusions in plant cells

To test whether the sequence variation between SYDV and CYDV influenced protein localization, we determined the subcellular localization patterns for six CYDV proteins *in planta* and compared these data to published results for SYDV (Bandyopadhyay *et al.*, 2010). Each GFP

fusion of N, X, P, Y, M and G proteins was expressed in the plant expressing RFP fused to histone 2B (Fig. 2.5). In contrast to GFP:SYDV-N, whose localization was distributed evenly across the nucleoplasm, GFP:CYDV-N localized in sub-nuclear loci with a cross-sectional area about 2 μ m (Fig. 2.6a). GFP:CYDV-X distributed throughout the cell, with accumulation in the nucleus. GFP:CYDV-P accumulated in puncta distributed throughout the nucleoplasm but was excluded from the nucleolus. GFP:CYDV-Y partitioned between the cell periphery and the nuclear envelope (Fig. 2.6b), suggesting a membrane association for this protein. Regarding the SYDV matrix protein, the cognate CYDV protein was exclusively nuclear when expressed as a GFP fusion. GFP:CYDV-G associated with endomembranes, with the most easily detectable signal localized on the nuclear envelope.

Interaction matrix for CYDV proteins

In addition to protein localization studies, we investigated whether the determined sequence divergence between the two viral strains impacted the interaction of CYDV proteins, relative to the interactions observed for SYDV (Bandyopadhyay *et al.*, 2010). In order to make direct comparisons, the same type of bimolecular fluorescence complementation (BiFC) assay was used to define the interaction and localization patterns of CYDV proteins (Fig. 2.7). While all pairwise interactions were tested, in the four protein fusion orientations possible with BiFC, only a subset of the data is reported here. The N, X, P, Y, M and G proteins were tested in all pairwise interactions and against glutathione-S-transferase (GST), which served as a non-binding control (Fig. 2.7). The L protein was not included in these experiments as we were unable to detect GFP fusion of this protein in planta (data not shown). None of the CYDV proteins showed interaction with GST. Positive BiFC interactions were detected for the pairs N/N, N/X, N/P, N/Y, N/M, N/G, P/P, X/P, X/Y, X/X, /M and M/M. No other interactions were detected. The X protein did not interact with the G protein. The resulting BiFC and localization data were integrated into a CYDV

PILM, which differs significantly from that of SYDV. The M/Y, Y/Y and G/G interactions were unique to SYDV (Fig. 2.8), while the P/P and X/M interactions were unique to CYDV.

Localization of PYDV proteins in virus-infected plant cells

It has been reported previously that localization patterns of plant-adapted rhabdovirus proteins can differ markedly in the context of infected cells compared to single protein expression in virus-free cells (Goodin *et al.*, 2007). Given this precedent, we expressed GFP fusion of proteins from both CYDV and SYDV in transgenic *N. benthamiana* plants expressing RFP targeted to the endomembrane system, which provided a facile means to track changes in plant nuclear proteins as well (Fig. 2.9-10).

GFP:CYDV-N was unevenly distributed throughout the nucleoplasm, while the GFP:CYDV-X and GFP:CYDV-P proteins exhibited a more even distribution throughout the nucleoplasm. In the case of the P protein, the punctate nuclear localization pattern observed when localized in virus-free cells was absent in virus-infected cells. The Y protein showed accumulation of the cell periphery, as well as the nuclear envelope. The GFP: CYDV-M protein co-localized with membranes that accumulated in intranuclear spherules. Regarding its localization pattern in virus-free cells, the GFP:CYDV-G protein accumulated primarily on perinuclear membranes and the nuclear envelope.

In contrast to its cognate protein, GFP:SYDV-N was distributed evenly across the nucleoplasm in virus-infected cells. GFP:SYDV-X protein showed greater partitioning between the nucleus and cytoplasm than GFP:CYDV-X, which was primarily nuclear in the context of infected cells. GFP:SYDV-P was observed on large sub-nuclear foci in virus-infected cells, in a pattern clearly distinguishable from that produced by GFP:CYDV-P. GFP:SYDV-M localized to intranuclear membranes in virus-infected cells, while GFP:SYDV-G was found on endomembranes in presence or absence of virus.

Discussion

We have produced a PILM for the CYDV strain of PYDV. The SYDV and CYDV strains represent the closest related plant-adapted rhabdoviruses for which PILMs have been produced. Despite their close sequence relatedness, there are significant contrasts in the protein interaction and localization patterns, which provides insights at the molecular and cellular levels for the contrasting biology of these viruses.

Of particular interest is the difference in CYDV-N of the region spanning the NLS that was mapped in SYDV-N protein (QKRANEEAPPAAQKR) (Anderson *et al.*, 2012). While the 10aa spacer is maintained between the paired KR residues essential for nuclear localization, the sequence of the spacer is not conserved, nor are the KR residues flanked by glutamines. Functional mapping will have to verify the KRTAEDATTQQTKR sequence in CYDV-N as being a bona fide NLS. If this is indeed the case, then the charge and sequence variation may explain the marked difference in localization patterns of the PYDV-N proteins, particularly as variation in NLS sequence greatly impacts affinity and isoform selectivity for nuclear import receptors including importin- α , which is the presumed karyopherin for SYDV-N (Anderson *et al.*, 2012; Kosugi *et al.*, 2009). If this is not the NLS region, then CYDV-N must utilize an entirely different signal to facilitate targeting of this protein to the nucleus. However, given the 71% sequence identity (83% similarity) of the CYDV- and SYDV-N proteins, there is no readily identifiable region that might encode an alternative NLS in CYDV-N.

In addition to differences in nuclear localization patterns per se, an intriguing result is the observation that CYDV-Y is targeted to the nuclear envelope, while its SYDV cognate is not. This difference is observed from virus infected cell as well. The primary structure of these proteins is 74% identical and 88% similar, with the dissimilar residues dispersed over the entire length of the proteins. As such, there is no obvious region in CYDV-Y that readily accounts for targeting of this protein to the nuclear envelope. However, differential interaction with a nuclear transport receptor

may account for the differential localization pattern (Boni *et al.*, 2015). Therefore, the nuclear envelope-targeting region will have to be mapped physically (Anderson *et al.*, 2012). The difference in partitioning of the Y proteins is maintained in the context of infection, with the SYDV-Y accumulating in the nucleus whereas the CYDV-Y does not. Assuming that the Y protein mediated cell-to-cell transport of PYDV strains, then a differential in the efficiency of transport of PYDV strains, then a differential in the efficiency of transport may, in part, account for the differential symptom severity of these viruses in plants.

The effect of any single difference in the localization and interactions of PYDV proteins of the general interaction of this virus with its plant host cannot be determined from the present study. Collectively, it stands to reason that a ‘summation’ of these differences has resulted in vector and plant selectivity. More broadly, it is interesting to note that every plant-adapted rhabdovirus has a unique PILM (Min *et al.*, 2010; Ramalho *et al.*, 2014; Martin *et al.*, 2012, Bandyopadhyay *et al.*, 2010). All of these PILMs were constructed using BiFC assay in leaf epidermal cells of *N. benthamiana*. Given the uniformity of assay conditions, the differential interactions should be a reflection of the intrinsic properties of each viral protein. BiFC is known to report only very stable interactions, and thus a lack of detecting any particular interaction, e.g. P/P for SYDV or N/N for CoRSV, does not mean that these interactions do not occur, but only that they are not stable enough to yield BiFC-positive results. Each protein-protein interaction in the BiFC, and every interaction in general, is governed by a particular dissociation constant (K_D) (Pusch *et al.*, 2011). Thus, variation in PILMs, in part, likely represents variation in K_D for each viral protein. Extrapolating from the PILMs, it is not uncommon for viral proteins to interact with at least one, and often many more, host cell proteins to interact with at least one, and often may more, host cell proteins (Nagy *et al.*, 2016, Min *et al.*, 2010; Mann *et al.*, 2016). Therefore, virus evolution, in particular adaptation to hosts and vectors, must be restricted or permitted according to the efficiency of binding of interaction domains in viral and host proteins (Koonin *et al.*, 1989; Duffy *et al.*, 2008; Cuevas *et*

al., 2015). Moreover, infection by viruses induced global changes in alternative splicing of host mRNAs (Boudreault *et al.*, 2016). This alternate splicing may alter protein-interaction domains in host factors (Scheckel *et al.*, 2015; Irimia *et al.*, 2014). Furthermore, interaction with viral proteins can cause dramatic changes in localization of host factors, which may alter their ability to associate with their normal interactors (Min *et al.*, 2010). Coupled with this is the extensive alteration of host cells, particularly nuclear structure, that is evident in CYDV- and SYDV-infected cells. In short, the protein interactome encountered by individual viral proteins is likely to be something quite different from that which exists in the absence of infection. Especially, the subcellular locations of N, P, and Y proteins of CYDV in the virus-infected cells revealed noticeably different localization patterns compared to those of SYDV that observed from SYDV-infected cells. The results revealed that SYDV-N GFP fusion signal was more focused on the central region of nucleus with higher intensity and SYDV-P GFP fusion localized multiple separated foci in nucleus. While we have not investigated their difference localization patterns in amino acid sequence level, considering the N and P proteins are major components of virus replication complex (Deng *et al.*, 2007; Luo *et al.*, 2007; Ruigrok *et al.*, 2011; Wu *et al.*, 2002 ;Yang *et al.*, 1999), each virus seems use the host plant nucleus in somewhat different way for their replication (Xu *et al.*, 2002). In our hands, SYDV is easier to purify given its higher titre in infected host compared to those of CYDV. We are assuming that the higher titre of SYDV would be directly related to the greater symptom severity of host plant by SYDV infection than CYDV infection (Ogbe *et al.*, 2003). The different N and P localization patterns of the two viruses could be the clue to explain different symptom development and severity. Systemic attempts using high-throughput protein interaction screening and revers genetic system to build the virus-host protein interaction map are needed to investigate the biological relevant between protein localization interaction pattern and *in-situ* virus life-cycle.

Taken together, we posit that virus-host cell compatibility is governed, in part, by summation of the efficiency by which viral proteins interact with each other and with host factors.

These interactions, in turn, are governed by the K_D for each interaction. By corollary, adaptation to new hosts or vectors will be governed by the existence of requisite interaction domains in host factors in new hosts, or sufficiently rapid selection of virus variants from the quasi-species cloud upon entry to a new host or vector. This hypothesis is supported by phylogenetic evidence, which demonstrates that plant-adapted species group according to their insect vector, thus it is likely that insects are the key driver of speciation for this group of viruses (Bandyopadhyay *et al.*, 2010). It is intriguing that the X protein of CYDV is more closely related to its cognate protein in EMDV than to SYDV. While there is no firm evidence for recombination between or among these viruses, the solanaceous hosts common to both may have provided such an opportunity (Parrella *et al.*, 2016). Thus, variation in PILMs is likely expected given the diverse host range that can be collectively infected by the plant-adapted rhabdoviruses for which PILMs have been generated. Furthermore, within a single-host species, e.g. *N. benthamiana*, plant-adapted rhabdovirus exhibit a wide range of pathogenicity, with some viruses expressing a recovery phenotype (SYNV) (Ghosh *et al.*, 2008), taking exceptionally long (weeks) to establish infections (PYDV) (Ghosh *et al.*, 2008), or requiring plants to be maintained at elevated temperatures in order to establish systemic infections (CoRSV) (Ramalho *et al.*, 2014).

Mechanistic investigation of the hypotheses above will require expansion of the availability of recombinant viral systems (Jackson *et al.*, 2016; Wang *et al.*, 2015) and detailed biochemical characterization of rhabdoviral protein complexes, with particular attention paid to the determination of K_{DS} for interactions contributing to PILMs, as well as a broader characterization of host factors that interact with plant rhabdoviral proteins (Min *et al.*, 2010). However, the availability of a significant number of PILMs raises intriguing questions about their underlying molecular basis, which have implications for understanding the evolutionary trajectories of these viruses.

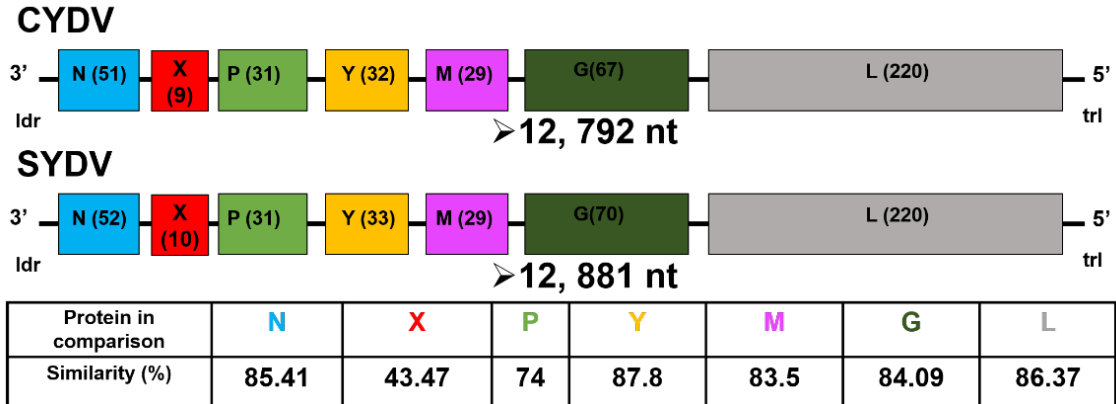


Figure 2.1. Comparison of the CYDV and SYDV genomes and proteins. The 12792 nt CYDV genome is organized into seven ORFs (open boxes) that are separated by conserved gene junctions and flanked by short leader (ldr) and trailer (trl) sequences, respectively. The predicted size of the encoded protein (in kDa) for each ORF is provided in parentheses.

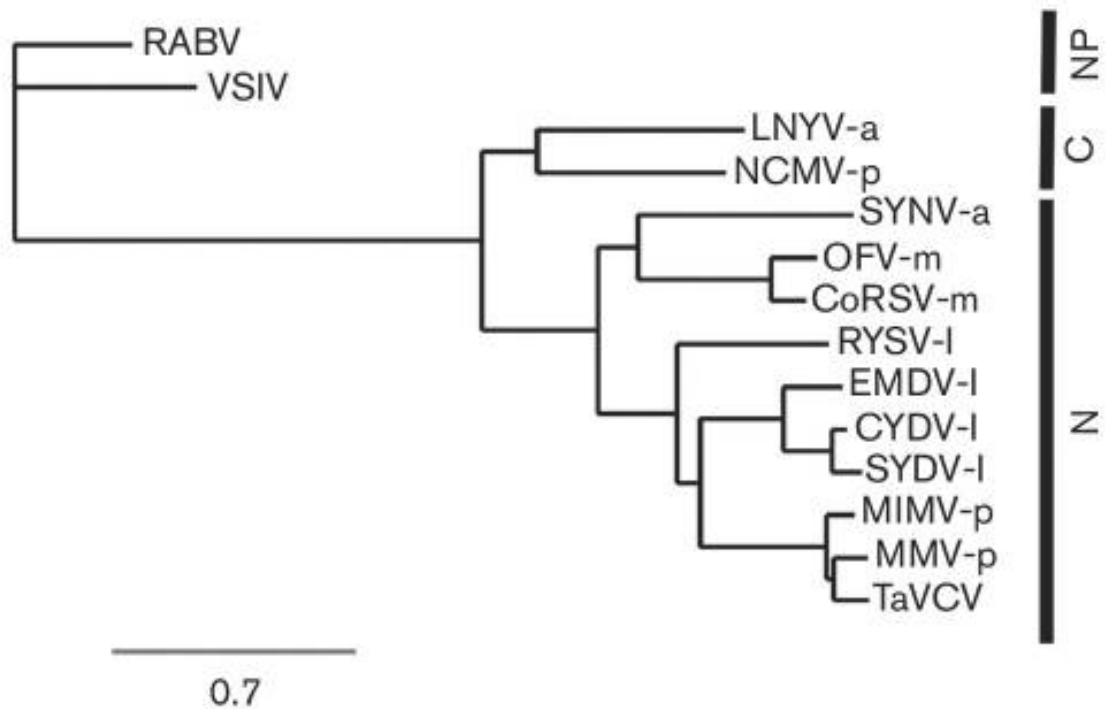


Figure 2.2. L protein derived phylogeny. Viruses infecting a variety of hosts were selected, including those that do not infect plants (NP) as well as plant-adapted species that replicate in nuclei (N) or cytoplasm (C) of infected cells. Vectors for the plant-adapted viruses are provided at the end of the virus abbreviation, namely: a, aphid; l, leafhopper; m, mite; or p, planthopper. Virus names and GenBank accession numbers are listed in Methods. CoRSV, coffee ringspot virus; MMV, *Maize mosaic virus*; TaVCV, *Taro vein chlorosis virus*; MIMV, *Maize Iranian mosaic virus*; OFV, *Orchid fleck virus*; SYDV, *Potato yellow dwarf virus-Sanguinolenta strain*; CYDV, *Potato yellow dwarf virus-Constricta strain*; RYSV, *Rice yellow stunt virus*; SYN, *Sonchus yellow net virus*; NCMV, *Northern cereal mosaic virus*; LNYV, *Lettuce necrotic yellows virus*; RABV, *Rabies virus*; VSIV, *Vesicular stomatitis virus* – Indiana serotype. All branch points had bootstrap values greater than 0.6. The scale bar indicates the number of aa changes per site.

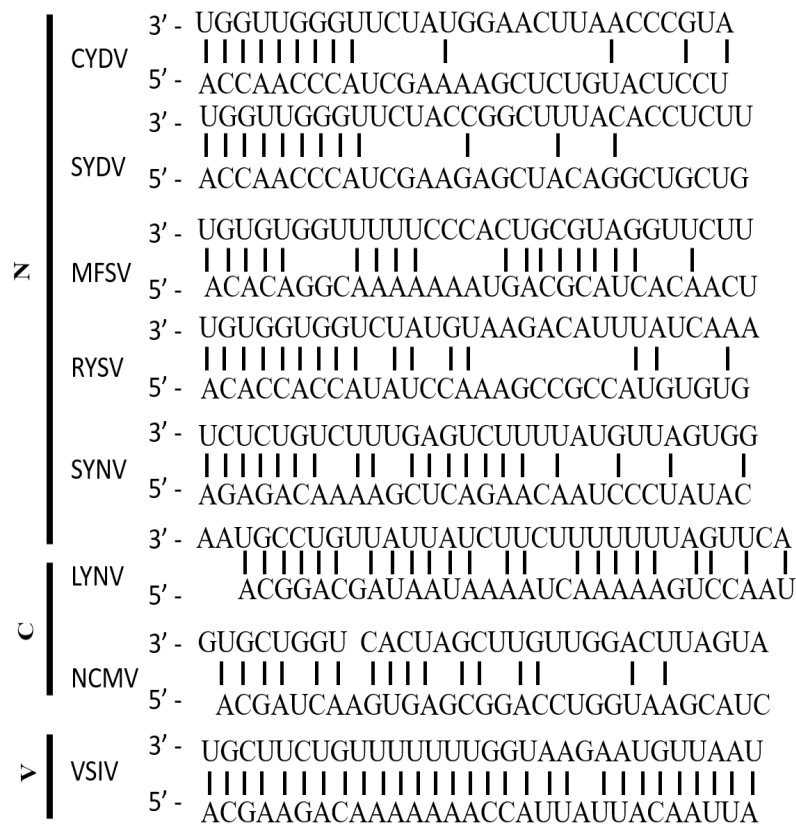


Figure 2.3. Complementarity in the leader (3') and trailer (5') regions of selected rhabdoviruses in the *Nucleorhabdovirus* (N), *Cytorhabdovirus* (C) and *Vesiculovirus* (V) genera.

(a)

| | polyadenylation signal | intergenic spacer | transcription start site |
|-----------|---------------------------|----------------------|-----------------------------|
| | 1 | 2 | 3 |
| ldr/N | AAUUUAUUUU | GGG | UUGUGU |
| N/X | GAAUUUAUUUU | GGGG | UUGUUG |
| X/P | GAAUUUAUUUU | GGG | UUGUGU |
| P/Y | GAAUUUAUUUU | GGG | UUGUUG |
| Y/M | GAAUUUAUUUU | GGG | UUGUUC |
| M/G | GAAUUUAUUUU | GGG | UUUGGU |
| G/L | GAAUUUAUUUU | GGGG | UUGAGU |
| L/Url | GAAUUGUUUU | GGG | AAUAAA |
| Consensus | AAUUUAUUUU | GGG | UUG |

(b)

| | polyadenylation signal | intergenic spacer | transcription start site | |
|---|---------------------------|----------------------|-----------------------------|-----|
| | 1 | 2 | 3 | |
| N | CYDV | UUAUUUUU | GGG | UUG |
| | PYDV | UUUAUUUU | GGG | UUG |
| | MFSV | UUUAUUUU | GUAG | UUG |
| | RYSV | AUUCUUUUU | GGG | UUG |
| | SYNV | AUUCUUUUU | GG | UUG |
| | TaVVCV | AAUUCUUUUU | GGG | UUG |
| C | LNYV | AUUCUUUUU | G(N) _n | CUU |
| | NCMV | AUUCUUUUU | GACU | CUA |
| V | VSIV | ACUUUUUUU | GU | UUG |

Figure 2.4. Comparison of the intergenic junction sequences of rhabdoviruses. (a) Sequence of each intergenic junction (IGJ) in the CYDV genomic RNA (drawn here in genomic orientation). The IGJs are divided into three regions to denote the poly-adenylation signal, intergenic spacer and transcription start site. The consensus IGJ is provided at the bottom. (b) Consensus IGJ comparisons from rhabdoviruses in the *Nucleorhabdovirus* (N), *Cytorhabdovirus* (C) or *Vesiculovirus* (V) genera. n, variable number of nucleotides.

Table 2. Features of PYDV proteins determined by predictive algorithms.

TM, transmembrane; pI, isoelectric point.

| ORF | MW (kD) | TM | PI | Predicted NLS | Putative Function | Highest scoring Virus / E-value (BLAST) |
|-----|---------|------------|------|-----------------------|--------------------|---|
| 1 | 51 | None | 7.62 | <u>KRTAEDATTQQTKR</u> | Nucleocapsid (N) | PYDV-N /0.0 |
| 2 | 8.9 | None | 3.87 | - | Unknown (X) | PYDV-X/4e-04 |
| 3 | 31 | None | 6.23 | PAKSRKL | Phosphoprotein (P) | PYDV-P/2e-103 |
| 4 | 32 | None | 6.60 | - | Movement (Y) | PYDV-Y/3e-161 |
| 5 | 29 | None | 8.85 | KRTVADPFKNLLKRKSE | Matrix protein (M) | PYDV-M/2e-131 |
| 6 | 67 | aa 575-597 | 4.56 | - | Glycoprotein (G) | PYDV-G/0.0 |
| 7 | 222 | aa 510-529 | 6.75 | KKLPVTNIHPDNLLKKR | Polymerase (L) | PYDV-L/0.0 |

§ The putative NLS of N was not predicted computationally and is instead the regions of the CYDV-N protein corresponding to the mappe3d NLS in SYDV

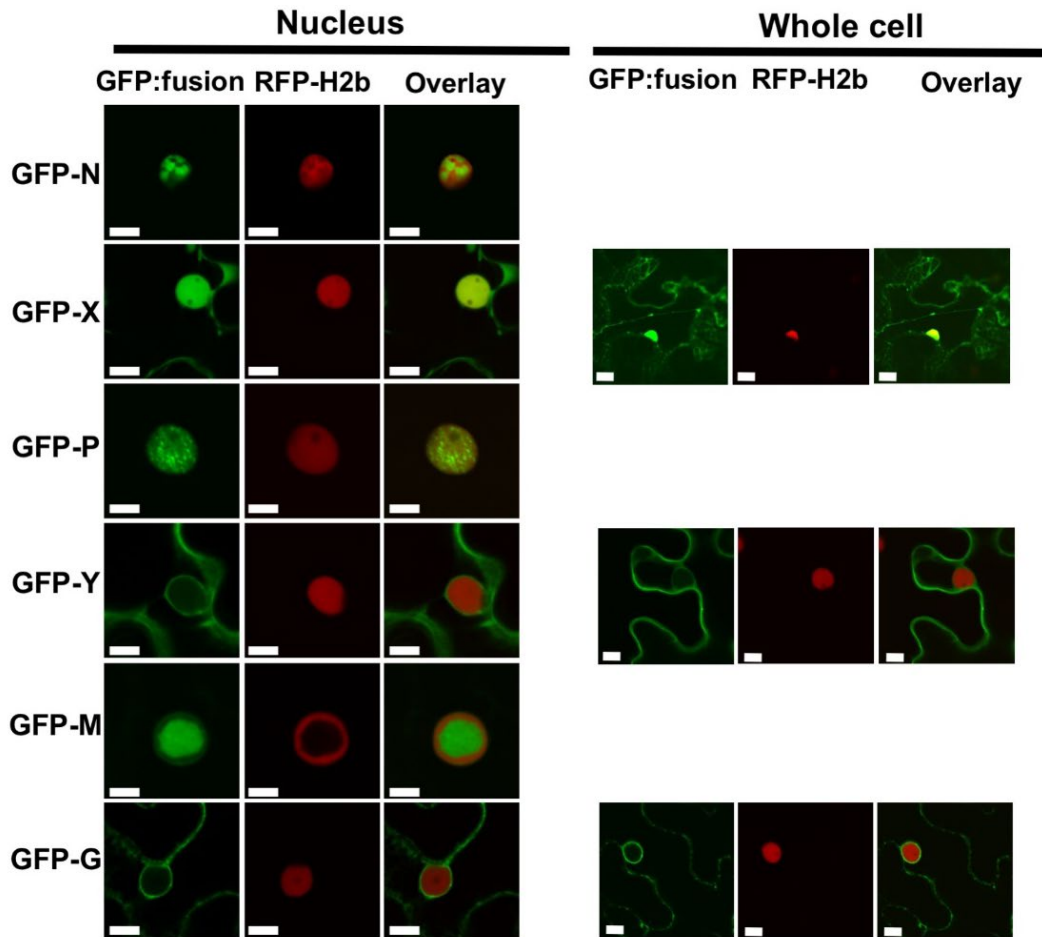


Figure 2.5. subcellular localization of CYDV proteins. CYDV proteins were expressed using agro-infiltration as amino-terminal fusions to GFP in leaf epidermal cells of *N. benthamiana* plants transgenic for RFP fused to the nuclear marker protein Histone 2B. Particular GFP fusions are listed on the left-hand side of the Figure 3 and their corresponding localization in nuclei and whole-cell views is shown to the right and far right, respectively. Whole-cell views are not shown for proteins whose localization was exclusively nuclear. Scale bar, 10 μ m.

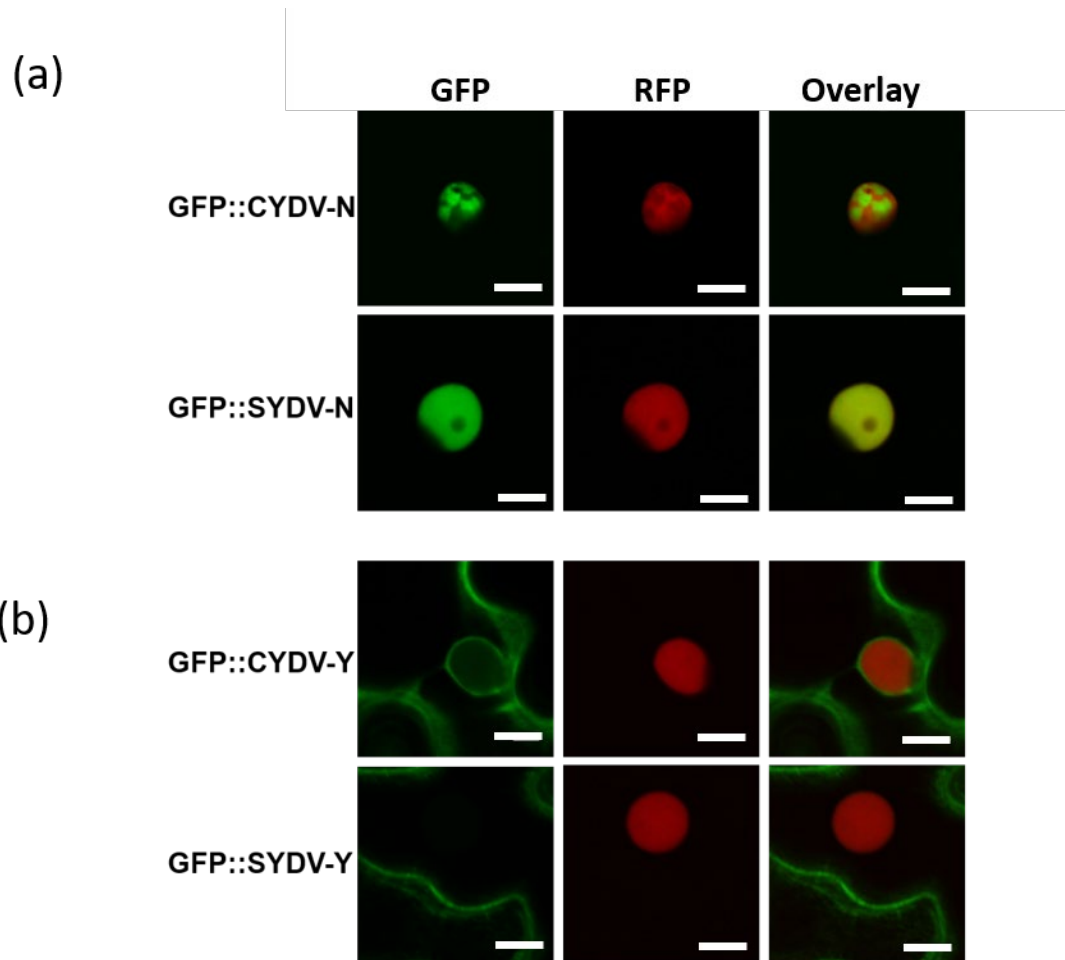
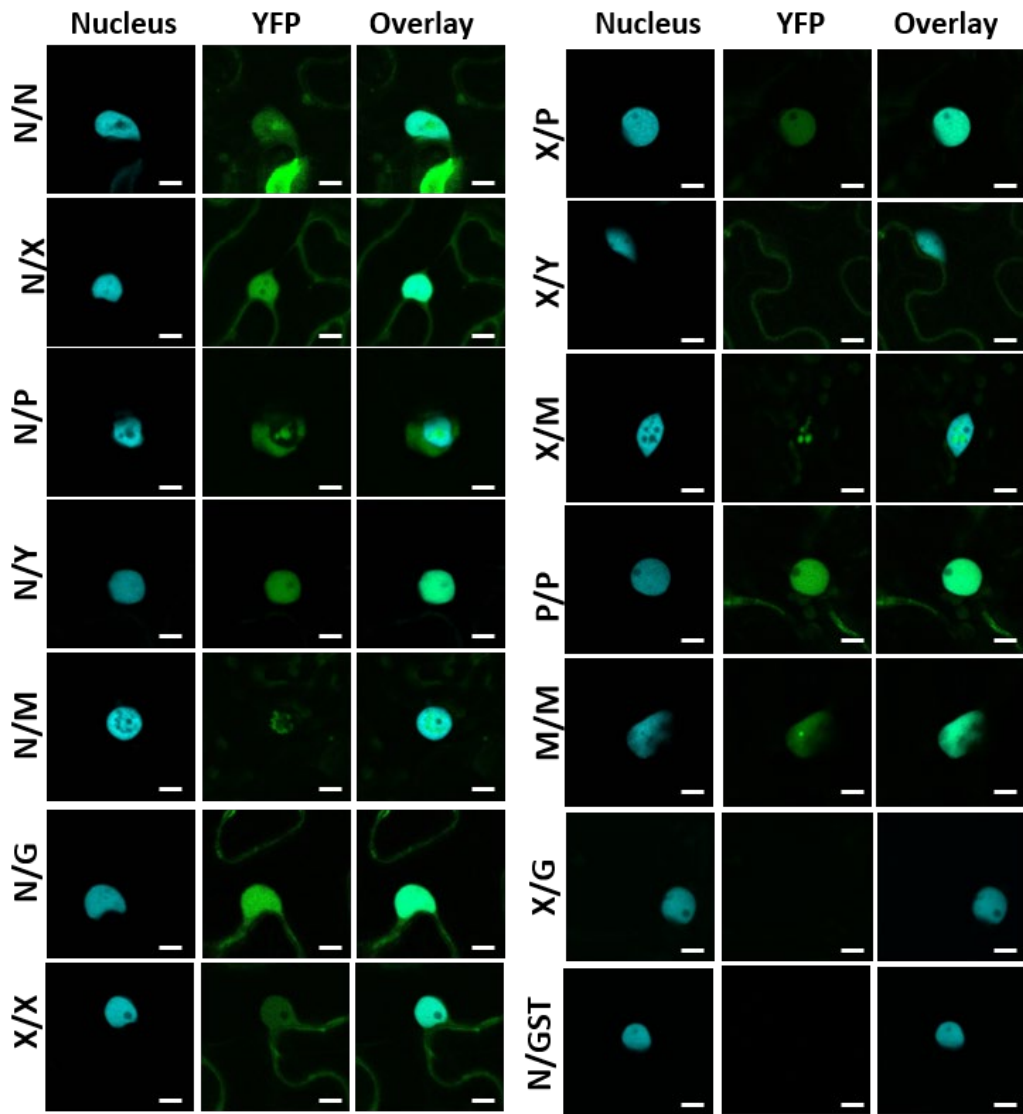


Figure 2.6. The different localization pattern of CYDV-N and -Y compared to their cognate proteins of SYDV. (a) Comparison of GFP fusion of CYDV N and SYDV N (b) Comparison of GFP fusion of CYDV Y and SYDV Y. Each protein was expressed using agro-infiltration as amino-terminal fusions to GFP in leaf epidermal cells of *N. benthamiana* plants transgenic for RFP fused to the nuclear marker protein Histone 2B. Particular GFP fusions are listed on the left-hand side of the Figure and their corresponding localization in nuclei and whole-cell views is shown to the right and far right, respectively. Whole-cell views are not shown for proteins whose localization was exclusively nuclear. Scale bar, 5 μ m.

(a)



(b)

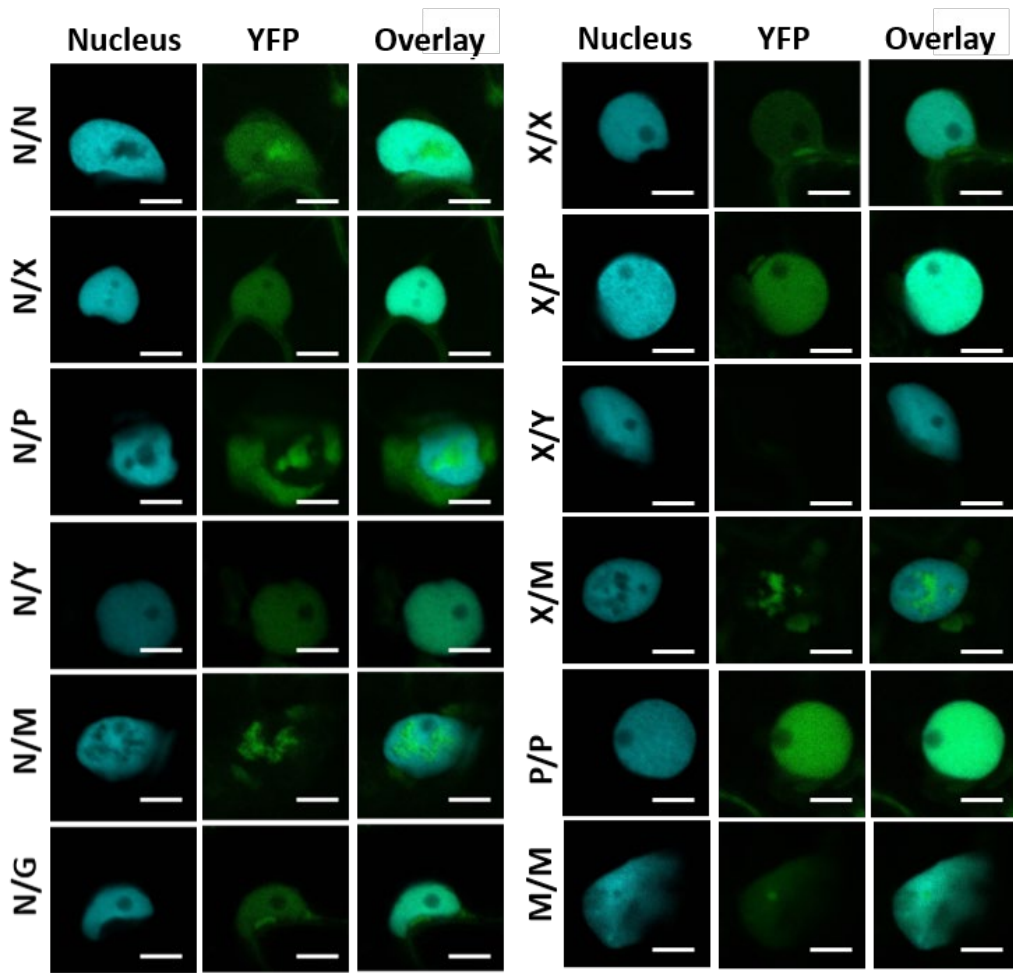


Figure 2.7. BiFC assay for all pairwise combinations for CYDV-encoded proteins, except L. The binary interactions of viral proteins were assayed in bimolecular fluorescence complementation experiments. Specific combinations are listed on the left-hand side of each column of single-plane confocal micrographs that show the location of YFP fluorescence (BiFC) relative to that of the CFP-marked nucleus (CFP). Interaction assays were conducted in leaf epidermal cells of transgenic *N. benthamiana* expressing CFP fused to the nuclear marker protein Histone 2B. The merger of the BiFC and CFP channels is also shown (Overlay). Protein fusions to each half of YFP were tested in all pairwise interactions, of which only a subset is shown here. Glutathione-S-transferase (GST) was used as a non-binding control. The majority of BiFC-negative results are not shown, save those necessary to confirm specificity of binding in the positive assays. Panel (a): Whole cell view ; panel (b): Nuclear view of positive interactions in panel (a). Scale bar, 10 μm .

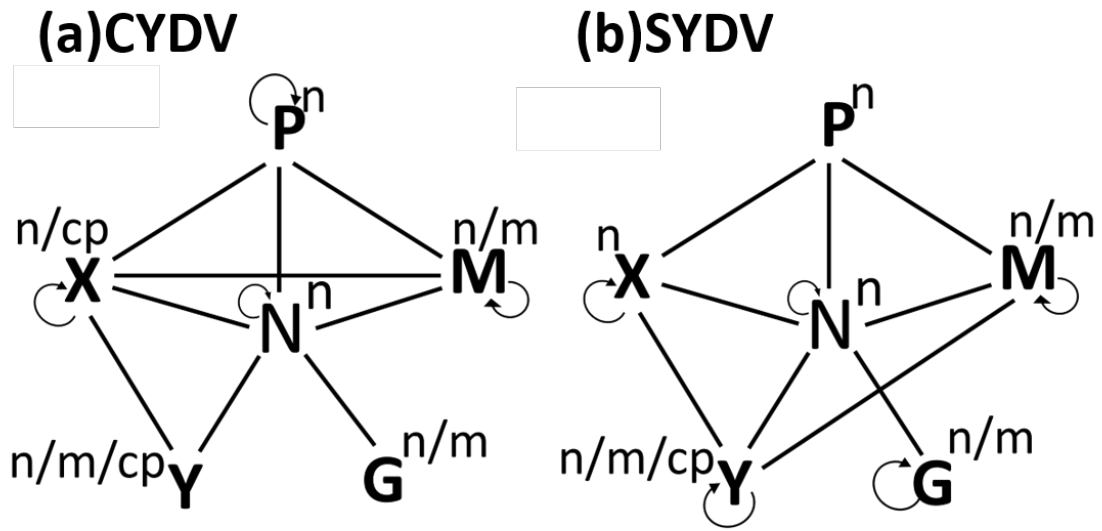


Figure 2.8. Comparison of integrated protein interaction and localization maps. (a) CYDV (b) SYDV. Self-interactions are indicated by curved lines. Lines indicate interactions between heterologous proteins. The subcellular localization of GFP-protein fusions is indicated in the superscripts: n, nucleus; n/m, nucleus/membrane; m, membrane; cp, cell periphery.

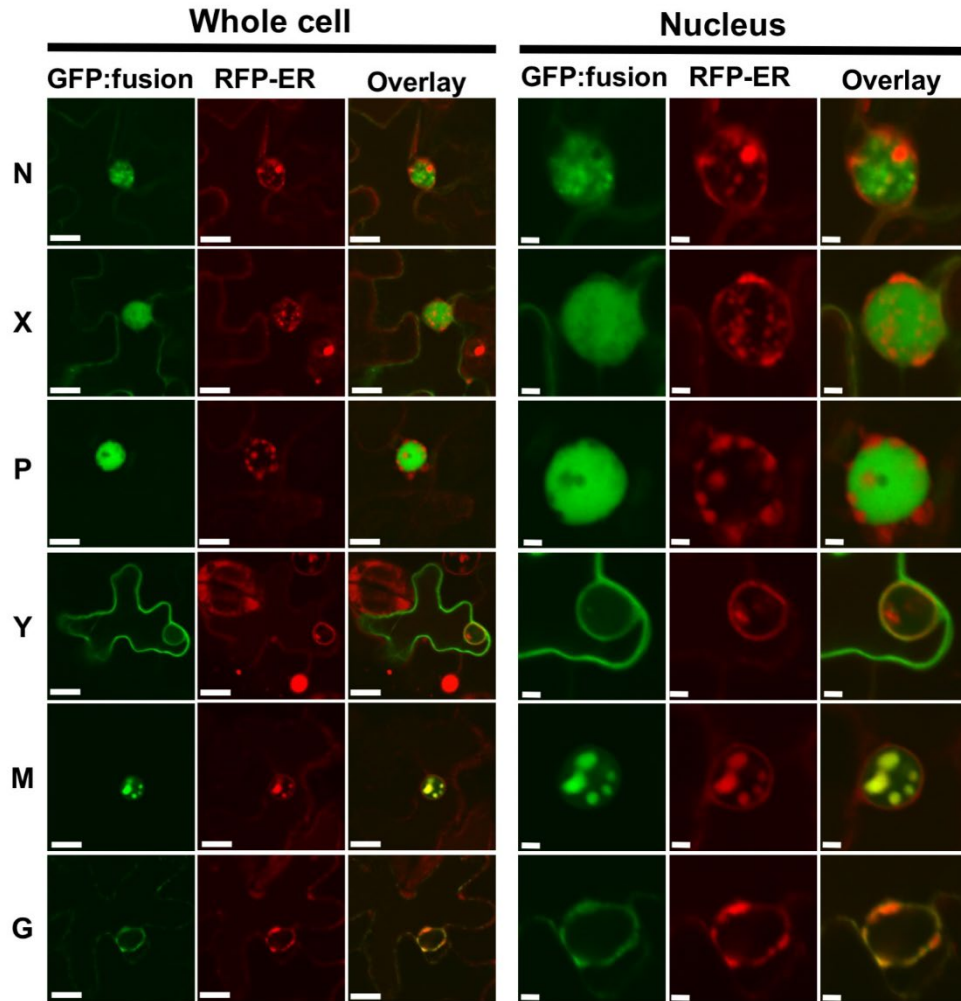


Figure 2.9. The localization pattern of CYDV-encoded proteins in the context of the virus-infected plant cell. CYDV-encoded proteins were expressed as amino-terminal fusions to GFP in CYDV-infected leaf epidermal cells of *N. benthamiana* plants transgenic for RFP targeted to endomembranes (RFP-ER). Specific CYDV proteins are listed on the left-hand side of the Figure and their corresponding localization in whole-cell or nuclear views is shown to the left and far left, respectively. Scale bars, 10 μm (whole-cell view) and 2 μm (nuclear view).

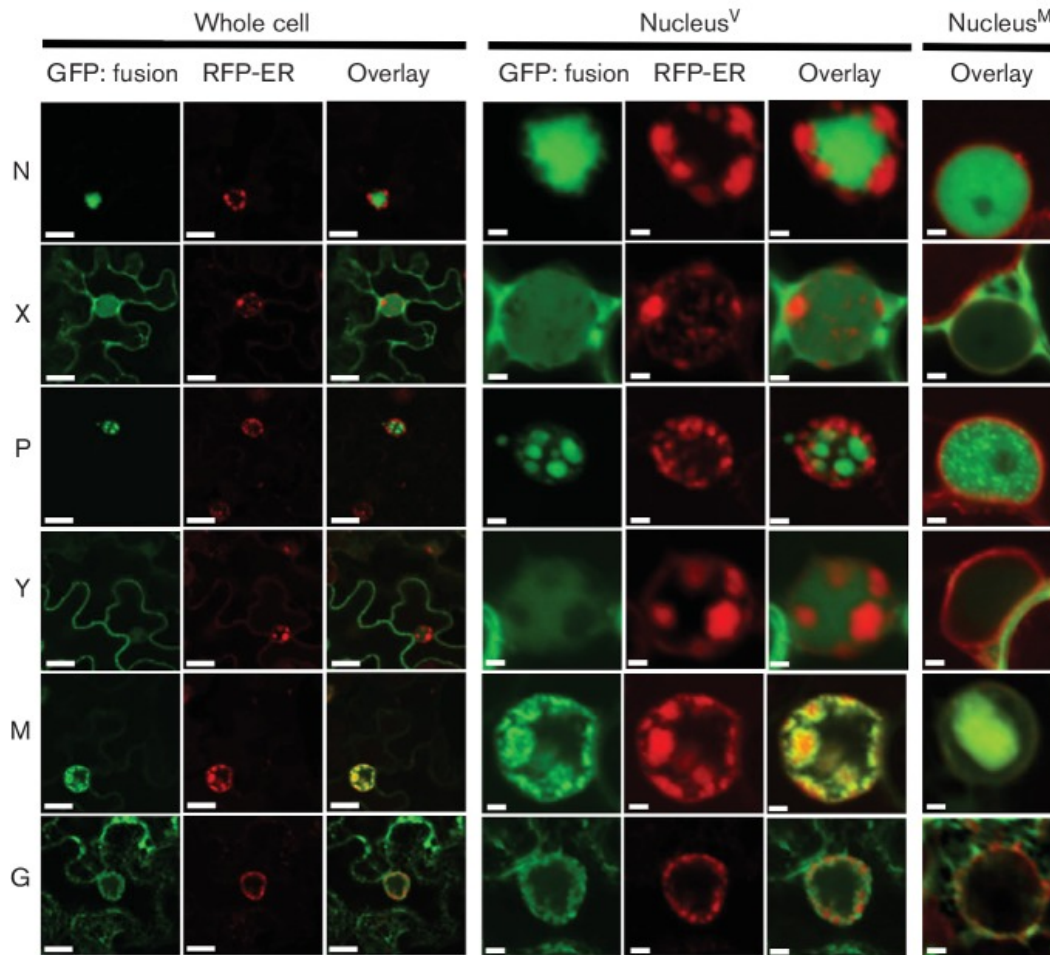


Figure 2.10. The localization pattern of SYDV-encoded proteins in the context of the virus-infected plant cell. SYDV proteins were expressed as amino-terminal fusions to GFP in SYDV-infected leaf epidermal cells of *N. benthamiana* plants transgenic for RFP targeted to endomembranes (RFP-ER). Specific SYDV proteins are listed on the left-hand side of the Figure 3 and their corresponding localization in whole cell or nuclear views is shown to the right and far right, respectively. Scale bars, 10 μm (whole-cell view) and 2 μm (nuclear view). For comparison, the overlay of SYDV protein-GFP fusions in mock-inoculated leaves is shown on the right-hand side (Images were taken by Joseph Wells in 2013).

Chapter 3

Validation of nuclear export function of the 3' terminal leucine-rich domain of PYDV matrix protein

Rhabdoviruses are members of the order mononegavirales which has a monopartite single-stranded negative-sense RNA genome (Ryu *et al.*, 2017). The members of the Rhabdoviridae family infect a wide range of hosts including vertebrates, invertebrates, and plants. (Redinbaugh *et al.*, 2005; Ryu *et al.*, 2017; Gubala *et al.*, 2011; Goldberg *et al.*, 2017). The plant-adapted rhabdoviruses are classified into four genera currently, *Varicosavirus*, *Dichoravirus*, *Nucleorhabdovirus* and *Cytorhabdovirus*, based on their sequence similarity to other rhabdoviruses (Liu *et al.*, 2018). *Nucleorhabdovirus* and *Dichoravirus* accomplish their replication, transcription, and morphogenesis in the nucleus. Otherwise, *Cytorhabdovirus* and *Varicosavirus* exclusively stay in the cytoplasm of the host cell during their infection (Redinbaugh *et al.*, 2005; Jackson *et al.*, 2005; Liu *et al.*, 2018).

Potato yellow dwarf virus (PYDV) is the type species of the genus *Nucleorhabdovirus* (Anderson *et al.*, 2012). This virus was first reported as a highly destructive pathogen of potato (*Solanum tuberosum*) in 1922 (Barrus *et al.*, 1922). This virus has contributed to the study of the virus-vector specificity and interaction, genetic variation of insect vectors, virus inoculation method for vector cell monolayer and development of density-gradient centrifugation for virus purification (Black *et al.*, 1940; Black *et al.*, 1941; Black *et al.*, 1943; Brakke *et al.*, 1951; Hsu *et al.*, 1973). The genome size is about 12 kb, and the negative-sense single-stranded genome encodes seven genes in order, N, X, P, Y, M, G and L (Bandyopadhyay *et al.*, 2010).

Given their limited coding capacity, the proteins of RNA viruses often have functions beyond their roles in structure or replication (Weber *et al.*, 2015). As such, plant virus replicase proteins have been shown to be suppressors of RNA silencing (Qu *et al.*, 2005) or have been shown to interact with myriad cellular factors (Denison *et al.*, 2008; Nagy *et al.*, 2016). In the case of

rhabdoviruses, their matrix proteins have been shown to target nuclear pore complexes, where they inhibit the export of host cell mRNAs (Petersen *et al.*, 2000). Plant-adapted rhabdoviruses such as PYDV and Sonchus yellow net virus (SYNV) have been shown to dramatically alter nuclear architecture in order to establish sites of replication and assembly (Ghosh *et al.*, 2008; Goodin *et al.*, 2007). In an earlier study, we reported that the M protein was capable of inducing intranuclear accumulation of the inner nuclear membrane in *Nicotiana benthamiana* (Bandyopadhyay *et al.*, 2010). This activity is likely required for establishing sites of virion assembly (Sun *et al.*, 2018), once the matrix protein associates with viral nucleocapsids, which then accumulate in perinuclear spaces (Jackson *et al.*, 2005; Mann *et al.*, 2014).

The functional domain assay using alanine scanning mutagenesis performed by Anderson (2014) revealed that K²²⁵ and R²²⁶ of SYDV-M are the functional domains for the nuclear localization *in-vivo*. At the time, lack of interaction between SYDV-M^{KK213AA} and NbImp- α 1 supported the possibility of that K²¹³ and K²¹⁴ motifs of M affect the affinity of the M-NLS for NbImp- α 1 (Anderson *et al.*, 2014; Anderson *et al.*, 2018). Interestingly, the aa 211-253 fragments of M^{wt} and M mutants were exclusively localized on the cytoplasmic space of plant cell, although the fragments still contained the functional NLS domain (Anderson *et al.*, 2014; Anderson *et al.*, 2018). The possible M-NES were predicted using NetNES on the carboxy-terminus of the M protein, at 244-LPSMLKML-251 which containing leucine-rich motif (Anderson *et al.*, 2018). This computational prediction was supported by the result of the BiFC interaction assays of full-length M protein and its carboxy-terminal fragment (aa 211-253) with the nuclear export receptor XPO1 (Anderson *et al.*, 2018). One of noticeable observation was the different spatial interaction patterns of XPO1 with full-length and aa 211-253 fragment of SYDV-M, inside and outside nucleus respectively (Anderson *et al.*, 2014).

In this study, The NES effect on the nuclear localization of M was tested using the short aa 211-243 fragments of M^{wt}, M^{LL223AA}, and M^{KR225AA} which do not contain the predicted NES domain.

The subcellular localization patterns of the GFP fusions of M^{wt} (aa 211-243), M^{LL2223AA} (aa 211-243), and M^{KR225AA} (aa 211-243) were compared to those of GFP fusion of M^{wt} (aa 211-253), M^{LL2223AA} (aa 211-253), and M^{KR225AA} (aa 211-253) to define the effect of NLS and NES on the nuclear localization of them. This research shows the absence of the NES on the C-terminal directs the GFP signal of the short fragments to the nucleus.

In previous research, we have shown that M/N interaction occurs in the nucleus and M/Y interaction results in intranuclear accumulation of Y which is exclusively localize to the periphery of cells in a self-interaction (Bandyopadhyay *et al.*, 2010). Also, we have shown that M/G interaction results in the relocation of M to cytoplasmic membranes. (Bandyopadhyay *et al.*, 2010).

Based on these data, this research suggests the ‘catch and release model’ for SYDV-M that explaining a role of the matrix protein in the inter- and intra- cellular movement of potato yellow dwarf virus. In this model, a portion of M proteins in nucleus ‘catch’ the nucleocapsid complex via N-M interaction in nucleus. M interacts with G and Y proteins in the nucleus. It seems M/G interaction promotes the expose of NES in SYDV-M to the exportin. The M/exportin interaction mediates the export of the nucleocapsid complex of the virus. And Y proteins of the complex deliver the complex to the plasmodesmata to ‘release’ the nucleocapsid complex to the neighbor cells for following cell-to-cell movement of the virus.

Methods

Plant materials and virus maintenance.

All plants, including transgenic autofluorescence marker lines (AFP fused histone 2B, a nuclear marker; AFP-HDEL, endomembrane marker), were maintained in the greenhouse under controlled conditions. *Sanguinolenta* strain of *Potato yellow dwarf virus* was maintained by continuous mechanical inoculation in *Nicotiana benthamiana* and *Nicotiana rustica* in isolation cage (Martin *et al.*, 2009).

Isolation of total RNA, RT-PCR

Total RNA was extracted from virus-infected and virus-free plant tissues using the Qiagen RNeasy Plant Minikit (Qiagen). The first strand cDNA synthesis and PCRs were carried out using Superscript reverse transcriptase IV (Thermo Fisher Scientific) and SeqAmp™ high-fidelity DNA polymerase (Takara), respectively. All of the primers designed in this research was made using SYDV sequence deposited in NCBI with GenBank accession no, NC_016136.

Computational prediction of the export signal using expasy server

To predict nuclear export signal on the primary structure of SYDV M protein *in silico*, we used NET-NEX algorithm which is provided from expasy proteomic server (la Cour *et al.*, 2004).

Site-directed mutagenesis.

Site-directed mutagenesis was performed using the Q5 site-directed mutagenesis kit (NEB) following the protocol provided by the manufacturer. Sequence validated full-length SYDV M cloned into gateway cloning donor vector pDONR221 was used as a template for the mutagenesis. Mutagenized clones were sequenced to validate the presence of the planned mutation (Anderson *et al.*, 2014). The carboxy-terminal (aa 211- 243) fragments of wt and mutant SYDV M generated by PCR targeting that specific region and cloned into pDONR 221 (Invitrogen).

Protein expression in plant cells

Expression of translational GFP fusion protein in plant cells for protein localization assay was performed using pSITE-2CA (GFP-fusion) vector (Chakrabarty, 2007). Recombinant vectors were transformed into *Agrobacterium tumefaciens* strain LBA 4404 (Anderson *et al.*, 2014; Ramalho *et al.*, 2014). The grown agrobacteria cells were suspended in infiltration buffer (0.1M MgCl₂, 0.1M MES, Acetosyringone) to a density of OD 0.6 (Martin *et al.*, 2012). Agroinfiltration for expression of protein fusions into *Nicotiana benthamiana* was performed using a syringe to the abaxial leaves. About 1 cm² leaf was taken to examine each expression construct. Sampling performed from a minimum of three leaves, from a minimum of three plants (Goodin *et al.*, 2002).

Laser scanning confocal microscopy

Olympus FV1000 laser-scanning confocal microscope was used to take all microscopic. The dual color image of micrograph was acquired using sequential scanning mode to avoid interruption between the overlapped wavelength of GFP and RFP laser, as described in previous research (Goodin *et al.*, 2007).

Results

Deletion of 3' terminal 10 amino acids containing leucine-rich residues from aa211-253 fragments of SYDV-M^{wt}, -M^{LL223AA}, M^{KR225AA} directed the GFP signal into nucleus

The 10 amino acids spanning aa 244-253 which include putative NES domain were deleted from the carboxy-terminal fragments (aa 211-253) of SYDV-M^{wt}, -M^{LL223AA}, and, -M^{KR225AA} to explain the steady cytoplasmic-localization of their GFP fusions (Anderson *et al.*, 2018), although the carboxy-terminal fragments have functional NLS at the 225KR226 that confirmed using alanine-scanning mutagenesis, yeast-based nuclear import assay, and BiFC assay using NbImp- α 1 (Anderson *et al.*, 2018). Generally, natural karyophilic domains of nuclear proteins preserve their ability to direct nuclear localization of heterologous protein which is fused to the domain (Weninger *et al.*, 2015, Cressman *et al.*, 2001). We postulated that this discrepancy came from the nuclear export of the GFP fusion of the M^{wt} (aa 211-253) by the NES signal located on aa 244-251 (Anderson *et al.*, 2018). We amplified the sequence region that corresponding from the 211th to 243th amino acids of SYDV-M^{wt}, -M^{LL223AA}, and -M^{KR225AA}, hereafter namely, SYDV-M^{wt} (aa 211-243), -M^{LL223AA} (aa 211-243), and -M^{KR225AA} (aa 211-243), respectively.

The resulted shorter fragments (aa 211-243) GFP-fusions of the carboxy-terminal fragments directed the GFP signal into nuclei (Fig.3.1). The M^{wt} (aa 211-243) directed GFP to the nucleus, but the fusion also appeared to accumulate in perinuclear membranes [Fig.3.1(a-c)]. Otherwise, M^{LL223AA} (aa 211-243) fully localized GFP to the nucleus and did not show any nuclear

envelope association [Fig.3.1(d-f)]. Localization of the GFP fusion of M^{KR225AA} (aa 211-243) was indistinguishable from GFP alone, despite the fragment did not have functional NLS. These observations support the leucine-rich domain of the carboxy-terminal have function for regulation of nuclear export of SYDV-M protein in the cytoplasmic shuttling of the protein.

Discussion

The replication and maturation of nucleorhabdoviruses occur in the nuclei of the infected host cell (Bandyopadhyay *et al.*, 2010; Dietzgen *et al.*, 2015; Ghosh *et al.*, 2008; Goodin *et al.*, 2001; Lamprecht *et al.*, 2009). The viruses form viroplasm in nucleus which is enriched in the viral replicase complex and assembly machinery (Martins *et al.*, 1998; Deng *et al.*, 2007; Kondo *et al.*, 2013; Sen *et al.*, 2007). The rhabdovirus matrix proteins condense the ribonucleocapsid and mediate virus budding in association with G proteins (Chen *et al.*, 2008; Harty *et al.*, 1999; Jayakar *et al.*, 2004). While the detailed mechanisms of these processes are not yet determined, the fundamental requirements for their nucleotropic life cycle include the nucleocytoplasmic shuttling of the virus proteins required for replication and morphogenesis (Alber *et al.*, 2007; Alves *et al.*, 2008; Anderson *et al.*, 2012; Anderson *et al.*, 2014). The nuclear transport of viral proteins is mediated by the interaction of the protein functional domains with nuclear transport receptors (Alves *et al.*, 2008; Fornerod *et al.*, 1997; Goldfarb *et al.*, 2004; Sanderfoot *et al.*, 1996). Therefore, mapping of the functional domains for nuclear transport in a viral protein is essential to understand the biology of nucleorhabdoviruses.

In this research, deletion of 10 amino acids domain, 244-LPSMLKMLSP-253 which contains leucine (underlined) phasing common in NESs from SYDV-M^{wt} (aa 211-253), -M^{LL223AA} (aa 211-253), and -M^{KR225AA} (aa 211-253) directed the localization of their GFP fusion to the nucleus. These observations provide more reliable evidence of the nuclear export function of the domain that predicted from the BiFC assay using AtXPO1 (Arabidopsis thaliana nuclear exportin-1) and the NetNES algorithm. The M^{LL233AA} (aa 211-243) fully localized the GFP fusion signal to

the nucleus without the perinuclear membrane association which is observed from the aa 211-243 fragment of wild-type. This result supports the nuclear membrane association of the di-leucine residues at aa 223-224 which were previously shown that the substitution of these two residues to alanine inhibits the intranuclear membrane accumulating by GFP fusion of full-length SYDV-M (Anderson *et al.*, 2014). The subcellular localization pattern of the NLS mutant fragment, M^{KR225AA} (aa 211-243) was indistinguishable from GFP alone. The nuclear localization of this short GFP-fusion fragment likely comes from the protein size, 36.2 kDa, which is much smaller than the maximal size of protein for free-diffusion through nuclear pore complex, 60kDa (Wang *et al.*, 2007). The solitary and dominant effect of 225KR226 residues for nuclear import was previously tested using yeast-based nuclear import assay, BiFC assay using NbImp- α , and alanine-scanning mutagenesis. Therefore, we do not believe the short carboxy-terminal fragment of SYDV-M NLS mutant does have any additional NLS in its sequence and assume that the GFP signal in nucleus was derived by free-diffusion of the GFP fusion protein.

The nuclear export function of 244-LPSMLKMLSP-253 domain of SYDV-M is also supported by the BiFC interaction assays of full-length M protein or its carboxy-terminal fragment (aa 211-253) with nuclear export receptor, XPO1, which were conducted in our previous research (Anderson *et al.*, 2018). In the assay, the full-length SYDV-M interacted in the nucleus otherwise the aa 211-253 SYDV-M fragment interacted with the nuclear export receptor outside of nucleus. Taken together, these results strongly support the hypothesis that the 244-LPSMLKML-251 on the carboxy-terminal region is a bona fide nuclear export signal, along with the nuclear localization of the carboxy-terminal of M fragments lacking the predicted NES domain, SYDV-M (aa 211-243).

The comprehensive functional domains described above are mapped on the corresponding amino acid sequence of SYDV and CYDV in Fig. 4.2. The sequence conservation in the functional residues of SYDV and CYDV suggests that these two regions are critical in the biology of PYDV considering the role of those domains in the nucleocytoplasmic shuttling. If these functional

domains are active during virus infection, it is possible that M may mediate the cell-to-cell movement of PYDV by exporting the nucleocapsids to the cell periphery. According to our previous research, SYDV-M protein interacts with N, G, and Y in the PILM which was built in previous research (Bandyopadhyay *et al.*, 2010; Anderson *et al.*, 2018). The research showed that N and M exclusively localized in nucleus, while Y localized in cytoplasmic space. Also, G localized to endomembrane (Bandyopadhyay *et al.*, 2010). M/N and M/Y interactions occurred in nucleus (Anderson *et al.*, 2018). M/G interaction resulted in the re-localization of M to cytoplasmic membrane (Bandyopadhyay *et al.*, 2010). It is not clear how SYDV-G protein allows the NES domain of M protein expose to the export receptor yet. However, considering protein-protein interaction leads to conformational change of the participants and G protein does not have any predicted NES, the G interaction with M may mediates the M-XPO1 interaction to induce nuclear export of the partially condensed nucleocapsid complex. To refine the association of G/M interaction in nuclear export of SYDV-M, BiFC assay of G and M in the leptomycin-B (exportin inhibitor) treated plant tissue is required. SYDV-Y protein is putative movement protein which has high similarity to the SYN-Sc4 protein in amino acid sequence (Bandyopadhyay *et al.*, 2010). SYDV-N proteins form the ribonucleoprotein complex via encapsidating the genome RNA. Min *et al.*, (2010) suggested that partially condensed SYN nucleocapsid complex by its M is presumably the mobile form of the virus for cell-to-cell movement. According to Min's suggested model (2010), the SYN nucleocapsids are exported from nucleus to cytoplasmic space in the association with the host factors Ni67 and Mi7 which have functional NLS and predicted NES (Min *et al.*, 2010).

If the NLS and NES domains are relevant in the context of virus infections, the PYDV-M may assist cell-to-cell movement of PYDV nucleocapsids by exporting nucleocapsids to the cytoplasmic space which requires the interaction of M with N, G, and Y (Bandyopadhyay *et al.*, 2010). The role of M in the virus cell-to-cell movement can be explained using 'catch and release' model (Fig. 4. 3) whereby a subpopulation of M binds to N associated with the nucleocapsids to

mediate their nuclear export. Unmasking NES domain of M by M-G interaction may be required to initiate the interaction of M with exportin to export the M-nucleocapsid complex . Interaction of these same M of nucleocapsid complex to Y proteins at the cell cytoplasmic space may 'release' the nucleocapsids at, or in the vicinity of, plasmodesmata. To support this model more firmly, more evidence that proving Y association with plasmodesmata proteins and kinesin superfamily proteins, and mapping of host proteins that interact with nucleocapsid components are needed. According to Anderson's report (2018), SYDV-M uses same the sites to interact with N and Y. This suggests that competition for these sites by N and Y may finely modulate the cell-to-cell movement function of M.

We have not investigated the conformational change of SYDV-M masking or exposing its NLS or NES situationally. Furthermore, the NES domain was not defined at the amino acid level in this study. Establishment of reverse genetic system for PYDV will provide more clear answers for these demands to understand the multiple pathways of nucleocytoplasmic shuttling of viral proteins and nucleocapsid complexes.

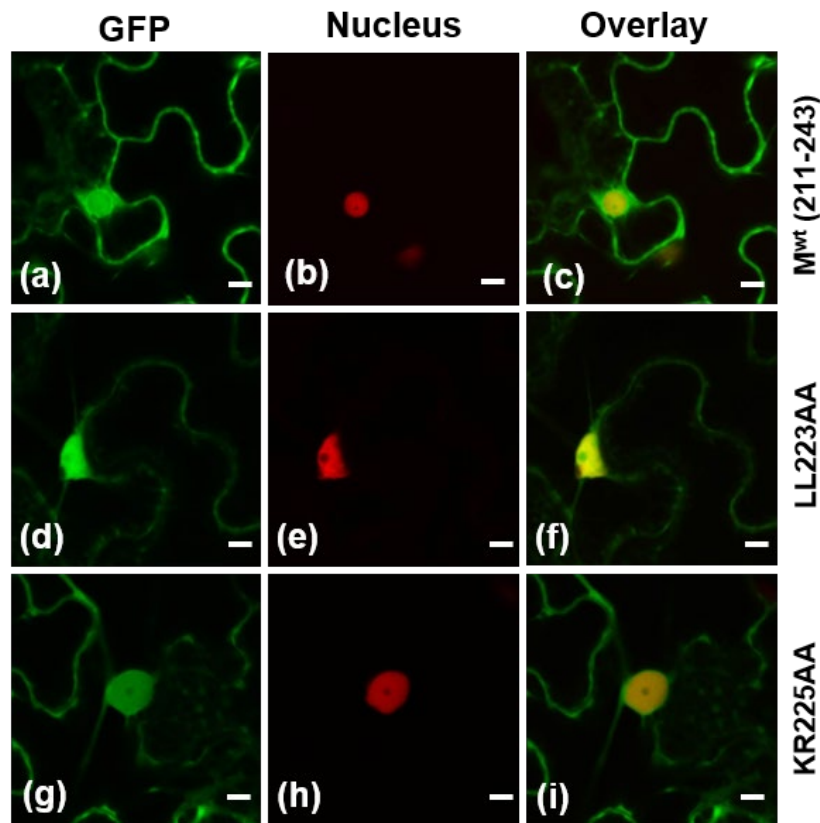


Figure 3.1. Confocal micrograph of the cellular localization of GFP tagged fragments of SYDV $M^{wt}(aa\ 211-243)$, $M^{LL223AA}(aa\ 211-243)$, and $M^{KR225AA}(aa\ 211-243)$. (a-c) confocal micrographs showing GFP fluorescence (a), RFP fluorescence (b), and overlay (c) of a and b, of the aa211-243 fragment from the wild-type M protein. (d-f) Confocal micrographs showing GFP fluorescence (d), RFP fluorescence (e), and overlay (f) of (d) and (e), of the aa211-243 fragment from M protein containing the LL223AA mutation. (g-i) Confocal micrographs showing GFP fluorescence (g), RFP fluorescence (h), and overlay (i) of (g) and (i), of the aa211-243 fragment from M protein containing the KR225AA mutation, which presents a similar localization pattern to GFP alone (data not shown). Similar results were obtained with fragments of M spanning residues 211–229 (data not shown). Scale bar, 10 μ m

Membranes
Import (Export)

```

SYDV 211 ELKKTVSDPLKNLLKRKSDTTIPTKTDGSKRAFLPSMLKMLSP 253
Cons.   ELK+TV+DP KNLLKRKS+ + PTK G KRA LPSMLKMLSP
CYDV 211 ELKR TVADPFKNLLKRKSEVSEPTKDAGGKRALLPSMLKMLSP 253

```

Figure 3.2. Functional domain map of amino acids 211–253 residue of the M protein of SYDV and CYDV. The amino acid domains highlighted in blue interacted with nuclear import receptor importin- α (Anderson *et al.*, 2018). The underlined KR, the second residue, showed the most profound effect on nuclear localization in the GFP fusion expression in plant (Anderson *et al.*, 2018). The di-leucine, LL in red, mediates the ability of M to be associated nuclear inner-nuclear membranes. The predicted nuclear export signal is marked in parentheses.

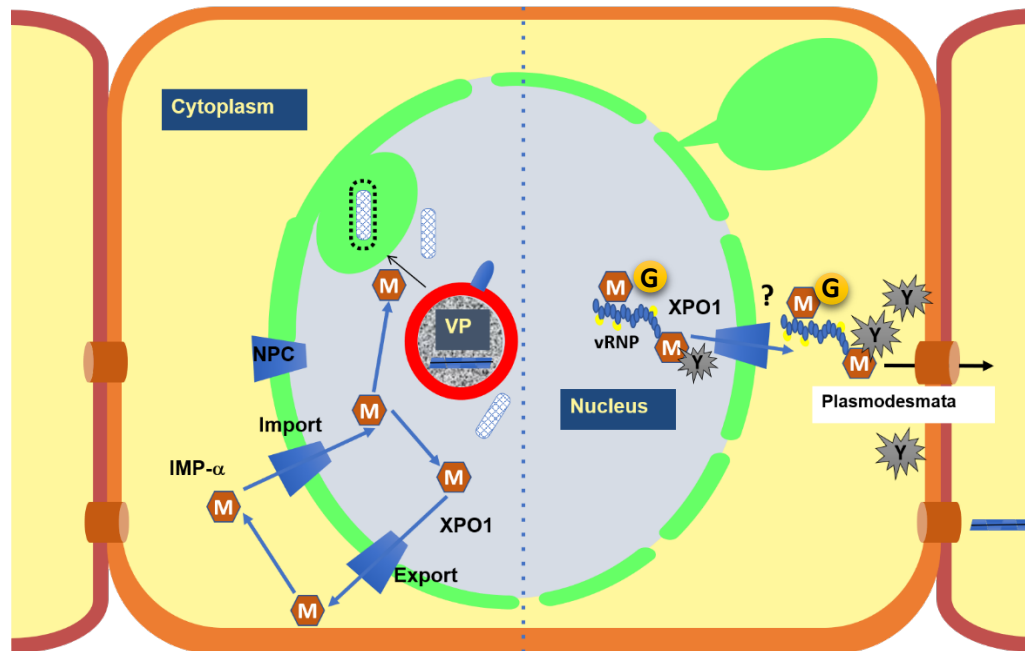


Figure 3.3. “Catch and release” model for SYDV-M. The interaction of M with N, Y, G, NbIMP- α , and XPO1 (Bandyopadhyay et al 2010; Anderson et al., 2018) and direction of GFP of short C-terminal fragments lacking the expected NES domain into nucleus suggest a possible role of PYDV-M protein in the inter- and intra- cellular trafficking of nucleocapsid complex of the virus. The interaction of the M ‘catching’ N of the viral nucleocapsids may result in XPOI-mediated nuclear export in the association with G. The M/Y interaction in the cell periphery region may ‘release’ the nucleocapsid at, or in the vicinity of, plasmodesmata to facilitate cell-to-cell movement of nucleocapsids of PYDV.

Chapter 4

Future studies

Attempt to establish the reverse genetic system for plant-adapted negative-strand RNA viruses.

Negative-sense single-stranded RNA viruses (NSRVs) consist of two orders, *Mononegavirales* and *Bunyavirales*, and three unassigned families, *Arenaviridae*, *Aspiviridae*, and *Orthomyxoviridae*, and an additional unassigned genera Deltavirus (Cann *et al.*, 2011). The viruses include many devastating pathogens such as rabies virus, ebola virus, influenza virus, and hepatitis delta virus, and so on (Conzelmann *et al.*, 1998; Beeching *et al.*, 2014; Strassburg *et al.*, 1986; Einer-Jensen *et al.*, 2004). Reverse genetics has been particularly useful to study these viruses because of the capability to rescue recombinant viruses from cDNA. The genetically manipulated viruses have been used widely to study their biologies including virus-host interactions, virus-vector specificity, and pathogenesis-related factor (Albariño *et al.*, 2011; Atieh *et al.*, 2018; Collins *et al.*, 2013; NeuMann *et al.*, 2002; Nolden *et al.*, 2017; Pekosz *et al.*, 1999; Pleschka *et al.*, 1996; Tierney *et al.*, 2005; Yun *et al.*, 2003). In reverse genetics for NSRVs, the following conditions must be met for the successful recovery of the infectious virus from cDNA: (1) The viral genome must be encapsidated entirely by nucleocapsid proteins. (2) The encapsidation process requires a precise terminal sequence of 5' and 3' ends of the viral genome. (3) The viral RNA-dependent RNA polymerase (P-L complex) is essential for transcription of viral genome and mRNA (4) the encapsidated genome and polymerase complex should produce ribonucleoprotein (RNP) complex in the susceptible cell (Fig. 4.1) (Pekosz *et al.*, 1999; Jackson *et al.*, 2016; Ganesan *et al.*, 2013; Nolden *et al.*, 2017).

While rescue of an animal-infecting negative-strand RNA virus (influenza virus) was achieved for the first time in 1989 (Palese *et al.*, 1989), the successful applications of the reverse

genetic system for plant-adapted NSRVs was delayed until a mini-replicon system for *Sonchus yellow net virus* was established (Ganesan *et al.*, 2013). Two years after that, the full-length infectious SYNV was rescued from cDNA through an *Agrobacterium*-mediated DNA transfer system (Wang *et al.*, 2015). In the system, the anti-genome of SYNV was flanked by modified Cauliflower mosaic virus 35S promoter and HDV-ribozyme in the vector to produce precise 5'- and 3'- termini. The three RNP components (N, P, and L), and the three gene silencing suppressors [barely stripe mosaic virus Yb (Yb), tomato bushy stunt virus p19 (p19), and tobacco etch virus HC-pro (HC-pro)] were co-expressed with the viral genome to inhibit host gene silencing.

Like other viruses, plant-adapted rhabdovirus genomes have various *cis*-regulatory elements to control virus transcription and replication (Barr *et al.*, 1997; Whelan *et al.*, 1999). Add to that, the viral proteins establish complicated interaction networks with host factors to hijack the host cell and its resources that required during infection (Anderson *et al.*, 2012; Bandyopadhyay *et al.*, 2010; Dietzgen *et al.*, 2012; Martin *et al.*, 2012). These interactions involve various functional motifs in the proteins (Sanderfoot *et al.*, 1996; Sen *et al.*, 2007; Vzorov *et al.*, 2005; Wang *et al.*, 2012; Ye *et al.*, 1994). Functional studies of viral proteins and *cis*-elements on the viral genomes of plant-adapted NSRVs are most commonly based on the use of predictive algorithms, proteins interaction and localization maps, and protein sequence homology with their counter partners infecting animals (Anderson *et al.*, 2012; Bandyopadhyay *et al.*, 2010; Ghosh *et al.*, 2008; Claudia R. F *et al.*, 1998; Claudia *et al.*, 1998; Deng *et al.*, 2007; Goodin *et al.*, 2001; Goodin *et al.*, 2007; Heaton *et al.*, 1989; Claudia *et al.*, 1998). Although these approaches have generated useful speculation about plant-adapted NSRV biology, the information may not reflect the *in-situ* functionalities of the viral proteins and regulatory sequences due to the absence of virus infection.

In this study, the reverse genetic system was applied to *Coffee ringspot virus* and *Potato yellow dwarf virus*. *Coffee ringspot virus* (CoRSV) is a member of the newly recognized genus *Dichoravirus*, a plant-infecting bipartite negative-stranded RNA virus that is transmitted by the

Brevipalpus mite (Ramalho *et al.*, 2014; Dietzgen *et al.*, 2014). The full-length genome sequence and gene organization of the virus were determined in 2014 by Ramalho *et al.* (2014). The virus has two segmented genomes namely, RNA 1 and RNA 2. RNA 1 encodes five open reading frames (ORFs) encoding N, P, movement protein, M, and G respectively, while RNA2 has a single ORF encoding large polymerase (L). The viral genes are separated by intergenic gene junctions (IGJs), and the gene coding region of each RNA genome is flanked by leader and trailer sequences (Ramalho *et al.*, 2014). The virus-specific protein interaction and localization map (PILM) for CoRSV was constructed using transient expression of GFP fusions and a BiFC assay in the model plant, *N. benthamiana* (Ramalho *et al.*, 2014). The nuclear localization of N, P, and M in the PILM, viroplasm-like structure (VpLS) formed by N and P co-expression (Ramalho *et al.*, 2014), and the accumulation of virus particles in nuclei and viroplasm formation in the infected plants (Kitajima *et al.*, 2003) strongly indicate that the virus has the nucleotropic life similar to that of nucleorhabdoviruses.

Potato yellow dwarf virus (PYDV) is the type species of the genus *Nucleorhabdovirus* (Bandyopadhyay *et al.*, 2010; Jones *et al.*, 1990). PYDV was first reported as a highly destructive pathogen of potato (*Solanum tuberosum*) (Barrus *et al.*, 1922). Early research on this virus has contributed significantly to the study of virus-insect interaction (Black *et al.*, 1941; Black *et al.*, 1943; Black *et al.*, 1965; Hsu *et al.*, 1973), lipid contents of the virus particle (Ahmed *et al.*, 1964, MacLeod *et al.*, 1968), and virus purification using sucrose gradient centrifugation (Brakke *et al.*, 1951; Hsu *et al.*, 1973). PYDV has two strains distinguishable by vector specificity and serotype, namely *Constricta* yellow dwarf virus (CYDV) and *Sanguinolenta* yellow dwarf virus (SYDV) respectively. They are selectively transmissible by the *Agallia constricta* and *Aceratagallia sanguinolenta*, respectively (Ghosh *et al.*, 2008; Black *et al.*, 1941; Hsu *et al.*, 1973). Those two virus genome sequences and genetic contents were characterized, and the protein interaction and

localization map (PILM) of each virus was completed (Bandyopadhyay *et al.*, 2010; Jang *et al.*, 2017).

To rescue the recombinant virus, the full-length antigenome of CoRSV and SYDV were cloned into the pCass4HDV vector (Annamalai *et al.*, 2006) and pCB301-2 μ -HDV (Sun *et al.*, 2017) and minigenomes were generated based on the virus genome sequence. The cDNA of RNP core proteins (N, P, and L) of each virus were cloned into protein expression vectors, pGD (Goodin *et al.*, 2002), pTRBO (Lindbo *et al.*, 2007), and pSITE systems (Chakrabarty *et al.*, 2007). This study aims to develop a reverse genetics system for generation of infectious CoRSV and SYDV from their cDNA clones. The recombinant viruses from the system will allow elucidating the wider portion of cytopathological properties of the plant-adapted negative-strand RNA viruses from their RNA sequence level. Furthermore, these approaches would be extended to the interaction of viral and vector proteins that regulate the vector specificities, disease control for the important crops in the global trade market and pharmaceutical use for public health.

Methods

Plant materials and virus maintenance

All plants, including transgenic marker lines of *Nicotiana benthamiana* and wild type *Chenopodium quinoa*, were maintained in the greenhouse on open benches or a 28° C growth chamber in the Kentucky Tobacco Research and Development Center (KTRDC) (Martin *et al.*, 2009; Anderson *et al.*, 2014; Ramalho *et al.*, 2014). The *Sanguinolenta* strain of *Potato yellow dwarf virus* (American Type Culture collection accession PV-234) was maintained by serial passage of mechanical inoculation in *N. benthamiana* and *Nicotiana rustica* (Martin, *et al.*, 2009; Anderson *et al.*, 2012). The mechanical serial passage in *Chenopodium quinoa* maintained *coffee ringspot virus*-Lavras strain. To maintain *Coffee ringspot virus* (CoRSV), *C. quinoa* was pre-incubated for three days in the 28°C chamber before mechanical inoculation using the virus reservoir and maintained five to seven days more after the inoculation in the same place to increase

the CoRSV infection efficiency. After the incubation, the plants were moved and maintained in the greenhouse until infection symptoms were visible (Ramalho *et al.*, 2014).

Isolation of total RNA, RT-PCR

Total RNA was extracted from plant tissues using the Qiagen RNeasy Plant minikit (Qiagen). Except where noted, first-strand cDNA synthesis and PCRs were carried out using Superscript reverse transcriptase IV (Thermo Fisher Scientific) and Phusion high-fidelity DNA polymerase (Finnzymes), respectively.

Cloning of the CoRSV full-length antigenome (ag) RNA 1 and RNA 2 into pGEM-T easy vector

cDNA of agRNA 1 and agRNA 2 were subcloned into pGEM-T easy vector (Promega) (Fig. 4.3a) before they are cloned into pCass4HDV (Fig. 4.2). The primer sets, ‘FspI_R1F’/‘KpnI_R1R’ and ‘FspI_R2F’/‘KpnI_R2R’ amplified agRNA 1 and agRNA 2 from CoRSV infected *C. quinoa* respectively. FspI and KpnI enzyme sites were introduced on 5’ and 3’ ends of agRNA 1 and agRNA2 respectively during the PCR. The PCR products were cloned directly into pGEM-teasy vector (Promega) via TA cloning to generate pGEM-R1 and pGEM-R2 (Fig. 4.3a).

Cloning of the full-length antigenomic cDNA of SYDV into pGEM-T easy vector

Three partial segments of antigenome of SYDV, SYDV_P1, SYDV_P2, and SYDV_P3, were amplified using the following primer pairs (‘SYDV-P1F’/‘SYDV-P1R’, ‘SYDV_P2F’/‘SYDV_P2R’, AND ‘SYDV_P3F’/‘SYDV_P3R’) and sub-cloned into pGEM-T easy vector (Promega), to construct pGEM_P1, pGEM_P2, and pGEM_P3. pGEM_P1 and pGEM_P2 were digested by KpnI and NotI and the resulted fragments were separated in the 0.8 % agarose gel. The SYDV_P2 fragment from pGEM_P2 was subcloned into pGEM_P1 backbone and pGEM_P1:P2 was produced. pGEM_P1:P2 and pGEM_P3 were digested by XmaI and NotI. The SYDV_P3 fragment from pGEM-R3 was inserted to the opening of the pGEM_P1:P2 to generate pGEM_agSYDV (Fig. 4.3b).

Construction of full-length antigenomic sequence of CoRSV RNA1 and RNA2 in pCass4HDV

The full-length CoRSV agRNA 1 and agRNA 2 were cut out from pGEM-R1 and pGEM-R2 using FspI and KpnI, respectively. The agRNA 1 (6.5 kb) and agRNA 2 (5.9 kb) fragments were separated from pGEM backbone on the 0.8 % agarose gel and purified from the gel using gel extraction and purification kit (Quiagen) (Fig. 4.4a-b). The CoRSV RNA1 and RNA2 were ligated into StuI and KpnI treated pCass4HDV by T4 ligase in vector/insert ratio, 1: 3 (Fig. 4.4c). The extra sequences between inserted viral genome and the regulatory elements of the vector, 35S promoter and ribozyme, were removed using site-directed substitution mutagenesis (NEB, Q5 Site-Directed Mutagenesis Kit) (Fig. 4.4d-e).

Construction of full-length antigenomic sequence of SYDV in pCass4HDV

pGEM_agSYDV was digested by HindIII to generate the two fragments ‘H-YD-H’ and linear pGEM_S-H-V [Fig. 4.5(1)]. The pGEM_S-H-V was religated [Fig. 4.5(2)] and used as a PCR template to amplify the 5’p-S-H-V-p3’ fragment [Fig. 4.5(3)]. The PCR product was inserted in the StuI site of the modified (m) pCass4HDV, the HindIII site removed [Fig. 4.5(4)]. The resulted mpCass4HDV_S-H-V was re-digested using HindIII. The 5’-H-YD-H-3’ fragment was inserted in the HindIII site in 5’-S-H-V-3’ to build pCass4HDV_agSYDV [Fig. 4.5(6)]. To remove the extra sequences between the 3’ terminus of the SYDV antigenome and the HDV-ribozyme of the vector, site-specific sequence deletion was carried using a Q5 Site-Directed Mutagenesis Kit (NEB) [Fig. 4.5(7)].

Cloning N, P, and L of CoRSV into pSITE vectors and pTRBO vector

The cDNAs of N, P, and L of CoRSV were amplified using the primer sets, ‘CoRSVNF/CoRSVNR’, ‘CoRSVPF/CoRSVNR’, and ‘CoRSVLF/CoRSVLR’. The primer sets introduced attB1-PacI and NotI-attB2 sequences on 5’ and 3’ ends of the PCR products respectively. The PCR products were recombined to pDONR 221 vector (Invitrogen) using BP clonase

(Thermofisher) (Fig. 4.6b). Subsequently, the pDONR constructs were utilized for LR reaction (LR clonase-II) to clone cDNAs of N, P, and L into pSITE 0A and pSITE-FLAG (Thermofisher) (Fig. 4.6c). The cDNAs of N, P, and L in pDONR 221 were cloned into the pTRBO vector using the PacI and NotI sites (Fig. 4. 6a) (Lindbo *et al.*, 2007, Martin *et al.*, 2009; Anderson *et al.*, 2014).

Cloning N, P, and L of SYDV into pGD vector

The cDNAs of SYDV-N, -P, and -L were amplified from SYDV infected *N. benthamiana* the primer set ‘SYDVNF/SYDVNR,’ ‘SYDVPF/SYDVPR’, and ‘SYDVLF/SYDVLR’. XhoI and BamHI sites were introduced on the 5’ and 3’ ends of the PCR products. The PCR products were subcloned into the pGEM-T easy vector. The pGEM constructs were digested using XhoI and BamHI, and the viral gene fragments were cloned into pGD vector (Goodin *et al.*, 2002) to produce pGD-SYDVN, pGD-SYDVP, and pGD-SYDVL (Fig. 4.6d).

Construction of pCASS4HDVRz-CoRSVMG_GFP

The multicloning site was generated between leader and trailer sequence of CoRSV in the pGEM-R1 using site-directed substitution mutagenesis. The primer pair ‘R1_Cassette F/R1_Cassette-R’ was used to replaced the gene encoding region of CoRSV to the synthesized multicloning site, 5’-GGATCCGACTCGAGTTAGATCTGTAAGCTT-3’. The XhoI and HindIII sites were introduced to 5’ and 3’ ends of GFP sequence respectively using the primer set, ‘XhoI-GFP/GFP-HindIII’. The PCR product was cloned into the multicloning site above to construct pCASS4HDVRz-CoRSVMG-GFP.

Plasmid purification from yeast and electrotransformation of Agrobacterium.

20 µl of yeast lysis buffer (2% Triton X-100, 1% SDS, 100mM NaCl, 10mM Tris-HCl pH 8.0, 1mM EDTA pH 8.0) was added to eppendorf tube. The 3-4 day old yeast colony was picked using pipet tip and resuspended in the 20 µl of yeast lysis buffer. 20 µl of phenol:chloroform was added along with half-volume of glass beads into the tube, and was vortexed with maximum speed

for 5 min. The tubes were centrifuged for 5 min at the maximum speed and the upper aqueous solution was taken for following steps. PCR targeting several parts of SYDV genome was performed to validate the plasmid using the aqueous phase. one μ l of aqueous phase was mixed with competent cells (electrocompetent *Agrobacterium* strain C58C1) on ice and then was pipetted into a precooled electroporation cuvette (0.1 cm). Electroporation was performed by using a Bio-Rad gene Pulse set at 1.8 kV, 25mF with Pulse controller of 200 ohms. The cells were grown at 25 °C for three hours and all *agrobacterium* culture was plated as described previously (Goodin *et al.*, 2007)

Construction of full-length antigenomic sequence of SYDV into pCB301-2 μ -HDV via Yeast homologous recombination.

To generate pCB301-2 μ _agSYDV, the antigenome of SYDV was amplified into four parts (SYDV_a, SYDV_b, SYDV_c, SYDV_d) using the primer pairs, ‘SYDVaF/SYDVaR’, ‘SYDVbF/SYDVbR’, ‘SYDVcF/SYDVcR’, and ‘SYDVdF/SYDVdR’, respectively. Yeast vector backbone was amplified from pCB301-2 μ -HDV using the ‘SYDV_backbone_F/SYDV_backbone_R’ primer pair (Figure 3.7a). The full-length SYDV-L was amplified into two parts, SYDVL-a and SYDVL-b using the primer sets ‘SYDVL-aF/SYDVL-aR’ and ‘SYDVL-bF/SYDVL-bR’ respectively (Fig A.7b). The primers were designed to generate at least 40 bp overlapping sequence between the neighboring fragments to facilitate the yeast mediated homologous recombination during yeast transformation process. The concentration of each PCR product and the vector pCB301-2 μ was measured on the agarose gel. The amount of each fragment was adjusted to about 0.8 μ g. The DNA mixture was transformed into L 40 yeast competent cells using the LiAC method (Gietz *et al.*, 2007). The total DNA mixture, 10 μ l of sheared salmon sperm DNA (10mg/ml), sterilized 300 μ l of PEG/LiAC solution (40% of PEG, 1X TE, 1X LiAC in total volume) was added to 50 μ l of competent cells. The tube was vortexed and incubated at 30 °C for 30 min with shaking. Heat shock was applied using 42 °C heat block for 30 min and the tube was chilled on ice for 1-2 min. The tube was centrifuged (3000rpm for 2min) to pellet the cells and the

supernatant was discarded. The pellet was resuspended in 100 µl of sterile 1 X TE buffer and spread onto tryptophan deficiency media for selection. After 3-4 days, the yeast colonies grown to an appropriate size were picked to confirm the cloning results using colony PCR (Fig. 4.7c).

Agrobacterium-mediated viral genome protein expression in plant cells

The viral genome and protein expression constructs were transformed into *Agrobacterium tumefaciens* strain LBA 4404 and grown on the LB plates containing proper antibiotics. The plates were incubated for 72 hours or until colonies were grown to a proper size. A single colony was transferred and spread onto a new media plate and grown for two days. The cells were scraped from the plates and resuspended in the infiltration buffer [10 mM of MgCl₂, 10 mM of 2-(N-Morpholino)-ethanesulfonic acid (MES)] (Goodin *et al.*, 2007). The final concentration of bacterial suspensions was adjusted to an OD 600 of 0.8 and incubated for 3hrs with 100 µM acetosyringone under room temperature for activation. The ribonucleocapsid components (N, P, and L) and the viral genome suspensions of each virus, were mixed in the desired combinations and volumes. The bacteria suspensions of pGD-HcPro (TEV), pGD-p19 (TBSV), and pGD- γb (BSMV) were added to inhibit the gene silencing effect by the plant.

Western blotting

For blotting and detection of proteins from plant samples, the soluble proteins were extracted from agroinfiltrated-, virus infected- and mock-inoculated plants. 200 mg of leaf tissues were collected using the cork borer and ground with tungsten beads (3 mm) and liquid nitrogen in eppendorf tube by vortex machine. The tissue powder was resuspended in the 200µl of 1x sample buffer (50mM Tris-HCl pH 6.8, 2% SDS, 10% glycerol, 1% β-mercaptoethanol, 12.5mM EDTA, 0.02% bromophenol blue) and boiled for 5 minutes. The total proteins were separated in SDS-PAGE of the desired concentration. The separated proteins were visualized using Coomassie blue on the SDS gel or transferred to polyvinylidene difluoride (PVDF) membrane by application of an

electrical current. The targeted proteins were visualized on the membrane using the proper primary and secondary antibodies and detection agents.

Laser scanning confocal microscopy

Agroinfiltrated *N. benthamiana* leaves were examined on an Olympus FV1000 laser-scanning confocal microscope as described previously. Micrographs for overlapped two-channel image were acquired sequentially, as described in previous (Goodin *et al.*, 2007)

Results

Expression of CoRSV RNA 1 and RNA 2 from pCass4HDV constructs was detected using RT-PCR.

Expression of antigenomic viral RNA is one of the essential elements to rescue infectious negative-strand RNA virus from cDNA (Horimoto *et al.*, 1994; Pleschka *et al.*, 1996; Pekosz *et al.*, 1999; Desselberger *et al.*, 2017). To express agRNAs in *N. benthamiana*, the cDNAs agRNA 1 and agRNA 2 were cloned into pCass4HDV vector and pCass4HDV-R1 and pCass4HDV-R2 were constructed. The cDNA constructs were digested by HindIII for restriction analysis; Comparison of the enzyme digestion pattern to in-silico (Fig. 4.8a-b). The expression of agRNA1 and agRNA2 was detected from the RT-PCR using each RNA of pCass4HDV-R1 and pCass4HDV-R2 agroinfiltrated *N. benthamiana*. The primer sets, 'R1_1657F/R1_3357R' and 'R13284F/R14947R' amplified about 1.7 kb PCR products from pCass4HDV-R1 infiltrated plants (Fig. 4.8c, lane 1, 2). 'R2_1471F/R2_3015R' and 'R2_4431F/R2_5945R' amplified about 1.5kb PCR product pCass4HDV-R2 infiltrated plants (Fig. 4.8c, lane 3, 4). DNA contamination of the RNA samples was not detected (Fig. 4.8c. lane 5-8).

Coffee ringspot virus nucleoprotein (N), Phosphoprotein (P), and RNA dependent RNA polymerase (L) were expressed using pSITE gateway system and FLAG fusion proteins were visualized by western blot.

The three RNP complex proteins, (N, P, and L) are compulsory to produce functional RNA complex along with ag-vRNA (WalPita *et al.*, 2005, Pekosz, 1999). The cDNAs encoding CoRSV-N, -P, and -L were cloned to pSITE-0A and pSITE-FLAG (Fig. 4.5). pSITE-FLAG-CoRSV-N, pSITE-FLAG-CoRSV-P, and pSITE-FLAG-CoRSV-L were expressed in *N. benthamiana* via agroinfiltration. FLAG-CoRSV-N and FLAG-CoRSV-P were detected by colorimetric development (Fig. 4.9a). In the result, the major band size for FLAG-CoRSV-N was 60kDa and other multiple bands were also detected in various sizes. FLAG-CoRSV-P was detected on the PVDF membrane as about 35 kDa in size. The expression level of FLAG-CoRSV-P was lower than FLAG-CoRSV-N. Otherwise, FLAG tagged CoRSV-L was not detected from the colorimetric development. To detect FLAG-CoRSV-L, Chemiluminescent development was used to increase the detection sensitivity, and the FLAG-CoRSV-L expression was detected through X-ray film development. The detected size of CoRSV L on X-ray film was about 230 kDa (Fig. 4.9b).

Expression of native CoRSV-N and -P using pTRBO, the *Tobacco mosaic virus* (TMV)-based transient expression vector.

pTRBO-CoRSV-N and pTRBO-CoRSV-P were transformed to the *Agrobacterium* strain LBA 4404 and infiltrated to *N. benthamiana* to express the native CoRSV-N and CoRSV-P. The protein samples were extracted from the infiltrated leaves after 48 hours post-infiltration. The extracts were subjected to western blot using CoRSV N antibody or gel staining using Coomassie blue. The western blot using CoRSV N specific antibody showed four protein bands on the membrane (Fig. 4.10a). Approximately 55 kDa, 50 kDa, 45 kDa, and 40 kDa bands were detected from the CoRSV-N sample (Fig. 4.10a). The P expression was tested on the gel stained by Coomassie brilliant blue due to absence of proper antibody (Fig. 4.10b). About 35 kDa single band was detected from the proteins samples which collected from the pTRBO-CoRSV-P agroinfiltrated plants (Fig. 4.10b).

CoRSV N and P co-expression induces viroplasm-like structure in the nucleus and nuclear expansion

Several studies have shown that the transient co-expression of nucleoproteins (N) and phosphoproteins (P) of plant negative-strand RNA viruses are sufficient to form VpLS in the plant and insect cells and various N and P interactions have been characterized (Wang *et al.*, 2018; Deng *et al.*, 2007; Kondo *et al.*, 2013, Jang, 2018, Ramalho *et al.*, 2014). In the previous research about CoRSV protein localization, the co-expression of N-GFP and RFP-P promoted the relocalization of the RFP-P to the cytoplasm by N-GFP. The nuclear co-localization of CoRSV N-GFP and CoRSV RFP-P did not induce the VpLS, while N and P interaction signal was localized in the VpLS in the BiFC assay (Ramalho *et al.*, 2014).

Due to the absence of polyclonal antibodies for CoRSV proteins, the functionality of the native N and P was tested in the transgenic RFP-H2B *N. benthamiana* using a confocal microscope, at 48 hours post-infiltration. The single expression of CoRSV-N did not induce any morphological change of nuclei in the infiltrated plants (Fig. 4.11a, left panels). Otherwise, CoRSV-P single expression formed an irregular shaped subnuclear structure (Fig. 4.11a, middle panels). The subnuclear structure formed by single P expression (Fig. 4.11a) was different from the nuclear viroplasm induced by the virus infection (Fig. 4.11b). The boundary of the subnuclear space formed by single P expression was irregular. The noticeable effect in the size of nuclei by P was not observed. The N and P co-expression induced VpLS in the nuclei of the infiltrated plants (Fig. 4.11a, right panels). This VpLS was very similar to the nuclear viroplasm induced by the CoRSV which has smooth spherical shape. Considering the feature of RFP-H2b and the confocal images, the chromatin and nucleolus seemed not to be in the VpLS. The results reported here were reproduced at least five times. And the N and P expression using pSITE-0A showed the same results (Fig. 4.11a).

GFP-ER signal re-direction was observed in the nuclei by the single P expression.

Host membrane remodeling by virus infection has been reported from various viruses including plant rhabdovirus (Carette *et al.*, 2000; Jackson *et al.*, 2005; Suhy *et al.*, 2000; Reichel *et*

al., 1998). Especially, significant ER membrane signal re-direction from the cytoplasm to nucleoplasm in *N. benthamiana* 16C plant by SYNV infection was reported by Jackson *et al.*, (2005). In this research, GFP-ER signal rearrangement was observed in 16c *N. benthamiana* (GFP-ER marker plant) transiently expressing CoRSV-P. The nuclei of the cells in the 16C *N. benthamiana* plants were stained using DAPI, and the nuclei appeared to have an irregular shaped subnuclear space like those of nuclei in the transgenic RFP-H2b *N. benthamiana* plants expressing P (Fig. 4.11a and Fig. 4.12). The accumulation of GFP signal in the subnuclear space seemed to reflect that the ER membrane is re-directed into the P-induced inner space of nuclei. Moreover, the GFP signal intensity in the cell periphery region and nuclear membrane was noticeably lower than those in the mock-inoculated plant. A bulk of GFP signal was concentrated on the subnuclear space which is induced by P expression (Fig. 4.12). The results reported here were reproduced at least five times.

Inhibition of DAPI staining of nuclei of cells expressing CoRSV RNAs and N, P, L

The extremely low efficiency of DAPI staining of nuclei was observed while testing the cellular effect of the coexpression of CoRSV-N, -P, -L, and antigenomic viral RNAs in GFP-ER line of *N. benthamiana* at the three days post infiltration. A very limited number of stained nuclei were found. It was almost impossible to distinguish nuclei using DAPI staining. Otherwise, extremely swollen nuclei-like membrane patterns were detected (Fig. 4.13). This phenomenon was not observed in the N, P, and N/P co-expression. DAPI staining of the RFP-H2B plant expressing CoRSV N, P, L, and, RNA1 and RNA2 revealed that the DAPI staining of the nucleus was substantially inhibited (Fig. 4.14a). In most of the cases, the inhibition of DAPI staining was limited to the nuclei which are enlarged and containing VpLS (Fig. 4.14a-c). A total of 155 nuclei were counted using the confocal microscope and the nuclei were classified into four types: type 1, the undyed nucleus with clear subnuclear space and expansion; type 2, the undyed nucleus with expansion, but unclear VpLS; type 3, dyed nucleus with expansion and/or subnuclear structure; type 4, nucleus in usual shape (5-10 μm) (Fig. 4.14c). 30 % of nuclei had clear subcellular

nucleoplasm and expansion in size (47/155), type 1 and type 3. Only three of the 47 nuclei were DAPI-labeled. About 52% of the nuclei among the counted (80/155) showed clear DAPI-label (type 4). The rest (18%) showed relatively bigger size and very weak or undetectable DAPI-label (type 2) (Fig. 4. 14b). The difference in the DAPI density seemed to be directly correlated to the morphological variation of the nuclei. (Fig. 4.14b, 14c). More than 99% of the nuclei of the cells in the mock infiltrated samples were DAPI-labeled strongly. The data obtained from this measurement was similarly reproduced more than twice with the slight deviation (data not shown).

The temperature may affect the morphology of VpLS induced by CoRSV RNA1, RNA2, N, P, and L

In our previous research, exposure of plants to 28°C increased the rate of systemic infection of *C. quinoa* and *N. benthamiana* by CoRSV (Ramalho *et al.*, 2014). It seemed that the heat stress applied to the plants allowed CoRSV the chance to overcome the plant resistance to the virus (Ramalho *et al.*, 2014). The plants infiltrated by *Agrobacterium* suspensions harboring all components (agRNA1/agRNA2/N/P/L/GSSs) for the CoRSV rescue were maintained in a 28 °C chamber pre- and post-infiltration to maximize the chance of virus infection and symptom development. Leaf tissues were collected at 72-hour post infiltration to observe the morphological aspect of the nuclei of cells in the RFP-H2B *N. benthamiana*. About 34% (42/123) of nuclei showed clear and typical nuclear expansion accompanying viroplasm-like subnuclear space under the microscopic view, immediately after sampling from the 28°C chamber (Fig. 4. 15a-b). However, from the observation taken three hours after the temperature change to 23°C, the number of nuclei having VpLS (2/147) was noticeably reduced (Fig. 4. 15c-d). Three more observations were repeated to acquire the arithmetic mean of the phenomenon. In individual observation, 100 nuclei were randomly counted under microscopic view and the number of nuclei with clear VpLS were compared before and after the temperature change. An average of 30% of nuclei in each observation appeared to be enlarged and to have clear VpLS structure under 28°C. Otherwise, the observation after 3 hours incubation under 23 °C revealed that 38% of nuclei among the counted remained in

the expanded state, but the subnuclear structure was observed to be missing. Only seven nuclei among the total 300 nuclei were observed with VpLS. Similar morphological change of nuclei according to the temperature change was reproducibly observed (Table 3).

ER signal accumulation and size contraction of the enlarged nuclei were detected from the DAPI-stained RFP-ER *N. benthamiana* expressing CoRSV RNAs and N, P, L, after low temperature (23°C) treatment.

For more detailed observation, the three enlarged nuclei (>15nm) which are visibly well-stained by DAPI were picked and numbered from 1 to 3 in the Agroinfiltrated tissue sample of the RFP-ER *N. benthamiana*. Two nuclei (No. 1 and 2 in Fig. 4.16a-b) of the three picked nuclei showed ER-accumulation in the nucleus after 23°C treatment for 10hrs. The ER accumulation in the nucleus did not occur in the healthy ER marker transgenic plant (Fig. 4.16d). The nucleus No. 3 showed a significant size contraction at 1.5 hrs after first observation under 23°C (Fig. 4.16b). In addition to the three nuclei, at least 12 nuclei were found to be noticeably contracted over time. Among them, the three nuclei representing the nuclear size contraction were photographed (Fig 4. 16c). They showed nucleus volume reduction at 3 hours after 23°C exposure. The nuclear contraction was reproducibly obtained from the RFP-H2B *N. benthamiana* expressing all CoRSV RNP constituents (RNAs, N, P, and L) at least twice more (data not shown).

The simultaneous expression of the CoRSV viral antigenomes and N, P, L could not recover the infectious virus.

For the experiment in Fig. 4.17, a total of 108 plants (36 of wild-type, 18 of GFP-ER, 18 of RFP-ER, 18 of CFP-H2B, and 18 of RFP-H2B *N. benthamiana*) were infiltrated using the Agrobacterium suspension mixture. About three-weeks post infiltration, only four plants showed phenotypical changes including marginal yellowing, small yellow spots, and crinkle in the upper-leaves above the infiltrated leaves (Fig. 4.17a). Mock-inoculated plants did not show any change. RT-PCR targeting CoRSV-M (Fig. 4.17b), immunoblotting using CoRSV-N specific antibody (Fig. 4.17c), microscopic observation (Fig. 4.17d) and mechanical inoculation using the leaves showing

morphological change (not shown) revealed that no virus infection. The same experiment was reproduced 14 times more.

CoRSV N and P co-expression inhibited the GFP expression from CoRSV minigenome, but did not block the GFP expression from pSITE 0A

To evaluate the functionality of the cDNA clones of the CoRSV polymerase complex constituents (N, P, and L), various minigenome cassettes were cloned into pCass4HDV. The pCass4-CoRSV_MG_GFP induced a detectable background signal which came from leaky expression of the GFP gene in the minigenome cassette [Fig. 4.18(b)-a]. However, the co-expression of N and P inhibited the background GFP signal [Fig. 4.18(b)-c]. The single expression of N did not affect to the GFP expression [Fig. 4.18(b)-b]. N, P, and L co-expression with the minigenome showed a very limited number of GFP-foci under the microscope [Fig. 4.18(b)-d]. The western blot assay using GFP antibody for the samples used in Fig. 4.18(b) produced same results as the microscopic observation. The western results revealed that N/P and N/P/L co-expression inhibits the GFP expression [Fig. 4.18(c)]. Minigenome and CoRSV-P combination was tested separately. P expression did not prevent the GFP expression from the minigenome (data not shown). The N/P co-expression did not affect the expression of GFP from pSITE 0A [Fig. 4.18(e)]. The results obtained in this experiment were reproducible in the repeated experiments.

Expression of full-length SYDV antigenomic RNA and N, P, L protein to generate infectious virus from the cDNA.

To rescue infectious *Sanguinolenta* strains of PYDV from the antigenomic cDNA clone, the full-length anti-genomic sequence was cloned into pCass4HDV vector to generate pCass4HDV_agSYDV (Fig. 4.19b). The construct was digested by HindIII for restriction analysis (Fig. 4.19a). pGD vector was applied to express SYDV-N, -P, and -L proteins. RT-PCR specific to the SYDV genes coding N and P was performed using the cDNA obtained from the plant transiently expressing pCass4HDV_agSYDV. About 1.5kb of N and 750bp of P of SYDV was amplified from RT-PCR (Fig. 4.19c). DNA contamination from RNA sample was not detected. A negligible band

was amplified from the SYDV N specific PCR (Fig. 4.19c). The immuno-blotting assay using polyclonal SYDV antibody was performed to visualize N, P, and L of SYDV expression from the pGD constructs. The expression level of N and P was enough to visualize. Otherwise, SYDV L protein expression level was not detectable on the PVDF membrane (Fig. 4.19d). Chemiluminescence X-ray film development was not able to detect the L expression (data not shown). The L in the pGD vector was verified by sequencing (Retrogen). Multiple bands were detected from the protein sample of the plant expressing pGD-SYDVN. The major band size was detected around 50 kDa marker. The protein sample obtained from the plant expressing SYDV-P generated either multiple protein bands. The major band was about 33 kDa. (Fig. 4. 17d)

Discussion

Determining the functional role of proteins and regulatory elements in the genome of the plant-adapted rhabdoviruses is most commonly based on the use of predictive algorithms, transient expression of autofluorescence protein fusion in the cell, and the analogy by amino acid sequence homology to their animal infecting counter partners (Anderson *et al.*, 2018; Bandyopadhyay *et al.*, 2010; Ghosh *et al.*, 2008; Jang *et al.*, 2017). Despite the accumulation of much speculations from these approaches, the knowledge about the *in-situ* role of the viral genome and gene products in the context of virus infection is still limited (Goodin *et al.*, 2007; Jackson *et al.*, 2005; Jackson *et al.*, 2016; Pappi *et al.*, 2013; Jang *et al.*, 2017; Tsai *et al.*, 2005).

Recently, reporter gene expression using plant-adapted rhabdovirus mini-replicon system, and recovery of the infectious virus from model plant were achieved through the co-expression of a virus antigenome, RNP core proteins (N, P, and L) and gene silencing suppressors by *Agrobacterium*-mediated cDNA transfer mechanism (Ganesan *et al.*, 2013; Wang *et al.*, 2015). This promising system will allow generating recombinant plant-adapted negative-strand RNA viruses to study the relevance of their genetic sequence to the virus structure and protein functions.

Furthermore, these strategies will promote the extensive application of plant-adapted NSRVs to therapeutic and agricultural purposes.

In this research, agRNA1 and agRNA2 of CoRSV, and its RNP core proteins (N, P, and L) were expressed in *N. benthamiana* with gene silencing suppressors using an Agrobacterium-mediated gene delivery system. The expression of agRNA1 and agRNA2 was confirmed using RT-PCR (Fig. 4.9). The expression of three core proteins was visualized using FLAG-tag fusion proteins. In western blot tests, FLAG fusion N protein appeared to be multiple bands. The size of the major band was about 50 kDa (Fig. 4.10). The predicted size by computational calculation (SerialCloner v2.6.1, serialbasics) of N was 49kDa. N proteins of NSRVs have been shown to be highly self-associated (Ambroise-Desfosses *et al.*, 2013) and phosphorylated in previous reports (Yang *et al.*, 1999; Wu *et al.*, 2002). Post-translational modification and insufficient denature of the sample could be resulted in the multiple minor bands and larger major band. FLAG fusion P was detected around the 40kDa size marker. The predicted molecular weight of P was 26kDa. The FLAG-L protein was detected using a chemiluminescence western blot. The expression level was lower than other proteins even though it was expressed from the same 35S promoter-based protein expression system. The band was detected around the 230kDa region. The predicted size was 212kDa.

In previous research, CoRSV-N was localized on the nucleus and cell periphery region, and P was exclusively localized to the nucleus. While the GFP fusion of P did not induce any morphological change in the nucleus (Ramalho *et al.*, 2014), in this research, the untagged P expression induced subnuclear space in the RFP-H2b marker plants. This result is very intriguing because orchid fleck virus (OFV), the prototype virus of dichoravirus, needs both N and P protein to induce morphological change of host nucleus (Kondo *et al.*, 2013). The differential morphology of subnuclear space by P compared to the VpLS of N and P co-expression or viroplasm by CoRSV infection suggests the CoRSV-P protein has distinct functions compared to OFV-P. Indeed,

CoRSV-P enables to induce ER-membrane rearrangement from 16c *N. benthamiana* which is not reported from OFV-P single expression (Kondo *et al.*, 2013). The rearranged GFP-ER signal of the 16c plant accumulates in the subnuclear space generated by P expression. This may associate to that P interact with host cell cytoskeleton and with nucleocytoplasmic trafficking carriers (Leyrat *et al.*, 2011). In a similar case, the redirecting of ER-signal flow from the cytoplasm to the nucleus by SYNIV and PYDV infection in the 16c plant has been reported (Jackson *et al.*, 2005). CoRSV-P has 32% of amino acid similarity to the cognate of OFV, however, the differential amino acid residues are dispersed along with the P amino acid sequence. Therefore, physical scanning of the functional domain(s) of CoRSV-P that related to the ER-rearrangement (Anderson *et al.*, 2012).

Formation of VpLS without ER membrane disruption in CoRSV-N and -P co-expressed plant tissue suggests that CoRSV-N functions in maintaining intact nuclear structure during infection. Regarding overly perturbed host cellular condition is not always favorable to viruses, viruses need to make their host survive long enough to the viruses replicate and spread (Koyuncu *et al.*, 2013). Therefore, as a nucleotropic virus, maintaining the subcellular site for virus factory, nucleus, would be critically important to the virus and N protein may perform the role to keep host nuclei intact during its infection.

The unexpected DAPI staining pattern by simultaneous expression of all RNP components (agRNA1, agRNA2, N, P, and L) extended the areas of our concern to alteration of chromatin structure and perturbation of nucleocytoplasmic transport by the virus. During this research, most of nuclei in the virus-infected, CoRSV-N and P co-expressed, and all RNP components expressed cells are relatively bigger ($>15\mu\text{m}$) than normal nuclei of epidermal cells which have about 5~10 μm in size (Nagar *et al.*, 1995). In the RNP component expression experiment, the nuclei in the range of normal size ($\approx 10\mu\text{m}$) were stained by DAPI, which is not observed from enlarged nuclei having the VpLS ($>20\mu\text{m}$). The size-dependent inhibition of DAPI uptake suggests two collaborative factors possibly explaining the phenomenon; (1) Generation of swelling force by

impaired nucleocytoplasmic transport of host cell by viral factors and (2) Alteration of host chromatin structure by previous one.

Already, many research and reviews emphasized that the volume of nucleus are closely related to swapping of cytosolic and nuclear substances through nuclear pore complex, the nucleocytoplasmic transport (Ganguly *et al.*, 2016; Levy *et al.*, 2010; Edens *et al.*, 2013; Jevtić *et al.*, 2014). The extremely swelled nuclei by expression of RNP components and the inhibited translation of CoRSV leader and trailer sequence flanked GFP RNA by CoRSNV-N and -P co-expression in this research may indicate the inhibited nuclear export of the RNA molecules that encapsidated by CoRSV-N and P. This rises an intriguing question about the compatibility of the predicted NESs from CoRSV-N and -P of the RNP complex of CoRSV with *N. benthamiana* export receptors. Ramalho *et al.* (2014) reported the predicted-NESs of N and its capability of P re-localization from the nucleus to cell periphery by N-P interaction. However, according to the result, the formation of multimer during encapsidation may affect to the functionality of NES of N. More detailed information about what conformational changes of CoRSV-N occur by the interaction between RNA and the viral protein is required to solve this problem (Fernández-Coll *et al.*, 2018).

Nuclear chromatins form a dynamic architecture that maintains the stability and accessibility of the chromatin machinery. The viruses invading host nucleus must contend with, modulate and utilize the forces that drive chromatin formation and regulate chromatin structure (Knipe *et al.*, 2013, Lieberman *et al.*, 2006, Goodin *et al.*, 2001; Liu *et al.*, 2018; Wang *et al.*, 2018). Chromosome condensation by TGMV in plant nuclei (Bass *et al.*, 2000), the marginalization of condensed chromatin to the nuclear envelope in the rat prostatic adenocarcinoma 3 (AT3) by the rabies virus (Jackson *et al.*, 1997) were reported. The chromatin condensation directly related to the chromatin compactness that affects the fluorochrome uptake of nucleus, for example, *in-situ* DAPI staining of chromatin (Mascetti *et al.*, 2001). DAPI associates with the minor groove of dsDNA, with a preference for the A-T clusters (Chazotte *et al.*, 2011). The margination of the

RFP-H2B patterns and poor DAPI staining in the enlarged nuclei may indicate that the excessive accumulation of RNP or RNP components generates swelling force excluding the chromatin primarily around the nuclear membrane and expanding the nuclear envelope (Bass *et al.*, 2000, Jacson *et al.*, 1997). Meanwhile, the marginalized chromatins may be extremely condensed by the swelling force generated by impaired export of viral factors. We have not investigated the interaction between CoRSV factors and host factors that related to the nuclear morphology yet. High-throughput screening for global interaction between CoRSV and host plant is required to provide reliable answers for the gap of our knowledge about the viroplasm formation by virus infection.

In previous research, Ramalho *et al.*, reported that the pre-incubation of *C. quinoa* in a 28 °C chamber before inoculation with CoRSV developed systemic susceptibility (Ramalho *et al.*, 2014), and increased the chance of the infection of *N. benthamiana* by the virus (unpublished data). During the attempts of infectious virus recovery from cDNAs, the VpLS in the enlarged nuclei disappeared after the plants were exposed to 23 °C for 3 hours. We do not have apparent evidence explaining the morphological change of the nuclei by temperature change yet. Even the minimal temperature changes might cause great effects on the protein physiochemistry (Fields *et al.*, 2001; Greenfield *et al.*, 2006; Dong *et al.*, 1995), nucleocytoplasmic shuttling (Enami *et al.*, 1993; Koh *et al.*, 2015; Matthew *et al.*, 1995), and nuclear membrane architecture (Nägel *et al.*, 1977). The translation rate of encapsidation signal flanked RNA in different temperature will provide a more refined answer for relation between nuclear transport of encapsidated RNA by CoRSV-N and temperature changes.

Although the active cytopathological responses in the infiltrated cells, only a few plants show abnormal change on the upper-leaves above the infiltrated leaf compared to the mock-inoculated plants after 3-4 weeks post inoculation in each experiment. Infectious virus is not detected from RT-PCR, immunoblotting, and microscopic observation. If perturbed

nucleocytoplasmic transport is directly related to the failure of recovery of the CoRSV from the cDNA, then impaired NES function of CoRSV-N would be a major factor impeding the recovery of the virus from this system. Still, there is no direct evidence of accumulation of encapsidated GFP-RNA and antigenomic RNAs in the nuclei. The RNA visualization, localization, and quantification using in-situ hybridization (FISH) (Kliot *et al.*, 2014; Shargil *et al.*, 2015) would be helpful to explain these results. Also, RNA gel shift assay is required to confirm the formation of RNP complex.

In this research, the SYDV antigenomic RNA and the RNP core proteins (N, P, and L) were also expressed in *N. benthamiana* using *Agrobacterium*-mediated DNA delivery system. However, recovery of infectious SYDV from the agroinfiltrated *N. benthamiana* has not been detected.

Overall discussion and future direction

In this dissertation (1) The full-length genome sequence of CYDV was determined and its genetic contents were compared to those of SYDV and other rhabdoviruses, (2) the subcellular localizations of CYDV proteins and all pair-wise binary interactions of CYDV proteins, except L protein, were determined, and the data generated unique PILM for each strain, (3) the functional domains of PYDV-M protein that regulate the inter- and intracellular movement of the virus were mapped, and (4) viroplasm-like structure formation in the plant host nuclei by co-expression of nucleoprotein and phosphoprotein was confirmed using CoRSV-N and -P proteins during attempt of establishing reverse genetic system for plant-adapted rhabdoviruses.

Although the most of rhabdoviruses share almost universal replication mechanism across the family (Dietzgen *et al.*, 2017), nucleorhabdoviruses are slightly different compared to other members since they induce replication compartments in nucleus rather than cytoplasm where most of other rhabdoviruses replicate (Bandyopadhyay *et al.*, 2010; Goodin *et al.*, 2001; Lamprecht *et al.*, 2009). Hence, their infection process, cytopathology and proteins functions that regulate their

nucleotropic biology are not clearly understood so far compared to other cytotropic viruses in the family (Francki *et al.*, 1973; Jackson *et al.*, 2005; Mann *et al.*, 2014; Redinbaugh *et al.*, 2005). Moreover, despite the long history of the research about the vector-specificity for the two strains of PYDV, CYDV and SYDV (Black *et al.*, 1940; Black *et al.*, 1941; Hsu *et al.*, 1973), the comparative analysis for the viruses in genomic sequence level has not been made yet. Hence, there is a gap in our knowledge about what genotypic variations make the differential phenotypes between two strains of PYDV.

In this research, the two strains of PYDV showed the close sequence relatedness. The highly conserved consensus sequence of intergenic junction regions between CYDV and SYDV, and, exact same nine nucleotides complementarity of the leader and trailer sequences of each strain may supports that CYDV and SYDV presumably share common replication and transcription mechanism (Ivanov *et al.*, 2011). The sequence identity of these regulatory regions which are recognized by the polymerase complex indicates that they share common recognition mechanism for RNA synthesis by polymerase (Whelan *et al.*, 1999; Whelan *et al.*, 2002; Assenberg *et al.*, 2010; Ivanov *et al.*, 2011).

While they have highly similar regulatory sequences, the subcellular localization and interaction patterns of some of their proteins were distinct compared to each other. Particularly, this study shows remarkably different subcellular localization pattern of CYDV-N compared to that of SYDV in the subnuclear area. The amino acid region spanning the bipartite NLS of CYDV-N protein (**KRTAEDATTQQTKR**) was compared to that of SYDV-N protein (**QKRANEEAPPAAQKR**). While the 10 aa linker residue (underlined) is maintained between the bipartite KR residues (bolded), the sequence of the linker is not conserved. Also, the KR residues of CYDV-N NLS are not flanked by glutamines. The existence of di-proline residues in SYDV-N protein NLS which does not exist in the NLS of CYDV-N may explain the significant difference in localization pattern of the PYDV-N proteins. Proline is known as a structural disruptor of protein

secondary structure due to the conformational rigidity (MacArthur *et al.*, 1991; Morgan *et al.*, 2013). It also affects to the rate of peptide bond formation between proline and other amino acid (Tang *et al.*, 2014; Zarrinpar *et al.*, 2003) that may result in the affinity and isoform selectivity for nuclear import receptors including importin- α (Marfori *et al.*, 2011), which is presumed karyopherin for SYDV-N (Anderson *et al.*, 2018). The nuclear envelope association of CYDV-Y, which is not observed from the SYDV cognate, is a quietly intriguing result from this research. The CYDV-Y protein has 74% identity and 88% similarity compared to SYDV-Y and there are no significantly different amino acid residues between the two Y proteins. Otherwise, the dissimilar amino acids sequence residues dispersed over the entire length of the CYDV-Y in the alignment result (Clustal-omega, EMBL). Any membrane association domains (PSORTII, Nakai *et al.*, 1997), ER retention signal(PS-Scan, De Castro *et al.*, 2006), and cNLS (cNLS mapper, Kosugi *et al.*, 2009) of CYDV-Y were not predicted from the computational algorithm. Therefore, the nuclear envelope-targeting domain of CYDV-Y will have to be mapped physically.

The comparative analysis of subcellular localization of virus proteins in a virus-free and virus-infected host cell is very useful for in-depth studying of their function and mechanism in the virus biology (Grummer *et al.*, 2001; Shen *et al.*, 2007). The differentiation of the subcellular localization pattern of CYDV-N, -P, and -M, in the CYDV-infected host cell, compared to those in the virus-free cell indicates the extensive alteration of host cell environment by the virus infection, especially nucleus. Virus infections cause a global change in alternative splicing of host mRNAs (Boudreault *et al.*, 2016; Mach *et al.*, 2015). Also, this may result in the modification of interaction domains of host factors that mediate virus-host interaction (Wu *et al.*, 1993).

The phylogenetic tree demonstrates that plant-adapted rhabdoviruses are grouped according to their arthropod vectors (Grummer *et al.*, 2001; Shen *et al.*, 2007). The result supports that the host-vector interaction is an evolutionary driving force of speciation for this group of viruses (Bourhy *et al.*, 2005; Dietzgen *et al.*, 2016). The adaptation of viruses to their new vectors or hosts

will be affected by virus-compatible interaction domains in host factors that pre-exist in newly introduced hosts, or sufficiently rapid optimising of the virus population in the new vectors or hosts in the early stage of invasion into the cell that allows better utilising host cellular machinery, avoiding from host defense mechanism and optimising virulence (Longdon *et al.*, 2014). Interestingly, CYDV-X is more closely related to EMDV-X (Babaie *et al.*, 2015) than to SYDV-X. There is no obvious evidence for genome recombination between or among plant-adapted rhabdoviruses but regarding the viruses share common solanaceous hosts, they may have had such an opportunity (Parrella *et al.*, 2016).

Matrix protein of rhabdoviruses condenses the nucleocapsid and mediate association with the glycoprotein and acquirement of envelope (host-derived membrane) during morphogenesis (Anderson *et al.*, 2018; Graham *et al.*, 2008; Solon *et al.*, 2005). The detailed molecular mechanism and related functional domains of M proteins in the processes are still unclear for the nucleorhabdoviruses (Anderson *et al.*, 2018; Bejerman *et al.*, 2015; Sun *et al.*, 2018). However, an obvious thing is M proteins of nucleorhabdoviruses have to gain access to nucleus during their infection to perform their role for virus maturation (Anderson *et al.*, 2018). Therefore, mapping of the functional domains in matrix protein is essential for understanding the molecular and cellular aspect of the protein (Ozawa *et al.*, 2007; Sanderfoot *et al.*, 1996; Whittaker *et al.*, 1998). The re-direction of a portion of GFP-fusion signal into nucleus from cytoplasmic region by deletion of aa 244-553 residues from the aa 211-253 fragments of SYDV-M^{wt}, -M^{LL223AA}, and -M^{KR225AA} supports the functionality of previously expected NES domain in the deleted region. Lacking perinuclear membrane-associated GFP signal of the SYDV-M^{LL223AA} aa 211-243 fragment is supportive evidence of the membrane association of 223LL225 amino acid residues that reported by Anderson *et al.*, (2018). According to the amino acids alignment result, the NLS and NES domains are conserved in the matrix proteins of both CYDV and SYDV. This may indicate that the commonly shared regions critically function in the nucleotropic biology of PYDV (Fleith *et al.*, 2016). In our

previous research, Min *et al.*,(2010) suggested that partially condensed nucleocapsids by M mediate the cell-to-cell transmission of nucleorhabdovirus. If the functional domains of SYDV-M are active during virus infection, based on the collective information above, the role of M in cell-to-cell movement of PYDV exporting the nucleocapsids to the cell periphery using the interaction of M with N, Y, and G can be suggested (Anderson *et al.*, 2018; Bandyopadhyay *et al.*, 2010). Y protein is the cognate of SYNIV-sc4 protein which is characterized as a movement protein (Bandyopadhyay *et al.*, 2010; Min *et al.*, 2010). N is a structural protein which forms the ribonucleoprotein complex (Luo, 2007). SYDV G/M interaction mediated the cytoplasmic localization of SYDV-M (Bandyopadhyay *et al.*, 2010). Based on these data, we propose a “catch and release” model that explains the role of M protein in virus transmission from cell to cell. In this model, a portion of M in the nucleus ‘catch’ the N of RNP complexes to mediate the export of capsid cores from the nucleus to cytoplasm with G protein association. Afterward, Y protein in cytoplasmic space interacts with the M of the RNP complexes and then direct the infectious units to the vicinity of plasmodesmata to ‘release’ them into neighbor cells for following cell-to-cell movement.

While trying to rescue the infectious virus from cDNA clone of CoRSV, we observed several intriguing phenomena by CoRSV-N and -P proteins. In our research, co-expression of CoRSV-N and -P induced intranuclear viroplasm-like structure and particularly the CoRSV-P was capable of inducing a morphological change of nucleus via ER-membrane rearrangement which is the first report from dichoravirus. Kondo *et al.*, reported that *Orchid fleck virus* (OFV) could induce intranuclear viroplasm-like structure (VpLS) by OFV-N and -P co-expression, however, either single expression of N or P did not induce any morphological change of nucleus (Kondo *et al.*, 2013). We have not investigated the host membrane association of CoRSV-P in amino acids level in this research, however it has been reported that rhabdovirus P proteins interact with host endomembrane, cytoskeleton, and nucleocytoplasmic trafficking carriers (Hsieh *et al.*, 2010; Rowe *et al.*, 2016; Leyrat *et al.*, 2011; Leopold *et al.*, 2006). The inhibited DAPI uptake of nucleus by

simultaneous expression of CoRSV RNP components including RNA1, 2, N, P and L was observed. While we do not have clear answers to explain this phenomenon, the extremely swollen nuclei, chromatin margination, and inhibited translation of GFP which is flanked by CoRSV leader and trailer sequence indirectly indicate that the RNP complexes of CoRSV are not ordinarily exported from nucleus (Edens *et al.*, 2013; Ganguly *et al.*, 2016; Levy *et al.*, 2010). We are strongly suspect that the inhibited export of RNP from nucleus can be closely related to the alternation of chromatin structure of host cell (Knipe *et al.*, 2013; Lieberman *et al.*, 2006; Nagamine *et al.*, 2008).

To generate more experimental evidence supporting the hypotheses above, development of the reverse genetic system for these viruses and detailed biochemical characterization of rhabdoviral protein complexes are required, with particular attention paid to the determination of the binding affinities for viral protein interactions which are shown this research. Reverse genetic system for these viruses also will assists research to elucidate the *in-situ* functions of the proteins or the two strains of PYDV and CoRSV. To be specific, rescuing PYDV from cDNA clone will facilitate straight comparative analysis between CYDV and SYDV through modification cis-elementary sequences, gene deletion, swapping, and rearrangement between the two virus. In this research, CoRSV showed noticeable possibility as a research tool for study of plant nuclear factors and endomembrane system via the chromatin margination and ER-membrane rearrangement by its N and P protein expression. We also need to extend our focus for CoRSV study to that how the virus maintain the nuclear envelope structure during its infection even though the single expression of CoRSV-P capable to perturb the ER-membrane structure. This approach will provides more opportunities to understand the protein interactions and activities of the host and virus during nucleotropic infection. Establishing reverse genetic system is crucially required for the study. These future approaches will broaden our knowledge of the cellular and molecular aspects of the viral proteins in the interactions among plant-adapted rhabdoviruses, plant hosts and insect vectors.

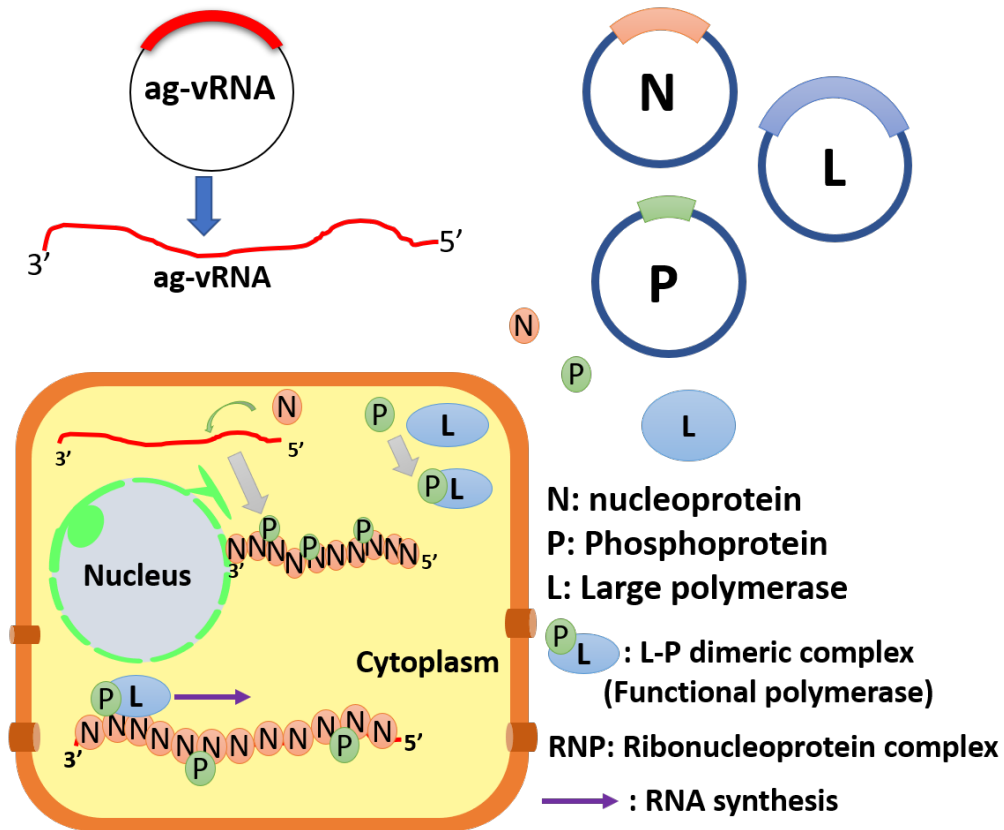


Figure 4.1. Common strategy for recovery of negative-strand RNA virus. (1) Expression of antigenomic viral RNA (ag vRNA) having precise 5' and 3' terminus is required. (2) The viral genome must be encapsidated by the nucleocapsid protein. (3) The viral RNA-dependent RNA polymerase (P-L complex) is essential for viral genome and mRNA synthesis. (4) The encapsidated viral genome and the polymerase should be produced in the host cell simultaneously to produce ribonucleoprotein (RNP) complex in the susceptible cell to initiate transcription.

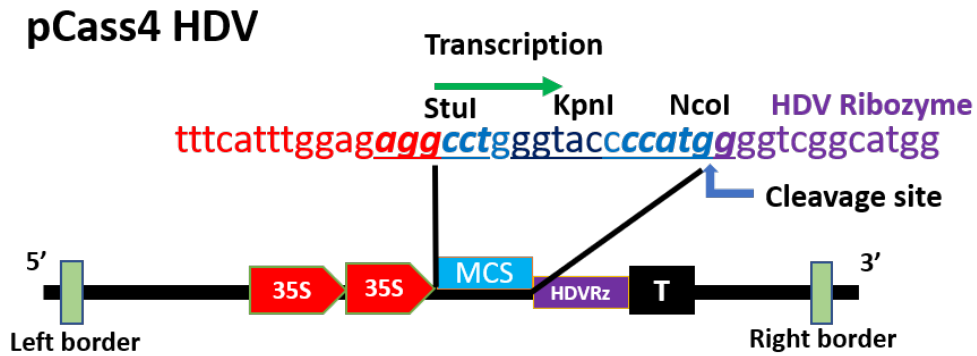


Figure 4.2. Map of pCass4HDV. The left border and right border are marked as a green box. Cauliflower mosaic virus duplicated 35S promoter is marked as a double red arrow in green outline. The 35S terminator is marked as a black box. The multi-cloning site is located between the 35S promoter and 35S terminator. The transcription start site of the modified 35S promoter and self-cleavage site of HDV ribozyme are marked using bold arrow.

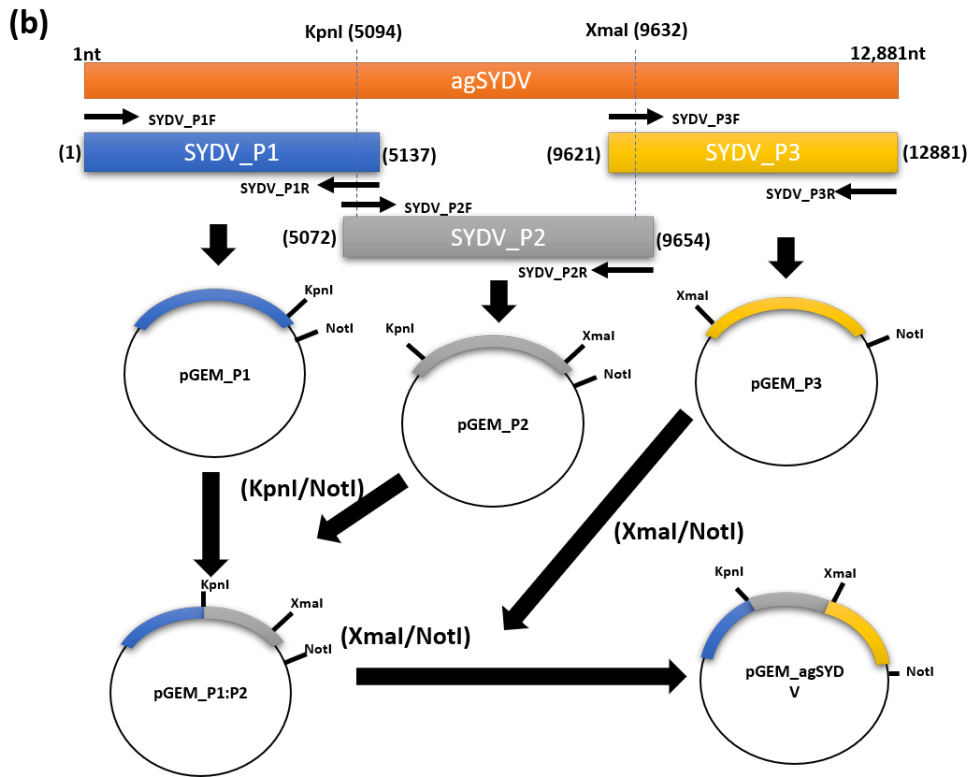
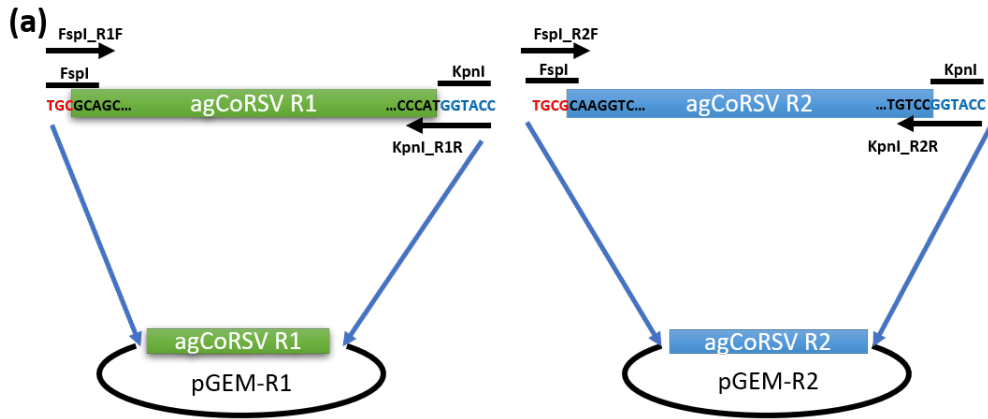


Figure 4.3. Schematic diagram for construction of full-length antigenomic sequence in the pGEM-T easy vector (a) Construction of pGEM-R1 and pGEM-R2. The antigenomic sequence of CoRSV RNA 1 and RNA 2 was amplified using corresponding primer sets, Fsp_R1F/KpnI_R1R and Fsp_R2F/KpnI_R2R. The primer sets introduced FspI and KpnI on the 5' and 3' termini of agRNA1 (green box) and agRNA2 (blue box) respectively. The antigenomic cDNAs were sub-cloned into pGEM T-easy vector. The nzyme sites were labeled using overbar on the corresponding sequence. (b) Construction of pGEM_agSYDV. The three PCR fragments were used to generate entire antigenome of SYDV. SYDV_P1 (blue box), SYDV_P2 (Gray box), and SYDV_P3 (yellow box) were sub-cloned into pGEM. The SYDV-P2 fragment which is excised from pGEM_P2 was sub-cloned into the KpnI /NotI treated pGEM_P1 to generate pGEM_P1:P2. The XmaI/NotI fragment including SYDV-P3 were cloned into XmaI/NotI treated pGEM_P1:P2 to assemble entire sequence in the pGEM T-easy vector.

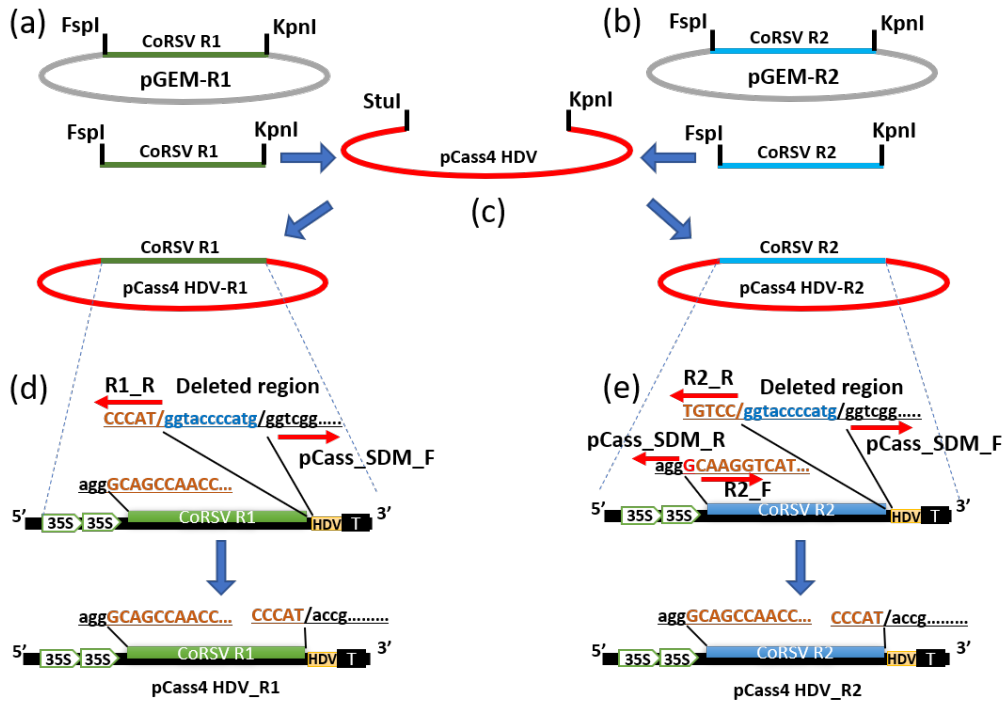


Figure 4.4. Schematic diagram for construction of pCass4 HDV_R1 and pCass4 HDV_R2 (a-b) Extraction of CoRSV R1 and CoRSV R2 from pGEM-R1. (c)The CoRSV RNA 1 and RNA2 were cloned into the pCass4HDV, StuI and KpnI treated (d-e) The extra sequences between, CoRSV R1/ribozyme, CoRSV R2/ribozyme, and 35Sp/RNA2 were removed using site-directed deletion mutagenesis.

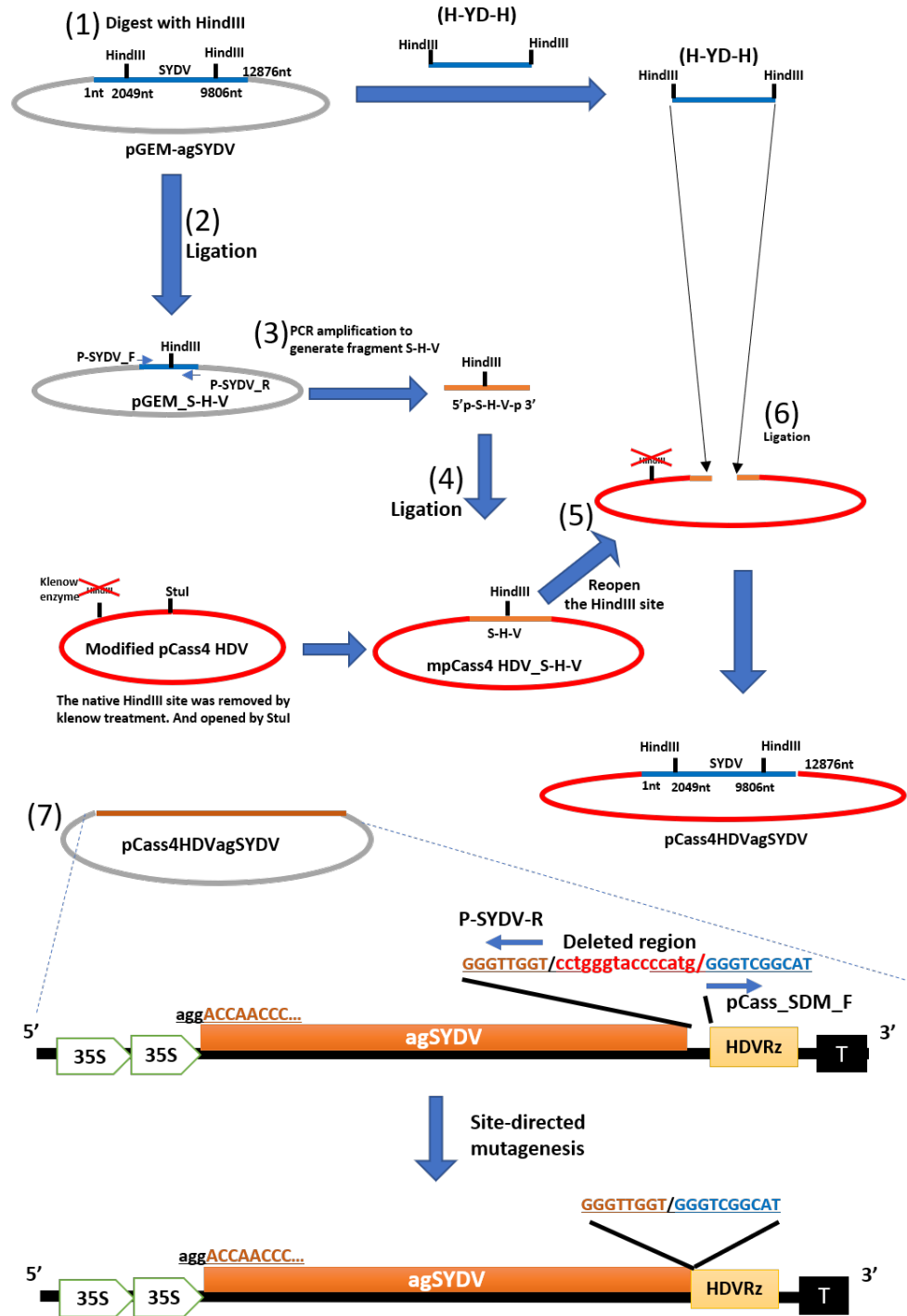
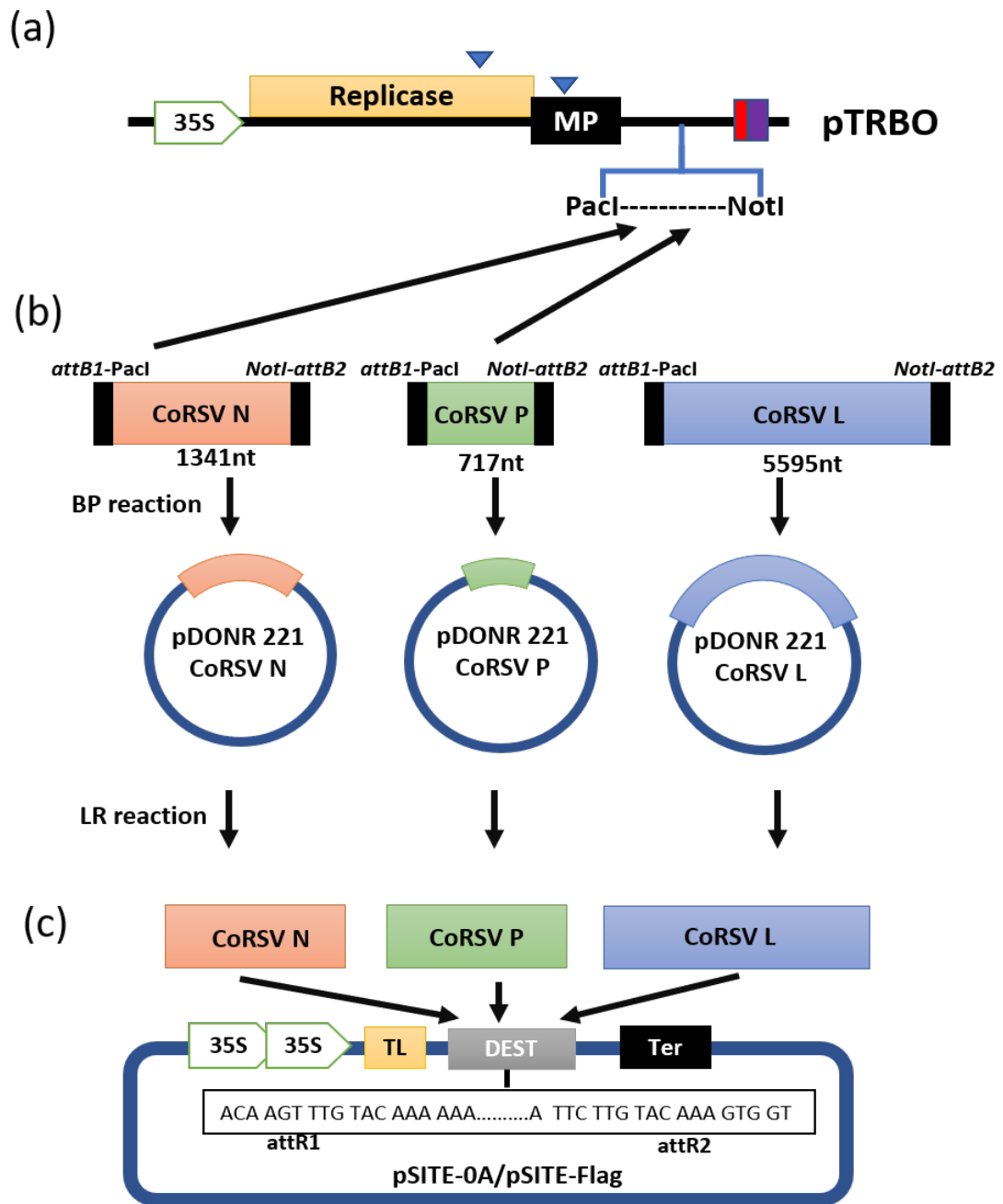


Figure 4.5. Schematic diagram of pCass4 HDVagSYDV construction. (1) HindIII digestion cut the pGEM-asSYDV into two fragments, 'H-YD-H' and the remaining. (2) Re-ligation of the remaining generates pGEM_S-H-V. (3) The S-H-V part was amplified using phosphorylated primer pair, P-SYDV_F/P_SYDV_R. (4) The 5' p-S-H-V-p 3' part was inserted to the StuI site of mpCass4HDV to generate mpCass4HDV_S-H-V. (5) mpCass4HDV_S-H-V was reopened by HindIII digestion. (6) The fragment 'H-YD-H', which was generated in the step (1), was inserted to the HindIII site located in S-H-V. The orientation of the insert was confirmed through KpnI digestion. (7) The extra region between agSYDV and HDV ribozyme was removed by site-directed PCR deletion.



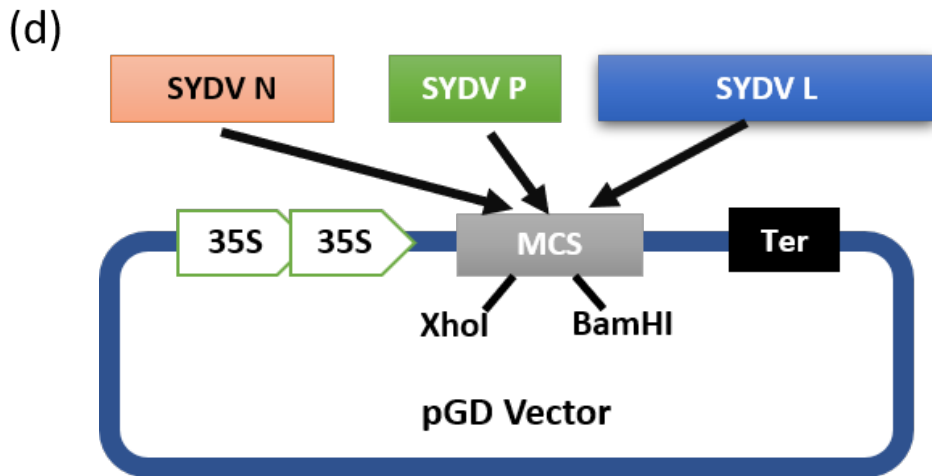


Figure 4.6. Construction of N, P, and L expression vectors for CoRSV and SYDV. (a) Map of the pTRBO vector (Lindbo, 2007). Green outlined arrow, CaMV 35S promoter. Reverse triangle, subgenomic promoter. Red box, CaMV polyA signal sequence/terminator. Violet box, Ribozyme. CoRSV-N and CoRSV-P was cloned into pTRBO (b) The cDNAs of CoRSV-N, -P, and -L were cloned into pDONR 221. The adapter ‘attB1-PacI’ and ‘NotI-attB1’ sequences were introduced to the 5’ and 3’ termini of the genes. (c) CoRSV-N, -P, and -L were cloned into pSITE-0A and pSITE-FLAG. (d) SYDV N, P, and L were cloned into pGD vector using XhoI and BamHI sites. Green box arrow, CaMV 35S promoter; Grey box, multi-cloning sites; Black box: 35S terminator.

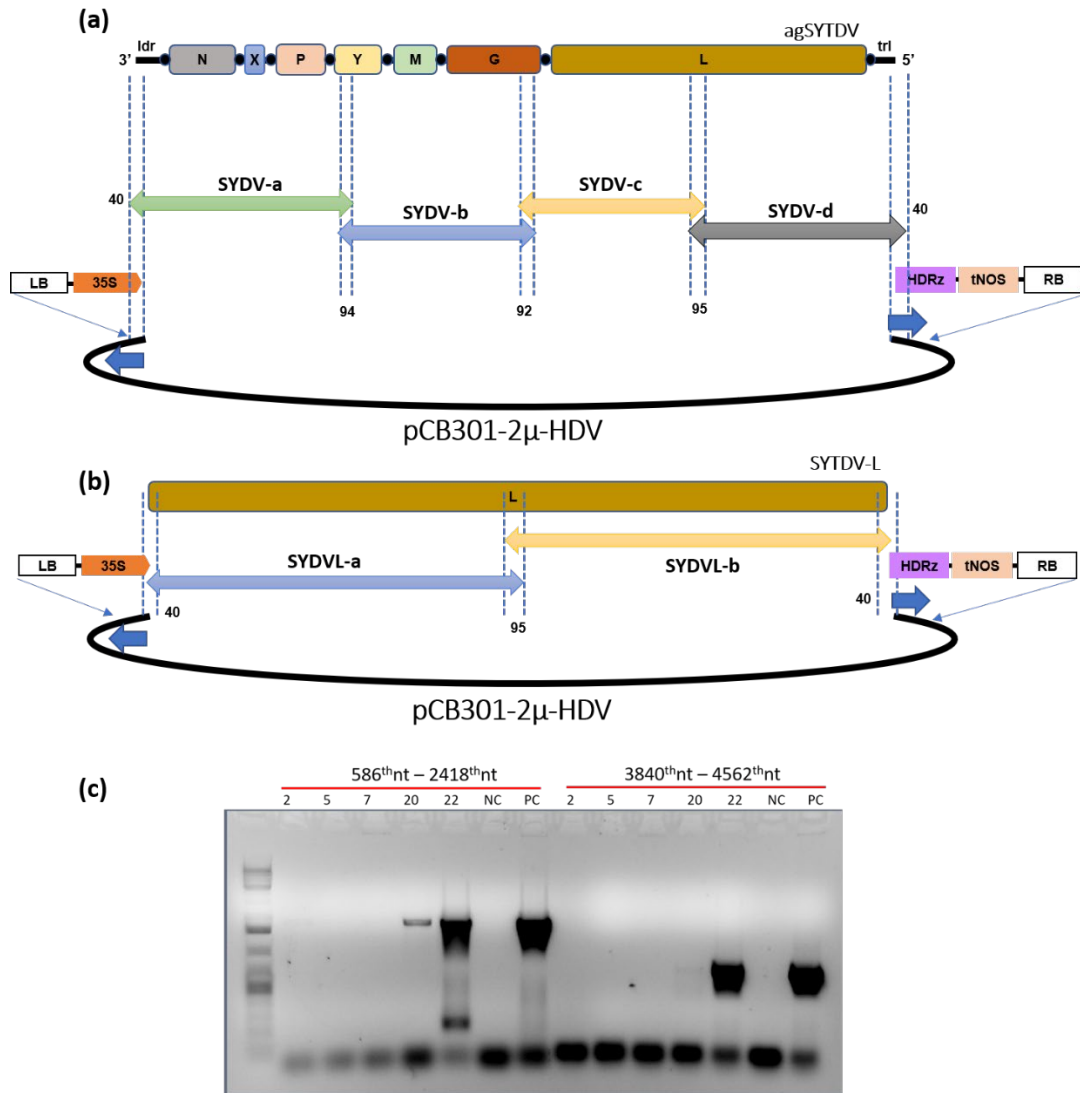


Figure 4.7. Construction of full-length antigenome and L of SYDV using yeast mediated homologous recombination. (a) Full-length agSYDV assembly by yeast. The four fragments a, b, c, and d were labeled as double arrow box with color (a, green; b, blue; c, yellow; d, grey). The heads of the arrows represent the overlapping region. Linearized pCB301-2μ-HDV is depicted as the black line. (b) assembly of SYDV L in the yeast cell through yeast homologous recombination. The two parts of SYDV L, SYDVL-a (blue double arrow box) and SYDVL-b (yellow double arrow box), were assembled to generate entire SYDV L. in pCB301-2μ-HDV. (c) The results of yeast mediated homologous recombination for SYDV L.

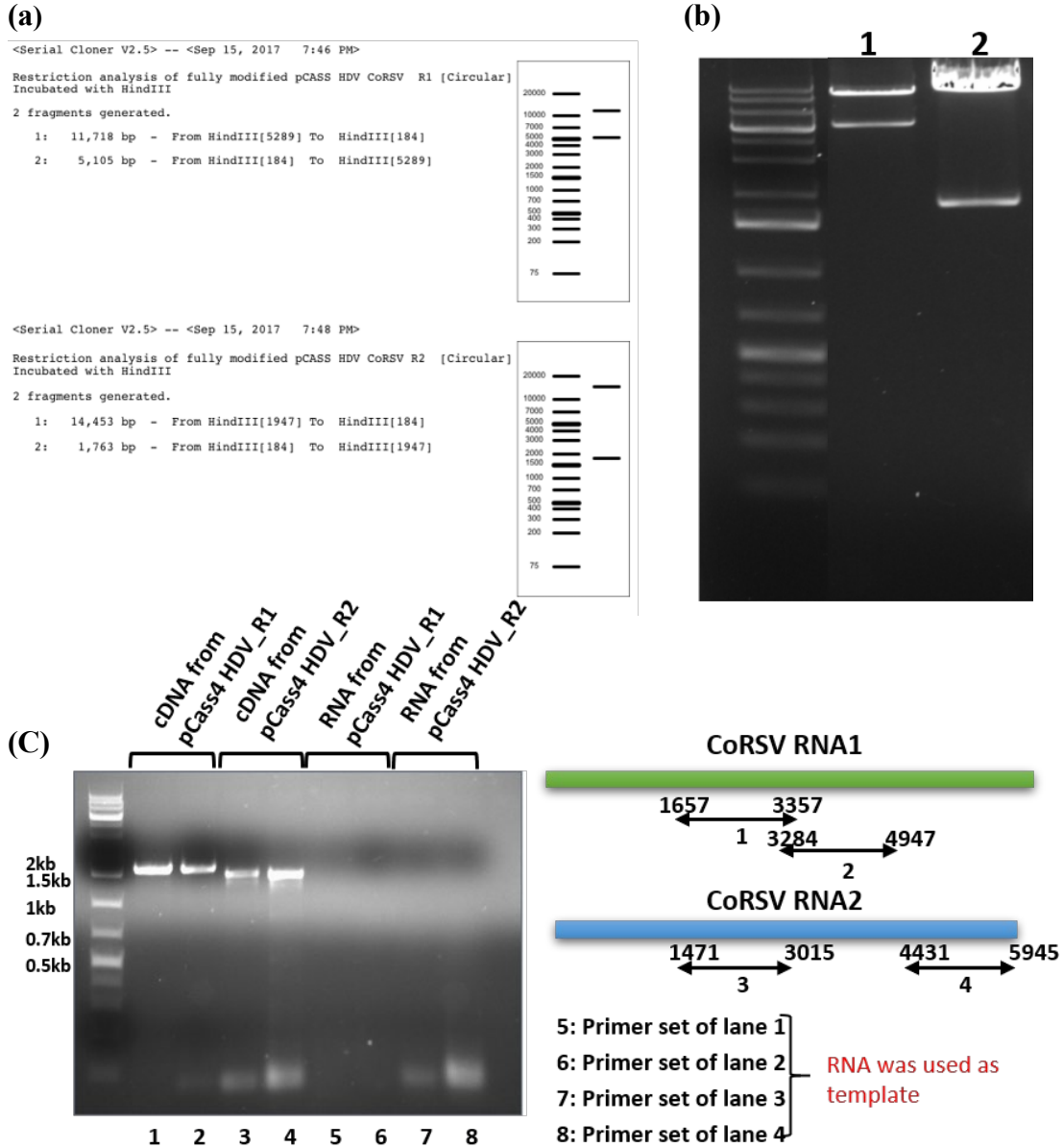


Figure 4.8. Expression of CoRSV RNA1 and RNA2 from pCass4HDV (a) *in silico* digestion pattern of pCass4 HDV-R1 and pCass4 HDV-R2 by HindIII. (b) The gel image of HindIII treated pCass4HDV-R1 (lane 1), and pCass4HDV-R2 (lane 2) (c) RT-PCR result from pCassHDV-R1 and pCassHDV-R2 infiltrated *N. benthamiana*. Lane 1: RNA1, 1657-3357, Lane 2: RNA1, 3284-4947, Lane 3: RNA2, 1471-3015, Lane 4: RNA2, 4431-5945. From lane 5-8: Same primer pairs corresponding to lane 1 to lane 4 respectively, but RNA was used as a PCR template instead of cDNA to confirm DNA contamination.

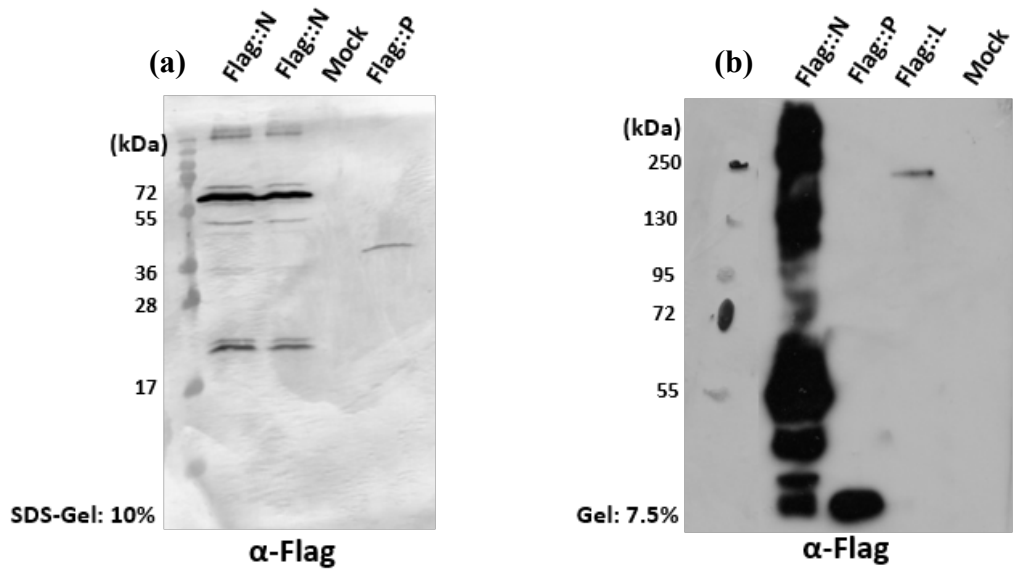


Figure 4.9. Expression of FLAG-fusion of CoRSV-N, -P, and -L from pSITE-FLAG. (a) Colorimetric development of FLAG fusion proteins, N and P of CoRSV, on PVDF membrane. (b) Chemiluminescent detection of FLAG-fusion of CoRSV-N, P, and L on X-ray film.

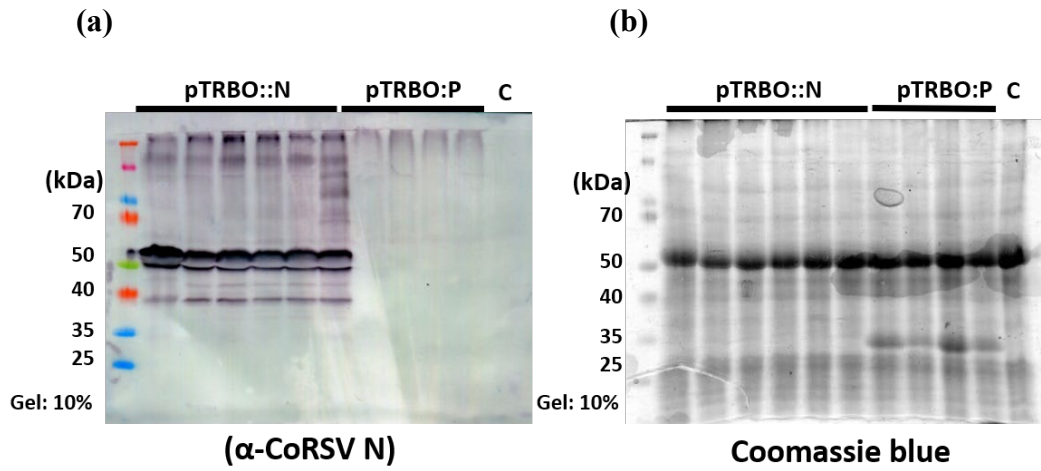


Figure 4.10. Expression of CoRSV-N and -P protein from pTRBO vector. (a) Immunoblotting assay specific to CoRSV-N. Two major bands were detected around 50 kDa size marker. (b) The CoRSV-P protein expression were detected from the SDS-PAGE gel by Coomassie blue staining. P protein bands were observed around 35kDa marker.

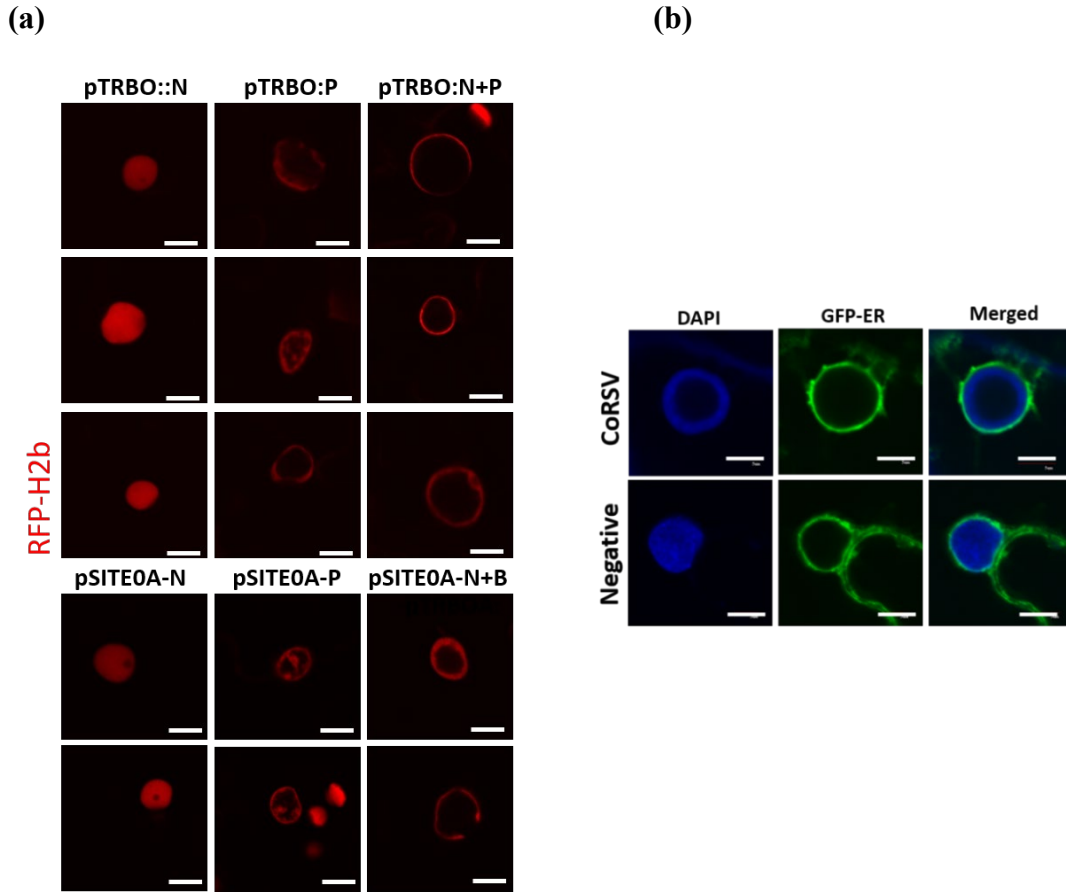


Figure 4.11. Formation of viroplasm like structure (VpLS) by CoRSV-N and -P, in the nuclei of RFP-H2b-expressing transgenic *N. benthamiana*. (a) Expression of CoRSV-N (left column), CoRSV-P (middle column), and co-expression of CoRSV-N and -P (right column) in transgenic nuclear marker, RFP-H2B, *N. benthamiana*. All images were taken 72 hours post infiltration. (b) CoRSV: The DAPI-stained nuclear in CoRSV infected transgenic GFP-ER marker plant, *N. benthamiana*, upper row. Mock: Nuclear DAPI staining of Mock inoculated (pTRBO only), *N. benthamiana* (GFP-ER), bottom row. Scale bar = 10 μ m.

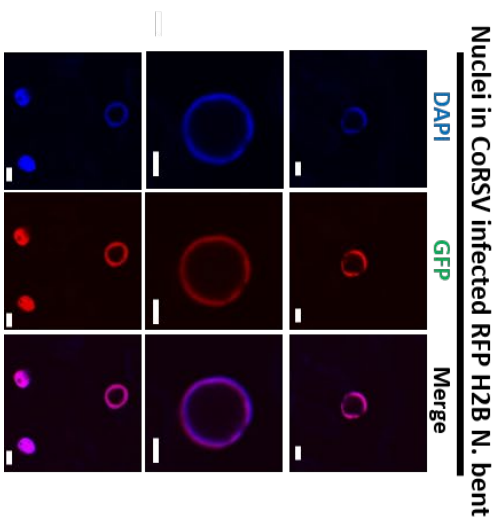
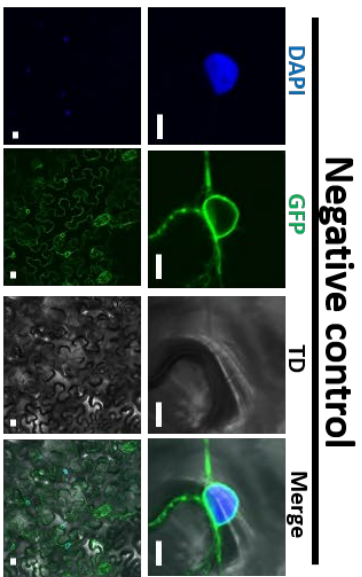
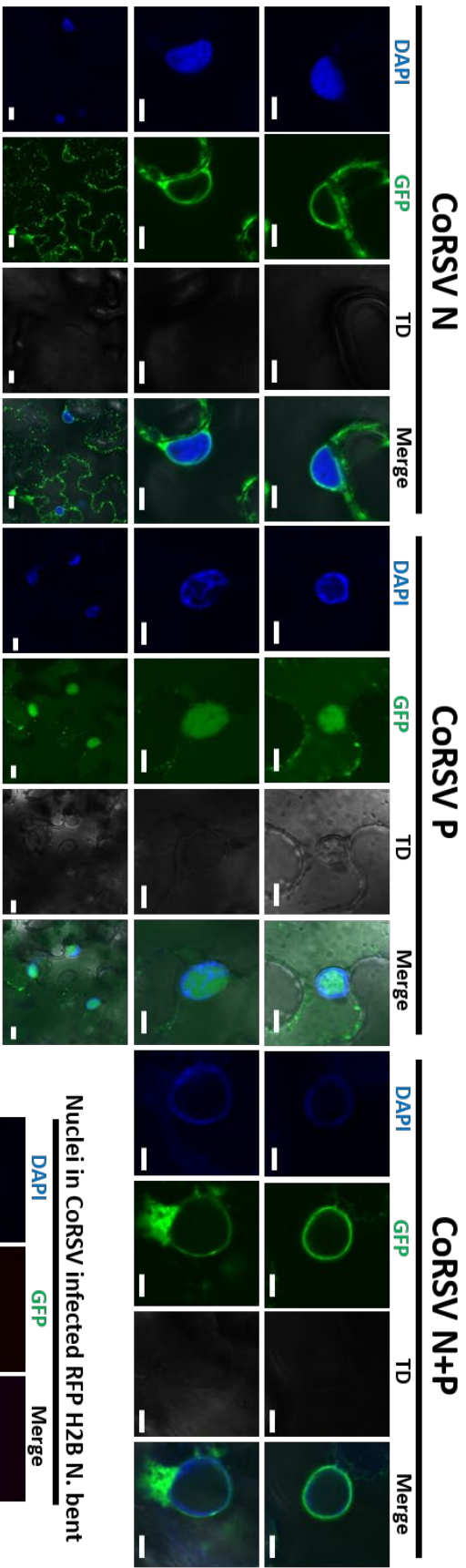


Figure 4.12. GFP-ER signal accumulation in the subnuclear space by CoRSV-P expression. N expression from pTRBO vector did not induce any difference in nucleus (DAPI) and ER-membrane (GFP) compared to mock. The single expression of P formed a subnuclear space in the nucleus (DAPI) and GFP-ER signal was accumulated in the subnuclear space (GFP). The inner boundary of the subnuclear space induced by P was more irregular than the VpLS formed by N and P co-expression and the true viroplasm induced by CoRSV. The size of nuclei under p expression was not different from those of N expression. ER accumulation in the sub-nuclear space was not detected. Scale bar = 5 μ m.

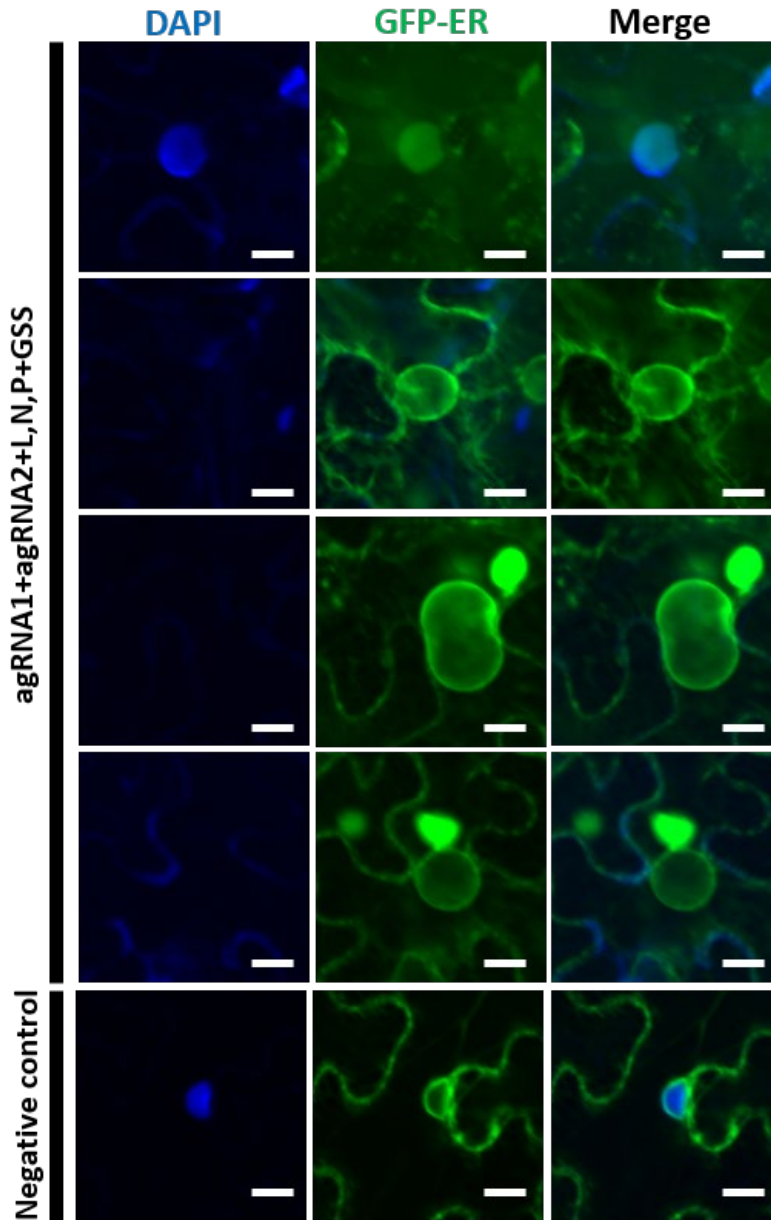
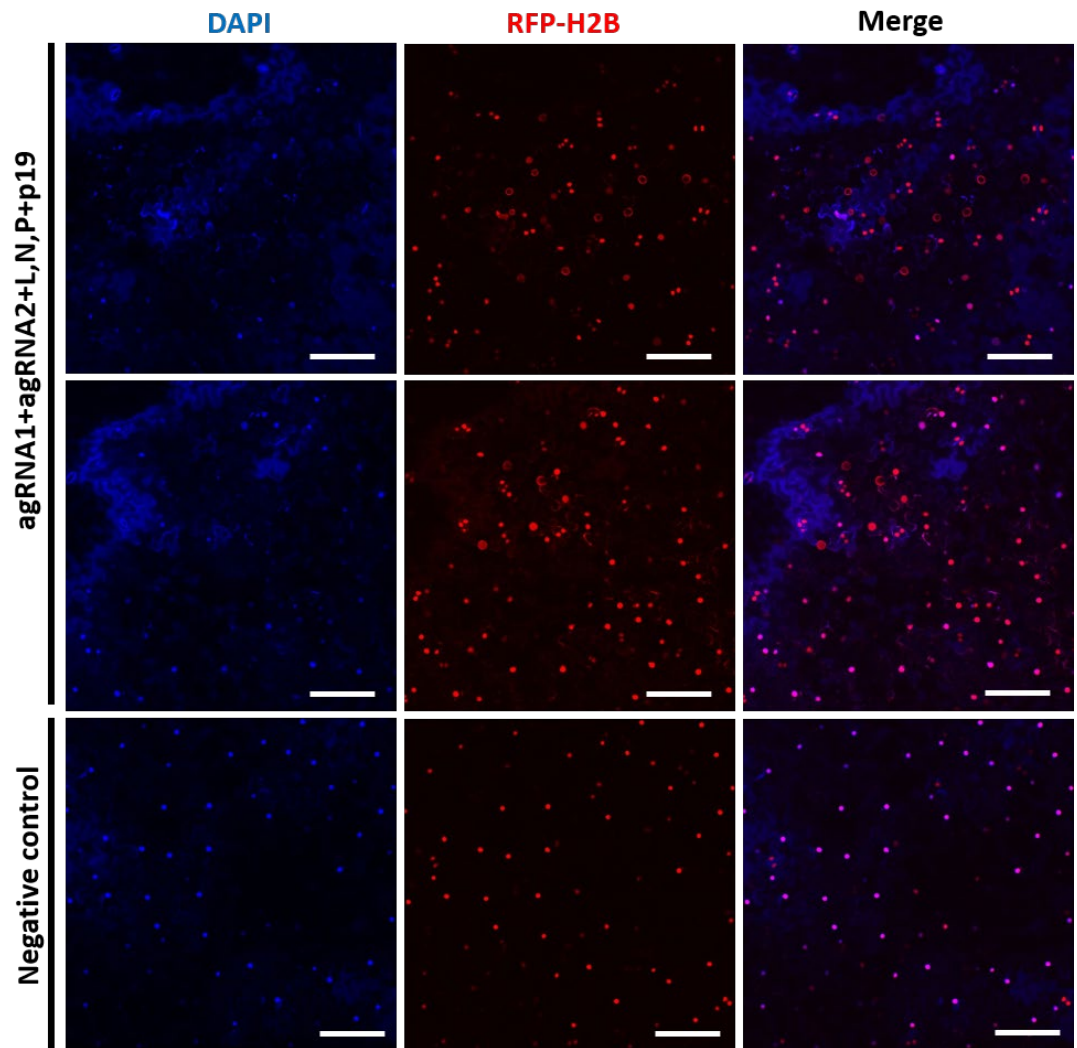
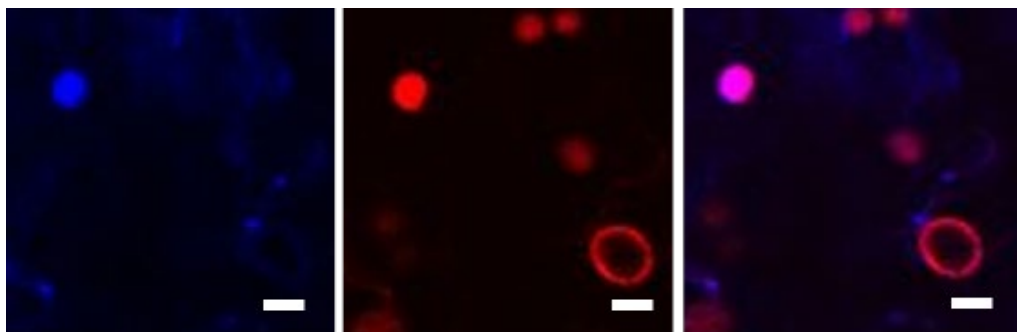


Figure 4.13. Inhibited DAPI staining of nuclei in GFP-ER *N. benthamiana* with simultaneous expression of CoRSV agRNA1, agRNA2, N, P, and L. Scale bar = 10 μ m.

(a)



(b)



(C)

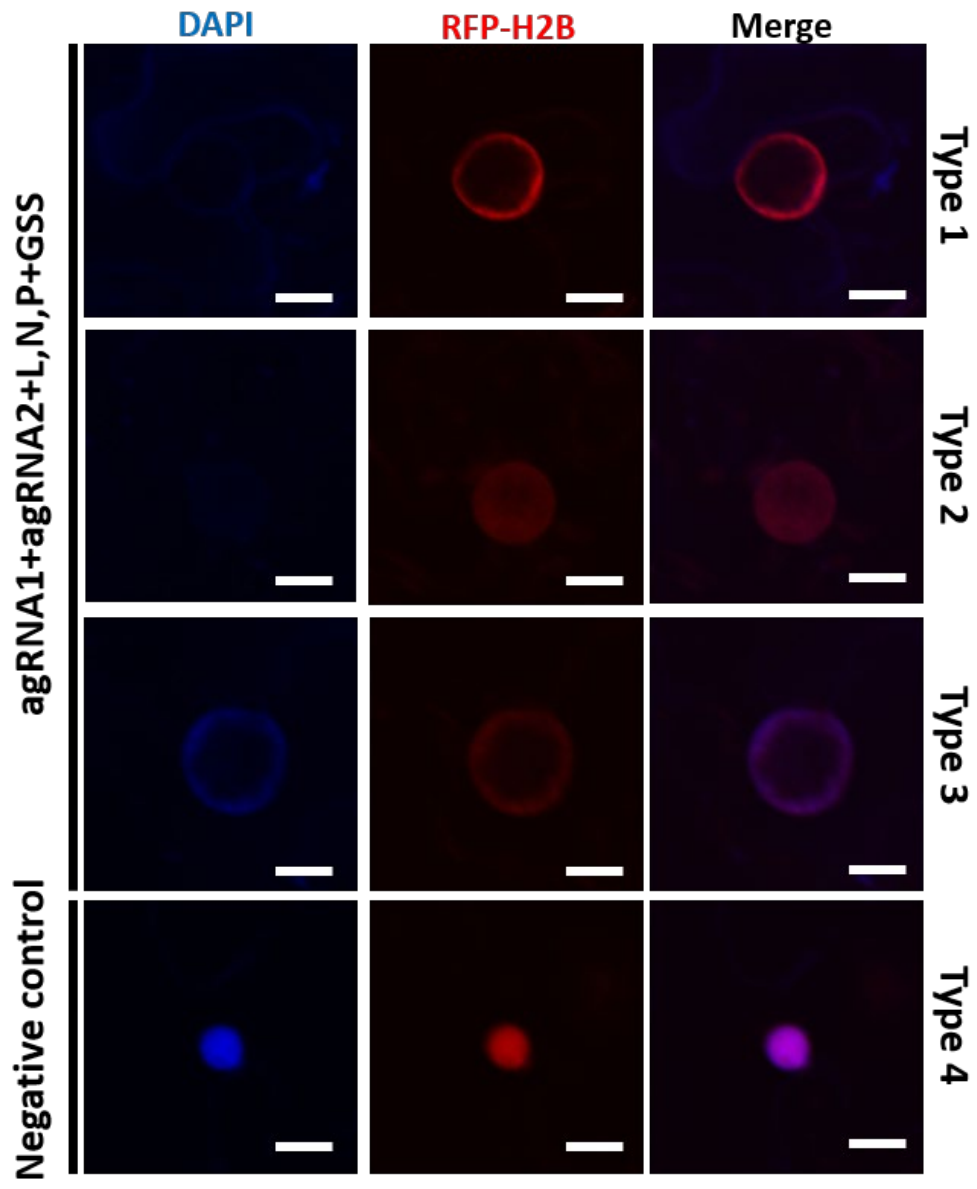


Figure. 4. 14. Size-dependently inhibited DAPI staining under simultaneous expression of viral RNAs, and N, P, and L in RFP H2b *N. benthamiana*. (a) Confocal image of DAPI stained RFP-H2B plant expressing agRNA1/agRNA2/N/P/L. The most of enlarged nuclei having VpLS remained red in merged image. Otherwise, nuclei in the of normal state compared to mock, appeared to be purple. (b) Comparison of the DAPI staining intensity according to size of nucleus. (C) The nuclei in the infiltrated plant were categorized into 4 types according to its appearance: Type1, the nucleus with VpLS, expansion, and no DAPI staining; Type 2, the expanded nucleus without VpLS, no DAPI staining; Type 3, Nucleus with expansion and staining; Type 4, Nucleus in normal state with DAPI staining. negative control. Total 155 nuclei were counted. Type 1: 28% (44/155); Type 2 18% (30/155); Type 3: 2% (3/144); Type 4: 52 % (80/155). Scale bar = 10 μ m.

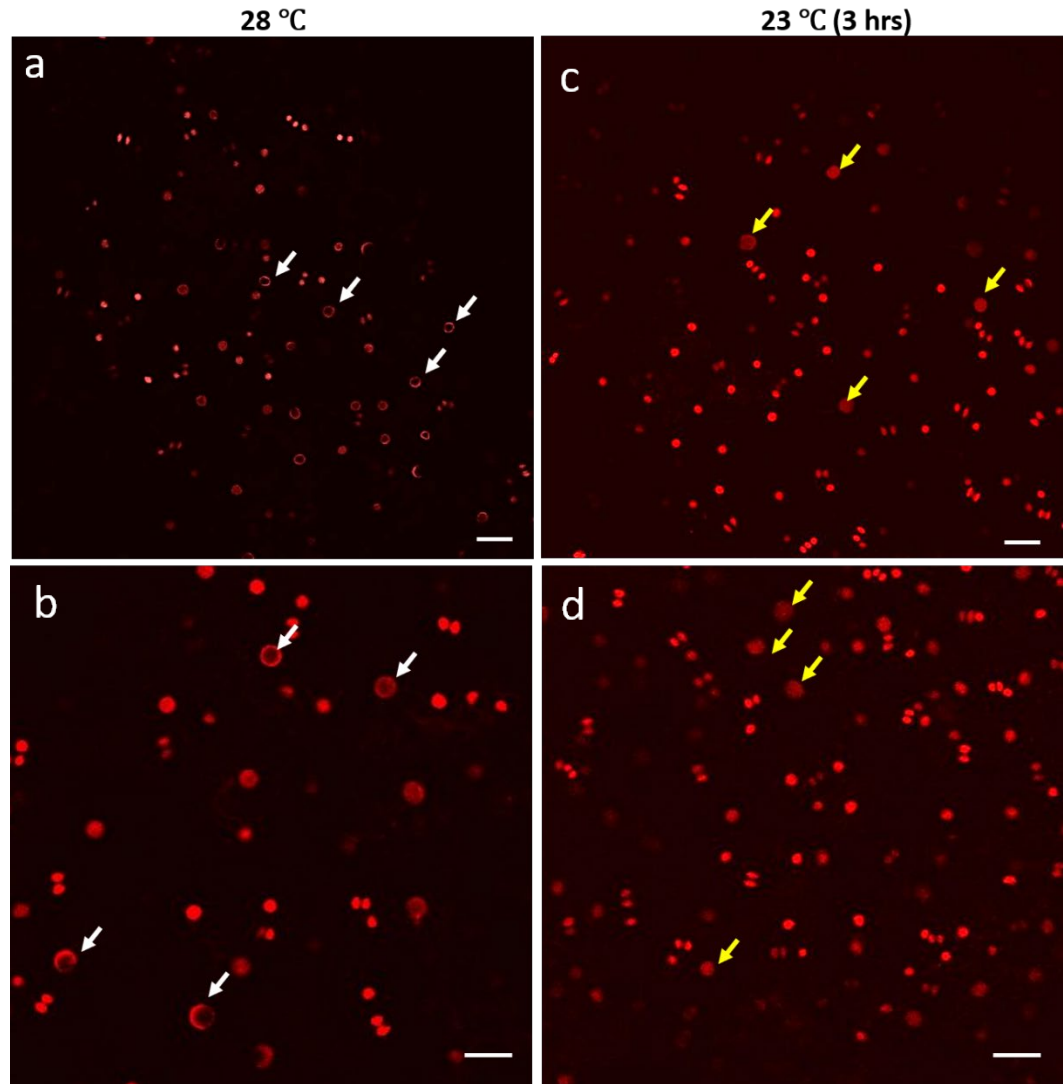


Figure 4.15. The alteration of VpLS pattern according to temperature in infiltrated plant. The Agroinfiltrated tissues were collected at 72 hpi. (a-b) At 28 °C, about 30% of nuclei were bigger than normal size (5-10 μ m) and the most of enlarged nuclei showed VpLS (white arrow). (c-d) After 3 hours incubation under 23°C, 38% of nuclei showed the size expansion, but without VpLS (Yellow arrow). Only 2 % of nuclei maintained the clear VpLS. The experiments were repeated three times and total 300 nuclei were randomly counted under the microscopic observation in each time (Table 3), Scale bar = 30 μ m.

Table 3. Number of the nuclei classified according to the shape at each temperature.

| Temp. | 28°C | | | 23°C (3 hrs) | | |
|--------------------------------|---|---------------------------------|------------------|------------------------------|---------------------------------|------------------|
| | No. of Enlarged Nuclei with VpLS | Enlarged nuclei without VpLS | Normal nuclei | Enlarged Nuclei with VpLS | Enlarged nuclei Without VpLS | Normal nuclei |
| 1 st observation | 42 | 4 | 54 | 4 | 48 | 48 |
| 2 nd observation | 17 | 1 | 82 | 0 | 25 | 75 |
| 3 rd observation | 32 | 5 | 63 | 3 | 41 | 66 |
| Avg (±SD) | 30 (±10.2) | 3(±1.7) | 66(±10.2) | 2(±1.7) | 38 (±9.6) | 63 (±11.2) |

(Temp., temperature; VpLS, viroplasm-like structure; Avg, average; SD, standard deviation)

Figure 4.16. Effect of temperature change on the ER localization pattern and the size of nucleus in the agroinfiltrated plant. Confocal (a) A low magnification view of microscopy (10X). The nuclei marked with arrow in the images were observed over time, at 0h (28°C), 1.5 h, 3 h, 10 h (23°C). (b) Two nuclei (1, 2) showed ER-signal accumulation (RFP) in the nucleus at 10h. The nucleus, No.3 showed rapid nuclear contraction at 1.5 h. (c) Noticeable size contraction were observed (yellow arrows). The targeted nuclei were photographed at 0h (28°C), 1.5h, 3h, and 10 h (23°C). (d) Mock inoculation. Red scale bar = 100 μm , White scale bar = 10 μm .

(a)

pSITE 0A::N
+
pSITE 0A::p
+
pSITE 0A::L
+
pCass4 R1 + pCass4 R2

Agroinfiltration.

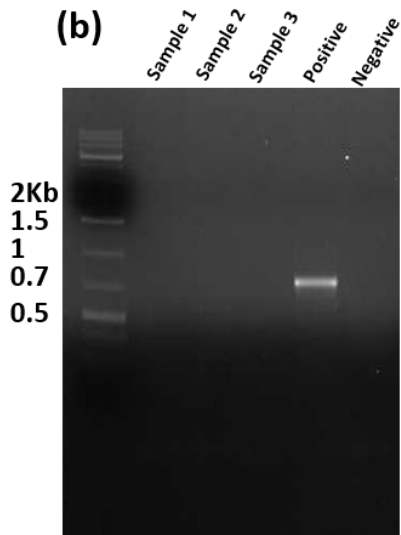


The plants are
incubated in 28 °C



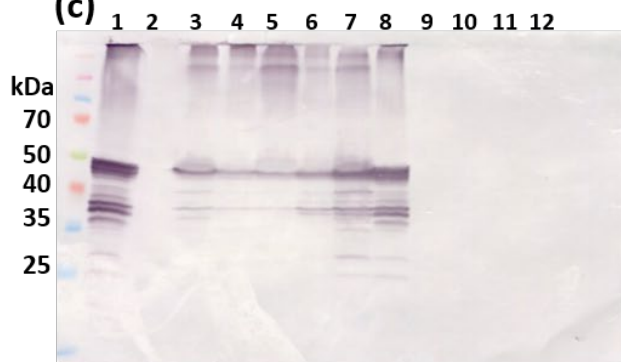
3WPI: Unusual appearances were
observed from the upper leaves.

(b)



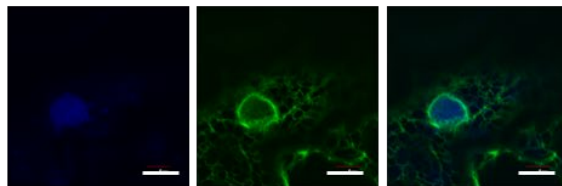
-Negative detection of
target gene (M).

(c)



α -CoRSV N

(d)



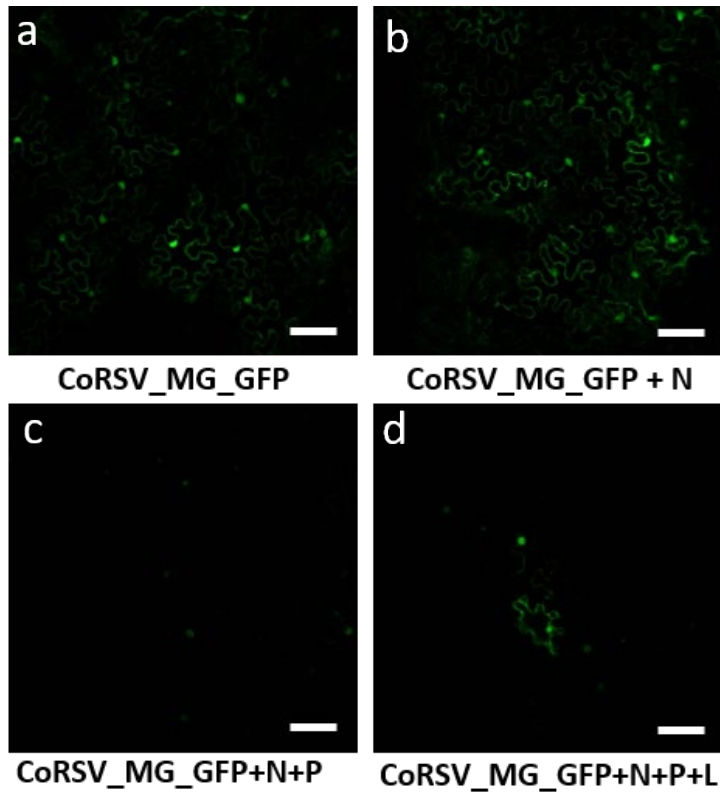
A cell image of the sample above

Figure 4.17. Test for recovery of infectious virus from the infiltrated plants (a) *Agrobacterium* cultures containing pCass4HDV-R1, pCass4HDV-R2, pSITE0A-N, pSITE0A-P, pSITE0A-L, pGD-p19, pGD-pYB, and pGD-HC-Pro were mixed and infiltrated to *N. benthamiana*. The plants were maintained in 28 °C. A few plants showed marginal yellowing, small yellow spots, and crinkling on the leaves above the infiltrated leaves that were distinct from mock, at 3 weeks post infiltration. (b) Non-detection of viral genome and/or mRNA in the plants showing distinct phenotype. (c) Non-detection of CoRSV-N protein in the plants. Lane 1, pSITE0A-N (positive sample); Lane2, pSITE0A-P (Negative); Lane 3-5, pSITE 0A-N/pSITE 0A-P/pSITE 0A-L/pCass4HDV-R/pCass4HDV-R2/pGD-GSSs (sampled at 3 DPI); Lane 6-8, repeat of lane 3-5 (sampled at 7 DPI); Lane 9-11, samples from the leaves showing phenotypical change; Lane 12, Mock inoculation. (d) Non-detection of viroplasm in the nuclei in the plants. Bar=10µm. Same experiments were repeated more than 10 times.

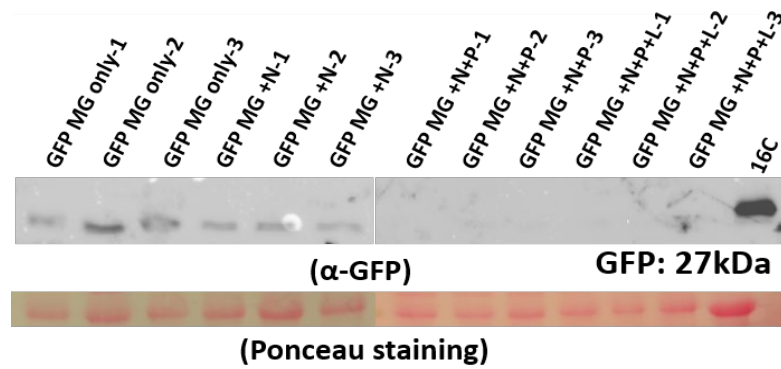
(a)



(b)



(c)



(d)



(e)

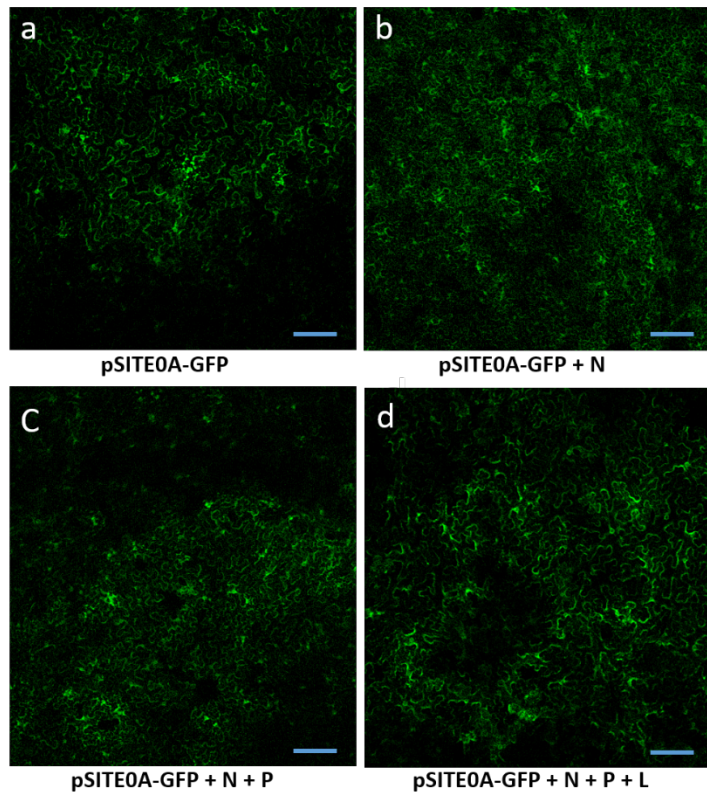


Figure 4.18. CoRSV leader and trailer sequence specific inhibition of GFP by CoRSV-N and -P co-expression. (a) Map of pCass4HDV-CoRSVMG_GFP. Green box arrow, CaMV 35S promoter; Red box, leader sequence of CoRSV; Green box, GFP; Blue box, trailer sequence of CoRSV, Yellow box; HDV ribozyme; Black box, 35S terminator. (b) N and P co-expression inhibited the GFP expression from pCass4HDV-CoRSVMG_GFP. A, pCass4HDV-CoRSVMG_GFP only; b, pCass4HDV-CoRSVMG_GFP+N; c, pCass4HDV-CoRSVMG_GFP+N+P; d, pCass4HDV-CoRSVMG_GFP+N+P+L. Bar = 100 μ m. (c) Detection of GFP protein from the protein samples that used in (b). (d) Map of pSITE0A-GFP. Green box arrow, CaMV 35S promoter; Yellow box, *Tobacco etch virus* translational leader; Green box, GFP; Black box, 35S transcriptional terminator (T). (e) GFP expression from pSITE0A with CoRSV-N and P proteins. a. pSITE0A-GFP only; b, pSITE0A-GFP+N, pSITE0A-GFP+N+P, pSITE0A-GFP+N+P+L. Bar = 200 μ m

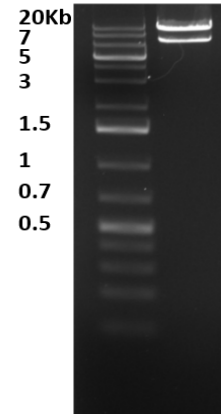
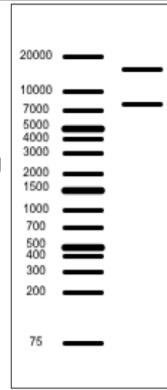
(a)

Restriction analysis of pCASS4HDV SYDV [Circular]
Incubated with HindIII

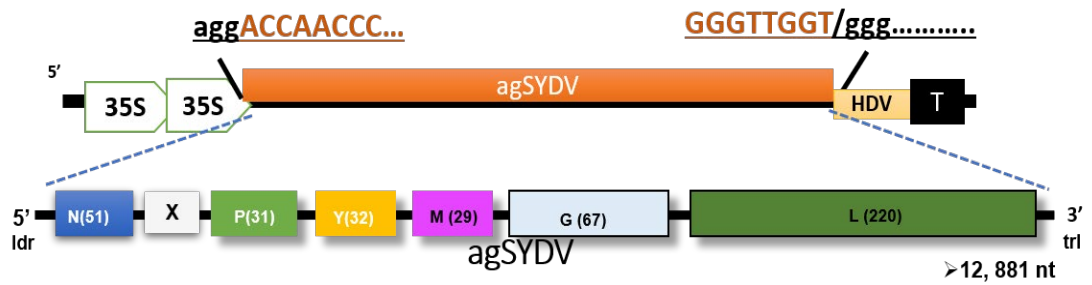
2 fragments generated.

1: 15,397 bp - From HindIII[10755] To HindIII[2998]

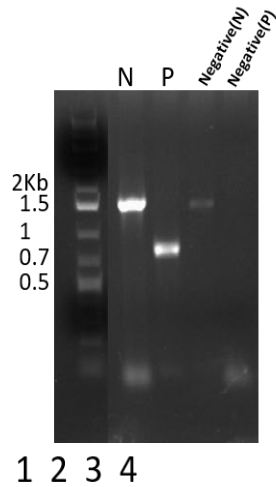
2: 7,757 bp - From HindIII[2998] To HindIII[10755]



(b)



(c)



(d)

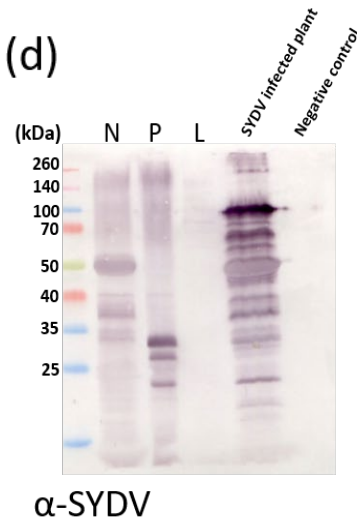


Figure 4.19. Expression of SYDV antigenomic RNA from pCass4 HDV_agSYDV, and SYDV -N, -P, and -L expression from pGD vector. (a) *in silico* HindIII digestion of pCass4 HDV_agSYDV and gel image of pCass4 HDV_agSYDV digested by HindIII. (b) Schematic representation of pCass4HDV_agSYDV (c) Detection of antigenomic RNA of SYDV using RT-PCR targeting N and P. Lane 1-2, PCR results using cDNA; Lane 3-4, PCR results using RNA. (d) Detection of N, P, and L protein expression using SYDV antibody

REFERENCES

1. Abraham, G. and A.K. Banerjee, Sequential transcription of the genes of vesicular stomatitis virus. *Proceedings of the National Academy of Sciences of the United States of America*, 1976. 73(5): p. 1504-1508.
2. Ahmed, M.E., et al., Lipid in Potato yellow dwarf virus. *Biochemical and Biophysical Research Communications*, 1964. 17(2): p. 103-107.
3. Albariño, C.G., et al., Reverse Genetics Generation of Chimeric Infectious Junin/Lassa Virus Is Dependent on Interaction of Homologous Glycoprotein Stable Signal Peptide and G2 Cytoplasmic Domains. *Journal of Virology*, 2011. 85(1): p. 112-122.
4. Alber, F., et al., The molecular architecture of the nuclear pore complex. *Nature*, 2007. 450: p. 695.
5. Albertini, A.A.V., et al., Molecular and Cellular Aspects of Rhabdovirus Entry. *Viruses*, 2012. 4(1): p. 117-139.
6. Alberts B, J.A., Lewis J, et al., *The Transport of Molecules between the Nucleus and the Cytosol. Molecular Biology of the Cell*. 4th edition. 2002.
7. Alves, C., N. Freitas, and C. Cunha, Characterization of the nuclear localization signal of the hepatitis delta virus antigen. *Virology*, 2008. 370(1): p. 12-21.
8. Ambroise Desfosses, E.A.R.J., Guy Schoehn, Danielle Blondel, Delphine Guilligay, Marc Jamin, Rob W. H. Ruigrok & Irina Gutsche, Self-organization of the vesicular stomatitis virus nucleocapsid into a bullet shape. *Nature Communications*, 2013. 4(1429).
9. Ammar, E.-D., et al., Cellular and Molecular Aspects of Rhabdovirus Interactions with Insect and Plant Hosts. *Annual Review of Entomology*, 2008. 54(1): p. 447-468.
10. Anderson, G., et al., Mapping the nuclear localization signal in the matrix protein of potato yellow dwarf virus. *Journal of General Virology*, 2018. 99(5): p. 743-752.
11. Anderson, G., et al., The Nucleocapsid Protein of Potato Yellow dwarf Virus: Protein Interactions and Nuclear Import Mediated by a Non-Canonical Nuclear Localization Signal. *Front Plant Sci*, 2012. 3: p. 14.
12. Anderson, G.L.F., Nuclear import and interactions of potato yellow dwarf virus nucleocapsid, matrix, and phosphoprotein. University of Kentucky, 2014.
13. Annamalai, P. and A.L.N. Rao, Packaging of Brome Mosaic Virus Subgenomic RNA Is Functionally Coupled to Replication-Dependent Transcription and Translation of Coat Protein. *Journal of Virology*, 2006. 80(20): p. 10096-10108.
14. Askjaer, P., et al., RanGTP-regulated interactions of CRM1 with nucleoporins and a shuttling DEAD-box helicase. *Mol Cell Biol*, 1999. 19(9): p. 6276-85.
15. Askjaer, P., et al., The Specificity of the CRM1-Rev Nuclear Export Signal Interaction Is Mediated by RanGTP. *Journal of Biological Chemistry*, 1998. 273(50): p. 33414-33422.
16. Assenberg, R., et al., Genomics and structure/function studies of Rhabdoviridae proteins involved in replication and transcription. *Antiviral Research*, 2010. 87(2): p. 149-61.
17. Atieh, T., et al., Haiku: New paradigm for the reverse genetics of emerging RNA viruses. *PLOS ONE*, 2018. 13(2): p. e0193069.

18. Babaie, G., et al., Complete Genome Sequence and Genome Analysis of Eggplant mottled dwarf virus-Iranian Isolate. *Journal of Phytopathology*, 2015. 163(5): p. 331-341.
19. Baldwin, R.L., Temperature dependence of the hydrophobic interaction in protein folding. *Proceedings of the National Academy of Sciences*, 1986. 83(21): p. 8069.
20. Ball, L.A. and C.N. White, Order of transcription of genes of vesicular stomatitis virus. *Proceedings of the National Academy of Sciences of the United States of America*, 1976. 73(2): p. 442-446.
21. Baltimore, D., A.S. Huang, and M. Stampfer, Ribonucleic Acid Synthesis of Vesicular Stomatitis Virus, II. An RNA Polymerase in the Virion. *Proceedings of the National Academy of Sciences of the United States of America*, 1970. 66(2): p. 572-576.
22. Bandyopadhyay, A., et al., An integrated protein localization and interaction map for Potato yellow dwarf virus, type species of the genus Nucleorhabdovirus. *Virology*, 2010. 402(1): p. 61-71.
23. Banerjee, A.K., Transcription and replication of rhabdoviruses. *Microbiol Rev*, 1987. 51(1): p. 66-87.
24. Barr, J.N., S.P. Whelan, and G.W. Wertz, cis-Acting signals involved in termination of vesicular stomatitis virus mRNA synthesis include the conserved AUAC and the U7 signal for polyadenylation. *Journal of Virology*, 1997. 71(11): p. 8718.
25. Barrus, M.F. and C.C. Chupp, Yellow dwarf of potatoes. *Phytopathology*, 1922. 12: p. 123-132.
26. Bass, H.W., et al., Chromosome condensation induced by geminivirus infection of mature plant cells. *J Cell Sci*, 2000. 113 (Pt 7): p. 1149-60.
27. Beeching, N.J., M. Fenech, and C.F. Houlihan, Ebola virus disease. *BMJ : British Medical Journal*, 2014. 349.
28. Bejerman, N., et al., Complete genome sequence and integrated protein localization and interaction map for alfalfa dwarf virus, which combines properties of both cytoplasmic and nuclear plant rhabdoviruses. *Virology*, 2015. 483: p. 275-83.
29. Bendtsen, J.D., et al., Improved prediction of signal peptides: SignalP 3.0. *J Mol Biol*, 2004. 340(4): p. 783-95.
30. Ben-Efraim, I. and L. Gerace, Gradient of Increasing Affinity of Importin β for Nucleoporins along the Pathway of Nuclear Import. *The Journal of Cell Biology*, 2001. 152(2): p. 411-418.
31. Bhasin, M., E.L. Reinherz, and P.A. Reche, Recognition and Classification of Histones Using Support Vector Machine. *Journal of Computational Biology*, 2006. 13(1): p. 102-112.
32. Bhattacharya, R., S. Basak, and D.J. Chattopadhyay, Initiation of encapsidation as evidenced by deoxycholate-treated Nucleocapsid protein in the Chandipura virus life cycle. *Virology*, 2006. 349(1): p. 197-211.
33. Bishop, D.H.L. and J.J. McSharry, *Rhabdoviruses*. 2018.
34. Bitancourt, A.A., A mancha anular, uma nova doenca do cafeeiro. . *O biologico* 1938. 4: p. 404-405.

35. Bitko, V. and S. Barik, Phenotypic silencing of cytoplasmic genes using sequence-specific double-stranded short interfering RNA and its application in the reverse genetics of wild type negative-strand RNA viruses. *BMC Microbiology*, 2001. 1(1): p. 34.
36. Bjellqvist, B., et al., The focusing positions of polypeptides in immobilized pH gradients can be predicted from their amino acid sequences. *Electrophoresis*, 1993. 14(10): p. 1023-31.
37. Black, L.M., Strains of Potato Yellow-Dwarf Virus. *American Journal of Botany*, 1940. 27(6): p. 8.
38. Black, L.M., Specific transmission of varieties of Potato yellow-dwarf virus by related insects. *American Potato Journal*, 1941. 18(8): p. 231-233 pp.
39. Black, L.M., Genetic Variation in the Clover Leafhopper's Ability to Transmit Potato Yellow-Dwarf Virus. *Genetics*, 1943. 28(3): p. 200-9.
40. Black, L.M., et al., Ultrastructure of potato yellow-dwarf virus. *Virology*, 1965. 27(3): p. 446-9.
41. Blom, N., et al., Prediction of post-translational glycosylation and phosphorylation of proteins from the amino acid sequence. *Proteomics*, 2004. 4(6): p. 1633-49.
42. Boche, I. and E. Fanning, Nucleocytoplasmic recycling of the nuclear localization signal receptor alpha subunit in vivo is dependent on a nuclear export signal, energy, and RCC1. *J Cell Biol*, 1997. 139(2): p. 313-25.
43. Bogerd, H.P., et al., Definition of a Consensus Transportin-specific Nucleocytoplasmic Transport Signal. *Journal of Biological Chemistry*, 1999. 274(14): p. 9771-9777.
44. Bohle, H., N. Lorenzen, and B.D. Schyth, Species specific inhibition of viral replication using dicer substrate siRNAs (DsiRNAs) targeting the viral nucleoprotein of the fish pathogenic rhabdovirus viral hemorrhagic septicemia virus (VHSV). *Antiviral Research*, 2011. 90(3): p. 187-194.
45. Boni, A., et al., Live imaging and modeling of inner nuclear membrane targeting reveals its molecular requirements in mammalian cells. *J Cell Biol*, 2015. 209(5): p. 705-20.
46. Boudreault, S., et al., Global Profiling of the Cellular Alternative RNA Splicing Landscape during Virus-Host Interactions. *PLoS One*, 2016. 11(9): p. e0161914.
47. Boudreault, S., et al., Global Profiling of the Cellular Alternative RNA Splicing Landscape during Virus-Host Interactions. *PloS one*, 2016. 11(9): p. e0161914-e0161914.
48. Bourhy, H., et al., Phylogenetic relationships among rhabdoviruses inferred using the L polymerase gene. *J Gen Virol*, 2005. 86(Pt 10): p. 2849-58.
49. Brakke, M.K., L.M. Black, and R.W.G. Wyckoff, THE SEDIMENTATION RATE OF POTATO YELLOW-DWARF VIRUS. *American Journal of Botany*, 1951. 38(5): p. 332-342.
50. Brakke, M.K. and N. Van Pelt, Linear-log sucrose gradients for estimating sedimentation coefficients of plant viruses and nucleic acids. *Anal Biochem*, 1970. 38(1): p. 56-64.
51. Burrell, C.J., C.R. Howard, and F.A. Murphy, Chapter 27 - Rhabdoviruses, in Fenner and White's Medical Virology (Fifth Edition), C.J. Burrell, C.R. Howard, and F.A. Murphy, Editors. 2017, Academic Press: London. p. 383-394.
52. cann, A., Principles of Molecular Virology. 2011.

53. Carette, J.E., et al., Cowpea Mosaic Virus Infection Induces a Massive Proliferation of Endoplasmic Reticulum but Not Golgi Membranes and Is Dependent on De Novo Membrane Synthesis. *Journal of Virology*, 2000. 74(14): p. 6556.
54. Chagas, C.M., Morphology and Intracellular Behaviour of Coffee Ringspot Virus (CRV) in Tissues of Coffee (*Coffea arabica* L.). *Journal of Phytopathology*, 1980. 99(4): p. 301-309.
55. Chagas, C.M., E.W. Kitajima, and J.C.V. Rodrigues, Coffee Ringspot Virus Vecteded by *Brevipalpus phoenicis* (Acari: Tenuipalpidae) in Coffee. *Experimental & Applied Acarology*, 2003. 30(1): p. 203-213.
56. Chakrabarty, R., et al., PSITE vectors for stable integration or transient expression of autofluorescent protein fusions in plants: probing *Nicotiana benthamiana*-virus interactions. *Mol Plant Microbe Interact*, 2007. 20(7): p. 740-50.
57. Chambers, T.C., N.C. Crowley, and R.I.B. Francki, Localization of lettuce necrotic yellows virus in host leaf tissue. *Virology*, 1965. 27(3): p. 320-328.
58. Chazotte, B., Labeling Nuclear DNA Using DAPI. *Cold Spring Harbor Protocols*, 2011. 2011(1): p. pdb.prot5556.
59. Chen, B.J. and R.A. Lamb, Mechanisms for enveloped virus budding: can some viruses do without an ESCRT? *Virology*, 2008. 372(2): p. 221-32.
60. Chenik, M., et al., Mapping the Interacting Domains between the Rabies Virus Polymerase and Phosphoprotein. *Journal of Virology*, 1998. 72(3): p. 1925-1930.
61. Cibulka, J., M. Fraiberk, and J. Forstova, Nuclear Actin and Lamins in Viral Infections. *Viruses*, 2012. 4(3): p. 325-347.
62. Ciska, M. and S. Moreno Diaz de la Espina, NMCP/LINC proteins: putative lamin analogs in plants? *Plant Signal Behav*, 2013. 8(12): p. e26669.
63. Claudia R. F. Martins, J.A.J., Diane M. Lawrence, Tae-Jin Choi,‡ Anna-Maria Pisi,§ Sara L. Tobin,|| Denise Lapidus, John D. O. Wagner,# Steven Ruzin, Kent McDonald,‡‡ and Andrew O. Jackson*, *Sonchus* Yellow Net Rhabdovirus Nuclear Viroplasms Contain Polymerase-Associated Proteins. *Journal of virology* 1998. 72(7): p. 5669–5679.
64. Coll, J.M., The glycoprotein G of rhabdoviruses. *Arch Virol*, 1995. 140(5): p. 827-51.
65. Collins, P.L., R. Fearn, and B.S. Graham, Respiratory Syncytial Virus: Virology, Reverse Genetics, and Pathogenesis of Disease. *Current topics in microbiology and immunology*, 2013. 372: p. 3-38.
66. Connor, J.H. and D.S. Lyles, Vesicular Stomatitis Virus Infection Alters the eIF4F Translation Initiation Complex and Causes Dephosphorylation of the eIF4E Binding Protein 4E-BP1. *Journal of Virology*, 2002. 76(20): p. 10177.
67. Conzelmann, K.-K., NONSEGMENTED NEGATIVE-STRAND RNA VIRUSES: Genetics and Manipulation of Viral Genomes. *Annual Review of Genetics*, 1998. 32(1): p. 123-162.
68. Craven, R.C., et al., Late Domain Function Identified in the Vesicular Stomatitis Virus M Protein by Use of Rhabdovirus-Retrovirus Chimeras. *Journal of Virology*, 1999. 73(4): p. 3359.
69. Cressman, D.E., et al., Mechanisms of nuclear import and export that control the subcellular localization of class II transactivator. *J Immunol*, 2001. 167(7): p. 3626-34.

70. Cronshaw, J.M., et al., Proteomic analysis of the mammalian nuclear pore complex. *The Journal of Cell Biology*, 2002. 158(5): p. 915-927.
71. Cruz-Jaramillo, J.L., et al., Characterization of a Proposed Dichorhavirus Associated with the Citrus Leprosis Disease and Analysis of the Host Response. *Viruses*, 2014. 6(7): p. 2602-2622.
72. Cuevas, J.M., et al., Temporal dynamics of intrahost molecular evolution for a plant RNA virus. *Mol Biol Evol*, 2015. 32(5): p. 1132-47.
73. D'Angelo, M.A. and M.W. Hetzer, Structure, dynamics and function of nuclear pore complexes. *Trends in Cell Biology*, 2008. 18(10): p. 456-466.
74. DeGrasse, J.A., et al., Evidence for a Shared Nuclear Pore Complex Architecture That Is Conserved from the Last Common Eukaryotic Ancestor. *Molecular & Cellular Proteomics*, 2009. 8(9): p. 2119.
75. Deng, M., et al., Role of the Sonchus Yellow Net Virus N Protein in Formation of Nuclear Viroplasms. *Journal of Virology*, 2007. 81(10): p. 5362-5374.
76. Denison, M.R., Seeking Membranes: Positive-Strand RNA Virus Replication Complexes. *PLOS Biology*, 2008. 6(10): p. e270.
77. Dereeper, A., et al., Phylogeny.fr: robust phylogenetic analysis for the non-specialist. *Nucleic Acids Res*, 2008. 36(Web Server issue): p. W465-9.
78. Desselberger, U., Reverse genetics of rotavirus. *Proceedings of the National Academy of Sciences*, 2017. 114(9): p. 2106.
79. Dietzgen, R.G., et al., Completion of the genome sequence of Lettuce necrotic yellows virus, type species of the genus *Cytorhabdovirus*. *Virus Res*, 2006. 118(1-2): p. 16-22.
80. Dietzgen, R.G., D.J. Innes, and N. Bejerman, Complete genome sequence and intracellular protein localization of *Datura* yellow vein nucleorhabdovirus. *Virus Res*, 2015. 205: p. 7-11.
81. Dietzgen, R.G., et al., The family Rhabdoviridae: mono- and bipartite negative-sense RNA viruses with diverse genome organization and common evolutionary origins. *Virus Research*, 2017. 227: p. 158-170.
82. Dietzgen, R.G., et al., Dichorhavirus: a proposed new genus for *Brevipalpus* mite-transmitted, nuclear, bacilliform, bipartite, negative-strand RNA plant viruses. *Arch Virol*, 2014. 159(3): p. 607-19.
83. Dietzgen, R.G., K.S. Mann, and K.N. Johnson, Plant Virus–Insect Vector Interactions: Current and Potential Future Research Directions. *Viruses*, 2016. 8(11): p. 303.
84. Dietzgen, R.G., et al., In planta localization and interactions of *impatiens* necrotic spot tospovirus proteins. *J Gen Virol*, 2012. 93(Pt 11): p. 2490-5.
85. Dittmer, T.A. and E.J. Richards, Role of LINC proteins in plant nuclear morphology. *Plant Signaling & Behavior*, 2008. 3(7): p. 485-487.
86. Dong, A., et al., Infrared spectroscopic studies of lyophilization- and temperature-induced protein aggregation. *Journal of Pharmaceutical Sciences*, 1995. 84(4): p. 415-424.
87. Duffy, S., L.A. Shackelton, and E.C. Holmes, Rates of evolutionary change in viruses: patterns and determinants. *Nat Rev Genet*, 2008. 9(4): p. 267-76.

88. Eckardt, N.A., The Nuclear Pore Complex in Arabidopsis. *The Plant Cell*, 2010. 22(12): p. 3878-3878.
89. Edens, L.J., et al., Nuclear size regulation: from single cells to development and disease. *Trends in Cell Biology*, 2013. 23(4): p. 151-159.
90. Einer-Jensen, K., et al., Evolution of the fish rhabdovirus viral haemorrhagic septicaemia virus. *J Gen Virol*, 2004. 85(Pt 5): p. 1167-79.
91. Enami, K., et al., An Influenza Virus Temperature-Sensitive Mutant Defective in the Nuclear-Cytoplasmic Transport of the Negative-Sense Viral RNAs. *Virology*, 1993. 194(2): p. 822-827.
92. Falk, B.W. and L.G. Weathers, Comparison of potato yellow dwarf virus serotypes. *Phytopathology*, 1983. 73(1): p. 81-85.
93. Fernández-Coll, L., K. Potrykus, and M. Cashel, Puzzling conformational changes affecting proteins binding to the RNA polymerase. *Proceedings of the National Academy of Sciences*, 2018. 115(50): p. 12550.
94. Fields, P.A., Review: Protein function at thermal extremes: balancing stability and flexibility. *Comparative Biochemistry and Physiology Part A: Molecular & Integrative Physiology*, 2001. 129(2): p. 417-431.
95. Finke, S., R. Mueller-Waldeck, and K.K. Conzelmann, Rabies virus matrix protein regulates the balance of virus transcription and replication. *J Gen Virol*, 2003. 84(Pt 6): p. 1613-21.
96. Fleith, R.C., et al., Genome-wide analyses reveal a highly conserved Dengue virus envelope peptide which is critical for virus viability and antigenic in humans. *Scientific reports*, 2016. 6: p. 36339-36339.
97. Follett, E.A., et al., Virus replication in enucleate cells: vesicular stomatitis virus and influenza virus. *J Virol*, 1974. 13(2): p. 394-9.
98. Formerod, M., et al., CRM1 is an export receptor for leucine-rich nuclear export signals. *Cell*, 1997. 90(6): p. 1051-60.
99. Fort, P., et al., Fossil rhabdoviral sequences integrated into arthropod genomes: ontogeny, evolution, and potential functionality. *Mol Biol Evol*, 2012. 29(1): p. 381-90.
100. Forwood, J.K., M.H.C. Lam, and D.A. Jans, Nuclear Import of Creb and AP-1 Transcription Factors Requires Importin- β 1 and Ran but Is Independent of Importin- α . *Biochemistry*, 2001. 40(17): p. 5208-5217.
101. Francki, R.I.B., Plant Rhabdoviruses, in *Advances in Virus Research*, M.A. Lauffer, et al., Editors. 1973, Academic Press. p. 257-345.
102. Freitas, N. and C. Cunha, Mechanisms and Signals for the Nuclear Import of Proteins. *Current Genomics*, 2009. 10(8): p. 550-557.
103. Fu, S.-C., et al., Correlation of CRM1-NES affinity with nuclear export activity. *Molecular Biology of the Cell*, 2018. 29(17): p. 2037-2044.
104. Fujino, K., et al., Temperature controls nuclear import of Tam3 transposase in *Antirrhinum*. *The Plant Journal*, 2010. 65(1): p. 146-155.

105. Fung, H.Y.J., S.-C. Fu, and Y.M. Chook, Nuclear export receptor CRM1 recognizes diverse conformations in nuclear export signals. *eLife*, 2017. 6: p. e23961.
106. Ganesan, U., et al., Construction of a *Sonchus Yellow Net Virus* Minireplicon: a Step toward Reverse Genetic Analysis of Plant Negative-Strand RNA Viruses. *Journal of Virology*, 2013. 87(19): p. 10598-10611.
107. Ganguly, A., et al., Perturbation of nucleo-cytoplasmic transport affects size of nucleus and nucleolus in human cells. *FEBS Letters*, 2016. 590(5): p. 631-643.
108. Gasteiger, E., et al., ExPASy: The proteomics server for in-depth protein knowledge and analysis. *Nucleic Acids Res*, 2003. 31(13): p. 3784-8.
109. Gaudier, M., Y. Gaudin, and M. Knossow, Cleavage of Vesicular Stomatitis Virus Matrix Protein Prevents Self-Association and Leads to Crystallization. *Virology*, 2001. 288(2): p. 308-314.
110. Gaudier, M., Y. Gaudin, and M. Knossow, Crystal structure of vesicular stomatitis virus matrix protein. *The EMBO Journal*, 2002. 21(12): p. 2886-2892.
111. Geisler, C. and D.L. Jarvis, Rhabdovirus-like endogenous viral elements in the genome of *Spodoptera frugiperda* insect cells are actively transcribed: Implications for adventitious virus detection. *Biologicals*, 2016. 44(4): p. 219-225.
112. Ghorbani, A., K. Izadpanah, and R.G. Dietzgen, Completed sequence and corrected annotation of the genome of maize Iranian mosaic virus. *Arch Virol*, 2018. 163(3): p. 767-770.
113. Ghosh, D., et al., Cloning and subcellular localization of the phosphoprotein and nucleocapsid proteins of Potato yellow dwarf virus, type species of the genus *Nucleorhabdovirus*. *Virus Res*, 2008. 135(1): p. 26-35.
114. Gietz, R.D. and R.H. Schiestl, High-efficiency yeast transformation using the LiAc/SS carrier DNA/PEG method. *Nat Protoc*, 2007. 2(1): p. 31-4.
115. GM., C., *The Nuclear Envelope and Traffic between the Nucleus and Cytoplasm. The Cell: A Molecular Approach*. 2nd edition. , 2000.
116. Goder, V. and M. Spiess, Topogenesis of membrane proteins: determinants and dynamics. *FEBS Letters*, 2001. 504(3): p. 87-93.
117. Goldberg, T.L., et al., Kanyawara Virus: A Novel Rhabdovirus Infecting Newly Discovered Nycteribiid Bat Flies Infesting Previously Unknown Pteropodid Bats in Uganda. *Scientific Reports*, 2017. 7: p. 5287.
118. Goldfarb, D.S., et al., Importin α : a multipurpose nuclear-transport receptor. *Trends in Cell Biology*, 2004. 14(9): p. 505-514.
119. Goodin, M.M., et al., Interactions and Nuclear Import of the N and P Proteins of *Sonchus Yellow Net Virus*, a Plant *Nucleorhabdovirus*. *Journal of Virology*, 2001. 75(19): p. 9393.
120. Goodin, M.M., et al., Membrane and protein dynamics in live plant nuclei infected with *Sonchus yellow net virus*, a plant-adapted rhabdovirus. *J Gen Virol*, 2007. 88(Pt 6): p. 1810-20.
121. Goodin, M.M., et al., pGD vectors: versatile tools for the expression of green and red fluorescent protein fusions in agroinfiltrated plant leaves. *Plant J*, 2002. 31(3): p. 375-83.
122. Graham, S.C., et al., Rhabdovirus Matrix Protein Structures Reveal a Novel Mode of Self-Association. *PLOS Pathogens*, 2008. 4(12): p. e1000251.

123. Green, T.J. and M. Luo, Structure of the vesicular stomatitis virus nucleocapsid in complex with the nucleocapsid-binding domain of the small polymerase cofactor, P. *Proceedings of the National Academy of Sciences*, 2009. 106(28): p. 11713.
124. Greenfield, N.J., Using circular dichroism collected as a function of temperature to determine the thermodynamics of protein unfolding and binding interactions. *Nature Protocols*, 2006. 1: p. 2527.
125. Griffiths AJF, M.J., Suzuki DT, Reverse genetics. . *An introduction of Genetic Analysis.* , 2000.
126. Grummer, B., et al., Localization of viral proteins in cells infected with bovine viral diarrhoea virus. *J Gen Virol*, 2001. 82(Pt 11): p. 2597-605.
127. Gu, L., et al., Intermolecular masking of the HIV-1 Rev NLS by the cellular protein HIC: Novel insights into the regulation of Rev nuclear import. *Retrovirology*, 2011. 8: p. 17-17.
128. Gubala, A., et al., Tibrogargan and Coastal Plains rhabdoviruses: genomic characterization, evolution of novel genes and seroprevalence in Australian livestock. *J Gen Virol*, 2011. 92(Pt 9): p. 2160-70.
129. Haas, B.J., et al., De novo transcript sequence reconstruction from RNA-seq using the Trinity platform for reference generation and analysis. *Nat Protoc*, 2013. 8(8): p. 1494-512.
130. Hardy, S., et al., Reverse genetics in eukaryotes. *Biology of the Cell*, 2010. 102(10): p. 561-580.
131. Harty, R.N., et al., A Proline-Rich Motif within the Matrix Protein of Vesicular Stomatitis Virus and Rabies Virus Interacts with WW Domains of Cellular Proteins: Implications for Viral Budding. *Journal of Virology*, 1999. 73(4): p. 2921.
132. Heaton, L.A., et al., Physical map of the genome of sonchus yellow net virus, a plant rhabdovirus with six genes and conserved gene junction sequences. *Proc Natl Acad Sci U S A*, 1989. 86(22): p. 8665-8.
133. Heim, F., et al., Complete nucleotide sequence of a putative new cytorhabdovirus infecting lettuce. *Arch Virol*, 2008. 153(1): p. 81-92.
134. Higgins, C.M., et al., Complete genome sequence of Colocasia bobone disease-associated virus, a putative cytorhabdovirus infecting taro. *Arch Virol*, 2016. 161(3): p. 745-8.
135. Horimoto, T. and Y. Kawaoka, Reverse genetics provides direct evidence for a correlation of hemagglutinin cleavability and virulence of an avian influenza A virus. *Journal of Virology*, 1994. 68(5): p. 3120-3128.
136. Hsieh, M.J., P.J. White, and C.W. Pouton, Interaction of viruses with host cell molecular motors. *Current Opinion in Biotechnology*, 2010. 21(5): p. 633-639.
137. HSU, G.A.a.H.T., Comparison of Structural Proteins from Two Potato Yellow Dwarf Viruses *Journal of General Virology*, 1984. 65: p. 991-994.
138. Hsu, H.T. and L.M. Black, Inoculation of vector cell monolayers with potato yellow dwarf virus. *Virology*, 1973. 52(1): p. 187-198.
139. Huang, D.M. and D. Chandler, Temperature and length scale dependence of hydrophobic effects and their possible implications for protein folding. *Proceedings of the National Academy of Sciences*, 2000. 97(15): p. 8324.

140. Huang, Y., et al., Novel structure of the genome of Rice yellow stunt virus: identification of the gene 6-encoded virion protein. *J Gen Virol*, 2003. 84(Pt 8): p. 2259-64.
141. Huang, Y.-W., et al., Identification of a Movement Protein of Rice Yellow Stunt Rhabdovirus. *Journal of Virology*, 2005. 79(4): p. 2108.
142. Hull, R., Chapter 7 - Replication of Plant Viruses, in *Plant Virology (Fifth Edition)*, R. Hull, Editor. 2014, Academic Press: Boston. p. 341-421.
143. Ibarra, A. and M.W. Hetzer, Nuclear pore proteins and the control of genome functions. *Genes & Development*, 2015. 29(4): p. 337-349.
144. Irimia, M., et al., A highly conserved program of neuronal microexons is misregulated in autistic brains. *Cell*, 2014. 159(7): p. 1511-23.
145. Iseni, F., et al., Characterization of rabies virus nucleocapsids and recombinant nucleocapsid-like structures. *J Gen Virol*, 1998. 79 (Pt 12): p. 2909-19.
146. Ishibashi, K., E. Matsumoto-Yokoyama, and M. Ishikawa, A Tomato Spotted Wilt Virus S RNA-based Replicon System in Yeast. *Scientific Reports*, 2017. 7(1): p. 12647.
147. Ivanov, I., et al., Structural insights into the rhabdovirus transcription/replication complex. *Virus Res*, 2011. 162(1-2): p. 126-37.
148. Iverson, L.E. and J.K. Rose, Localized attenuation and discontinuous synthesis during vesicular stomatitis virus transcription. *Cell*, 1981. 23(2): p. 477-84.
149. Izaurralde, E., et al., A Role for the M9 Transport Signal of hnRNP A1 in mRNA Nuclear Export. *The Journal of Cell Biology*, 1997. 137(1): p. 27-35.
150. Jackson, A.C. and J.P. Rossiter, Apoptosis plays an important role in experimental rabies virus infection. *Journal of Virology*, 1997. 71(7): p. 5603.
151. Jackson, A.O., et al., Biology of plant rhabdoviruses. *Annu Rev Phytopathol*, 2005. 43: p. 623-60.
152. Jackson, A.O. and Z. Li, Developments in Plant Negative-Strand RNA Virus Reverse Genetics. *Annual Review of Phytopathology*, 2016. 54(1): p. 469-498.
153. Jang, C., et al., Genome sequence variation in the constricta strain dramatically alters the protein interaction and localization map of Potato yellow dwarf virus. *The Journal of General Virology*, 2017. 98(6): p. 1526-1536.
154. Jayakar, H.R., E. Jeetendra, and M.A. Whitt, Rhabdovirus assembly and budding. *Virus Res*, 2004. 106(2): p. 117-32.
155. Jevtić, P., et al., Sizing and shaping the nucleus: mechanisms and significance. *Current Opinion in Cell Biology*, 2014. 28: p. 16-27.
156. Johannsdottir, H.K., et al., Host Cell Factors and Functions Involved in Vesicular Stomatitis Virus Entry. *Journal of Virology*, 2009. 83(1): p. 440.
157. Jones, R.W. and A.O. Jackson, Replication of sonchus yellow net virus in infected protoplasts. *Virology*, 1990. 179(2): p. 815-820.
158. Jovanovic-Talisman, T. and A. Zilman, Protein Transport by the Nuclear Pore Complex: Simple Biophysics of a Complex Biomachine. *Biophysical Journal*, 2017. 113(1): p. 6-14.

159. Kabachinski, G. and T.U. Schwartz, The nuclear pore complex – structure and function at a glance. *Journal of Cell Science*, 2015. 128(3): p. 423.
160. Kalab, P. and R. Heald, The RanGTP gradient - a GPS for the mitotic spindle. *J Cell Sci*, 2008. 121(Pt 10): p. 1577-86.
161. Kalderon, D., et al., A short amino acid sequence able to specify nuclear location. *Cell*, 1984. 39(3 Pt 2): p. 499-509.
162. Kehlenbach, R.H., et al., A Role for RanBP1 in the Release of CRM1 from the Nuclear Pore Complex in a Terminal Step of Nuclear Export. *The Journal of Cell Biology*, 1999. 145(4): p. 645.
163. Kim, I.S., et al., Mechanism of membrane fusion induced by vesicular stomatitis virus G protein. *Proceedings of the National Academy of Sciences*, 2017. 114(1): p. E28.
164. Kis, A., et al., Polycistronic artificial miRNA-mediated resistance to Wheat dwarf virus in barley is highly efficient at low temperature. *Molecular Plant Pathology*, 2015. 17(3): p. 427-437.
165. Kliot, A. and M. Ghanim, Fluorescent in situ hybridization for the localization of viruses, bacteria and other microorganisms in insect and plant tissues. *Methods*, 2016. 98: p. 74-81.
166. Kliot, A., et al., Fluorescence in situ hybridizations (FISH) for the localization of viruses and endosymbiotic bacteria in plant and insect tissues. *Journal of visualized experiments : JoVE*, 2014(84): p. e51030-e51030.
167. Knipe, D.M., et al., Snapshots: Chromatin Control of Viral Infection. *Virology*, 2013. 435(1): p. 141-156.
168. Knudson, D.L., Rhabdoviruses. *Journal of General Virology*, 1973. 20(Supplement): p. 105-130.
169. Kobayashi, J. and Y. Matsuura, Structural Basis for Cell-Cycle-Dependent Nuclear Import Mediated by the Karyopherin Kap121p. *Journal of Molecular Biology*, 2013. 425(11): p. 1852-1868.
170. Koh, J. and G. Blobel, Allosteric Regulation in Gating the Central Channel of the Nuclear Pore Complex. *Cell*, 2015. 161(6): p. 1361-1373.
171. Kondo, H., et al., Orchid fleck virus structural proteins, N and P, form intranuclear viroplasm-like structures in the absence of viral infection. *Journal of Virology*, 2013.
172. Kondo, H., et al., Orchid fleck virus is a rhabdovirus with an unusual bipartite genome. *J Gen Virol*, 2006. 87(Pt 8): p. 2413-21.
173. Koonin, E.V. and A.E. Gorbalenya, Evolution of RNA genomes: does the high mutation rate necessitate high rate of evolution of viral proteins? *J Mol Evol*, 1989. 28(6): p. 524-7.
174. Kormelink, R., et al., Negative-strand RNA viruses: the plant-infecting counterparts. *Virus Res*, 2011. 162(1-2): p. 184-202.
175. Kosugi, S., et al., Six classes of nuclear localization signals specific to different binding grooves of importin alpha. *J Biol Chem*, 2009. 284(1): p. 478-85.
176. Koyuncu, Orkide O., Ian B. Hogue, and Lynn W. Enquist, Virus Infections in the Nervous System. *Cell Host & Microbe*, 2013. 13(4): p. 379-393.

177. Krichevsky, A., et al., Nuclear import and export of plant virus proteins and genomes. *Mol Plant Pathol*, 2006. 7(2): p. 131-46.
178. Kurilla, M.G. and J.D. Keene, The leader RNA of vesicular stomatitis virus is bound by a cellular protein reactive with anti-La lupus antibodies. *Cell*, 1983. 34(3): p. 837-845.
179. Kuss, S.K., et al., Nuclear Imprisonment: Viral Strategies to Arrest Host mRNA Nuclear Export. *Viruses*, 2013. 5(7): p. 1824-1849.
180. Kutay, U., et al., Export of Importin α from the Nucleus Is Mediated by a Specific Nuclear Transport Factor. *Cell*, 1997. 90(6): p. 1061-1071.
181. Kuzmin, I.V., et al., The rhabdoviruses: biodiversity, phylogenetics, and evolution. *Infect Genet Evol*, 2009. 9(4): p. 541-53.
182. la Cour, T., et al., Analysis and prediction of leucine-rich nuclear export signals. *Protein Eng Des Sel*, 2004. 17(6): p. 527-36.
183. Lamprecht, R.L., Pietersen, G., Kasdorf, G.G.F., Characterisation of a proposed Nucleorhabdovirus new to South Africa. *Eur J Plant Pathol* 2009.
184. Lange, A., et al., Classical nuclear localization signals: definition, function, and interaction with importin alpha. *J Biol Chem*, 2007. 282(8): p. 5101-5.
185. Leopold, P.L. and K.K. Pfister, Viral Strategies for Intracellular Trafficking: Motors and Microtubules. *Traffic*, 2006. 7(5): p. 516-523.
186. Levy, D.L. and R. Heald, Nuclear Size Is Regulated by Importin α and Ntf2 in *Xenopus*. *Cell*, 2010. 143(2): p. 288-298.
187. Leyrat, C., et al., Structure, interactions with host cell and functions of rhabdovirus phosphoprotein. *Future Virology*, 2011. 6(4): p. 465-481.
188. Liang, B., et al., Structure of the L Protein of Vesicular Stomatitis Virus from Electron Cryomicroscopy. *Cell*, 2015. 162(2): p. 314-327.
189. Lieberman, P.M., Chromatin regulation of virus infection. *Trends in Microbiology*, 2006. 14(3): p. 132-140.
190. Lin, N.-S., Y.-H. Hsu, and R.-J. Chiu, Identification of Viral Structural Proteins in the Nucleoplasm of Potato Yellow Dwarf Virus-infected Cells. *Journal of General Virology*, 1987. 68(10): p. 2723-2728.
191. Lindbo, J.A., TRBO: A High-Efficiency Tobacco Mosaic Virus RNA-Based Overexpression Vector. *Plant Physiology*, 2007. 145(4): p. 1232-1240.
192. Liu, Y., et al., Identification and Characterization of Wheat Yellow Striate Virus, a Novel Leafhopper-Transmitted Nucleorhabdovirus Infecting Wheat. *Frontiers in Microbiology*, 2018. 9(468).
193. Longdon, B., et al., The evolution and genetics of virus host shifts. *PLoS pathogens*, 2014. 10(11): p. e1004395-e1004395.
194. Longdon, B., et al., The evolution, diversity, and host associations of rhabdoviruses. *Virus Evol*, 2015. 1(1): p. vev014.

195. Lui, K. and Y. Huang, RanGTPase: A Key Regulator of Nucleocytoplasmic Trafficking. *Mol Cell Pharmacol*, 2009. 1(3): p. 148-156.
196. Luo, M., et al., Conserved characteristics of the rhabdovirus nucleoprotein. *Virus research*, 2007. 129(2): p. 246-251.
197. Lusk, C.P., et al., Karyopherins in nuclear pore biogenesis: a role for Kap121p in the assembly of Nup53p into nuclear pore complexes. *The Journal of Cell Biology*, 2002. 159(2): p. 267-278.
198. Lvov, D.K., et al., Chapter 5 - Order Mononegavirales, in *Zoonotic Viruses in Northern Eurasia*, D.K. Lvov, et al., Editors. 2015, Academic Press: Boston. p. 77-106.
199. MacArthur, M.W. and J.M. Thornton, Influence of proline residues on protein conformation. *Journal of Molecular Biology*, 1991. 218(2): p. 397-412.
200. Mach, J., Sick as a...Grass? Viral Infection Causes Massive Changes in Alternative Splicing in *Brachypodium distachyon*. *The Plant Cell*, 2015. 27(1): p. 7.
201. Macleod, R., An interpretation of the observed polymorphism of potato yellow dwarf virus. *Virology*, 1968. 34(4): p. 771-777.
202. MacLeod, R., L.M. Black, and F.H. Moyer, The fine structure and intracellular localization of potato yellow dwarf virus. *Virology*, 1966. 29(4): p. 540-52.
203. Maertens, G.N., et al., Structural basis for nuclear import of splicing factors by human Transportin 3. *Proceedings of the National Academy of Sciences of the United States of America*, 2014. 111(7): p. 2728-2733.
204. Mallet, P.L. and F. Bachand, A proline-tyrosine nuclear localization signal (PY-NLS) is required for the nuclear import of fission yeast PAB2, but not of human PABPN1. *Traffic*, 2013. 14(3): p. 282-94.
205. Mann, K.S. and R.G. Dietzgen, Plant rhabdoviruses: new insights and research needs in the interplay of negative-strand RNA viruses with plant and insect hosts. *Arch Virol*, 2014. 159(8): p. 1889-900.
206. Mann, K.S., et al., Cytorhabdovirus P protein suppresses RISC-mediated cleavage and RNA silencing amplification in planta. *Virology*, 2016. 490: p. 27-40.
207. Marfori, M., et al., Molecular basis for specificity of nuclear import and prediction of nuclear localization. *Biochimica et Biophysica Acta (BBA) - Molecular Cell Research*, 2011. 1813(9): p. 1562-1577.
208. Martin, K., et al., Transient expression in *Nicotiana benthamiana* fluorescent marker lines provides enhanced definition of protein localization, movement and interactions in planta. *The Plant Journal*, 2009. 59(1): p. 150-162.
209. Martin, K.M., et al., Lettuce necrotic yellows cytorhabdovirus protein localization and interaction map, and comparison with nucleorhabdoviruses. *J Gen Virol*, 2012. 93(Pt 4): p. 906-14.
210. Martínez, F., et al., Interaction network of tobacco etch potyvirus NIa protein with the host proteome during infection. *BMC Genomics*, 2016. 17(1): p. 87.
211. Mascetti, G., S. Carrara, and L. Vergani, Relationship between chromatin compactness and dye uptake for in situ chromatin stained with DAPI. *Cytometry*, 2001. 44(2): p. 113-119.

212. Matthew Michael, W., M. Choi, and G. Dreyfuss, A nuclear export signal in hnRNP A1: A signal-mediated, temperature-dependent nuclear protein export pathway. *Cell*, 1995. 83(3): p. 415-422.
213. Melcher, U., The '30K' superfamily of viral movement proteins. *Journal of General Virology*, 2000. 81(1): p. 257-266.
214. Mendez-Rios, J. and P. Uetz, Global approaches to study protein-protein interactions among viruses and hosts. *Future microbiology*, 2010. 5(2): p. 289-301.
215. Min, B.E., et al., A host-factor interaction and localization map for a plant-adapted rhabdovirus implicates cytoplasm-tethered transcription activators in cell-to-cell movement. *Mol Plant Microbe Interact*, 2010. 23(11): p. 1420-32.
216. Miyamoto, Y., K. Yamada, and Y. Yoneda, Importin α : a key molecule in nuclear transport and non-transport functions. *The Journal of Biochemistry*, 2016. 160(2): p. 69-75.
217. Moore, M.S., Protein translocation: Nuclear export – out of the dark. *Current Biology*, 1996. 6(2): p. 137-140.
218. Morgan, A.A. and E. Rubenstein, Proline: the distribution, frequency, positioning, and common functional roles of proline and polyproline sequences in the human proteome. *PLoS one*, 2013. 8(1): p. e53785-e53785.
219. Nagamine, T., et al., Nuclear Marginalization of Host Cell Chromatin Associated with Expansion of Two Discrete Virus-Induced Subnuclear Compartments during Baculovirus Infection. *Journal of Virology*, 2008. 82(13): p. 6409.
220. Nagar, S., et al., A geminivirus induces expression of a host DNA synthesis protein in terminally differentiated plant cells. *The Plant Cell*, 1995. 7(6): p. 705.
221. Nägel, W.C. and F. Wunderlich, Effect of temperature on nuclear membranes and nucleocytoplasmic RNA-transport in *Tetrahymena* grown at different temperatures. *The Journal of Membrane Biology*, 1977. 32(1): p. 151-164.
222. Nagy, P.D., Tombusvirus-Host Interactions: Co-Opted Evolutionarily Conserved Host Factors Take Center Court. *Annu Rev Virol*, 2016. 3(1): p. 491-515.
223. Naim, B., et al., Passive and Facilitated Transport in Nuclear Pore Complexes Is Largely Uncoupled. *Journal of Biological Chemistry*, 2007. 282(6): p. 3881-3888.
224. Nakai, K. and M. Kanehisa, Expert system for predicting protein localization sites in gram-negative bacteria. *Proteins*, 1991. 11(2): p. 95-110.
225. Neumann, G., et al., Reverse Genetics Demonstrates that Proteolytic Processing of the Ebola Virus Glycoprotein Is Not Essential for Replication in Cell Culture. *Journal of Virology*, 2002. 76(1): p. 406-410.
226. Nolden, T. and S. Finke, Rapid Reverse Genetics Systems for Rhabdoviruses: From Forward to Reverse and Back Again. *Methods Mol Biol*, 2017. 1602: p. 171-184.
227. Ogbe, F.O., et al., Symptom severity of cassava mosaic disease in relation to concentration of African cassava mosaic virus in different cassava genotypes. *Plant Pathology*, 2003. 52(1): p. 84-91.
228. Onischenko, E. and K. Weis, Nuclear pore complex—a coat specifically tailored for the nuclear envelope. *Current Opinion in Cell Biology*, 2011. 23(3): p. 293-301.

229. Ozawa, M., et al., Contributions of Two Nuclear Localization Signals of Influenza A Virus Nucleoprotein to Viral Replication. *Journal of Virology*, 2007. 81(1): p. 30.
230. Palmeri, D. and M.H. Malim, Importin β Can Mediate the Nuclear Import of an Arginine-Rich Nuclear Localization Signal in the Absence of Importin α . *Molecular and Cellular Biology*, 1999. 19(2): p. 1218-1225.
231. Pappi, P.G., et al., A novel strategy for the determination of a rhabdovirus genome and its application to sequencing of Eggplant mottled dwarf virus. *Virus Genes*, 2013. 47(1): p. 105-113.
232. Parrella, G. and B. Greco, Sequence variation of block III segment identifies three distinct lineages within Eggplant mottled dwarf virus isolates from Italy, Spain and Greece. *Acta Virol*, 2016. 60(1): p. 100-5.
233. Parry, G., Components of the Arabidopsis nuclear pore complex play multiple diverse roles in control of plant growth. *Journal of Experimental Botany*, 2014. 65(20): p. 6057-6067.
234. Patil, B.L. and C.M. Fauquet, Light intensity and temperature affect systemic spread of silencing signal in transient agroinfiltration studies. *Molecular Plant Pathology*, 2014. 16(5): p. 484-494.
235. Pekosz, A., B. He, and R.A. Lamb, Reverse genetics of negative-strand RNA viruses: Closing the circle. *Proceedings of the National Academy of Sciences*, 1999. 96(16): p. 8804.
236. Petersen, J.M., et al., The matrix protein of vesicular stomatitis virus inhibits nucleocytoplasmic transport when it is in the nucleus and associated with nuclear pore complexes. *Molecular and cellular biology*, 2000. 20(22): p. 8590-8601.
237. Picard, D. and K.R. Yamamoto, Two signals mediate hormone-dependent nuclear localization of the glucocorticoid receptor. *Embo j*, 1987. 6(11): p. 3333-40.
238. Pita, J.S., V. Morris, and M.J. Roossinck, Mutation and Recombination Frequencies Reveal a Biological Contrast within Strains of Cucumber Mosaic Virus. *Journal of Virology*, 2015. 89(13): p. 6817-6823.
239. Pleschka, S., et al., A plasmid-based reverse genetics system for influenza A virus. *J Virol*, 1996. 70(6): p. 4188-92.
240. Pusch, S., N. Dissmeyer, and A. Schnittger, Bimolecular-fluorescence complementation assay to monitor kinase-substrate interactions in vivo. *Methods Mol Biol*, 2011. 779: p. 245-57.
241. Qu, F. and T.J. Morris, Suppressors of RNA silencing encoded by plant viruses and their role in viral infections. *FEBS Letters*, 2005. 579(26): p. 5958-5964.
242. Raikhel, N., Nuclear targeting in plants. *Plant Physiol*, 1992. 100(4): p. 1627-32.
243. Ramalho, T.O., et al., Characterization of Coffee ringspot virus-Lavras: a model for an emerging threat to coffee production and quality. *Virology*, 2014. 464-465: p. 385-396.
244. Ramalho, T.O., et al., Detection and survey of coffee ringspot virus in Brazil. *Arch Virol*, 2016. 161(2): p. 335-43.
245. Raux, H., et al., The Matrix Protein of Vesicular Stomatitis Virus Binds Dynamin for Efficient Viral Assembly. *Journal of Virology*, 2010. 84(24): p. 12609.
246. Redinbaugh, M.G. and S.A. Hogenhout, Plant rhabdoviruses. *Curr Top Microbiol Immunol*, 2005. 292: p. 143-63.

247. Reed, S.E., et al., Shotgun sequencing of the negative-sense RNA genome of the rhabdovirus Maize mosaic virus. *Journal of Virological Methods*, 2005. 129(1): p. 91-96.
248. Reeder, G.S., D.L. Knudson, and R. Macleod, The ribonucleic acid of potato yellow dwarf virus. *Virology*, 1972. 50(1): p. 301-4.
249. Regan, A.D. and G.R. Whittaker, Entry of Rhabdoviruses Into Animal Cells, in *Viral Entry into Host Cells*, S. Pöhlmann and G. Simmons, Editors. 2013, Springer New York: New York, NY. p. 167-177.
250. Reichel, C. and R.N. Beachy, Tobacco mosaic virus infection induces severe morphological changes of the endoplasmic reticulum. *Proceedings of the National Academy of Sciences*, 1998. 95(19): p. 11169.
251. Renault, L., et al., Structural basis for guanine nucleotide exchange on Ran by the regulator of chromosome condensation (RCC1). *Cell*, 2001. 105(2): p. 245-55.
252. Revill, P., et al., Taro vein chlorosis virus: characterization and variability of a new nucleorhabdovirus. *J Gen Virol*, 2005. 86(Pt 2): p. 491-9.
253. Richardson, W.D., B.L. Roberts, and A.E. Smith, Nuclear location signals in polyoma virus large-T. *Cell*, 1986. 44(1): p. 77-85.
254. Rihs, H.P., et al., The rate of nuclear cytoplasmic protein transport is determined by the casein kinase II site flanking the nuclear localization sequence of the SV40 T-antigen. *The EMBO Journal*, 1991. 10(3): p. 633-639.
255. Rout, M.P., et al., The Yeast Nuclear Pore Complex: Composition, Architecture, and Transport Mechanism. *The Journal of Cell Biology*, 2000. 148(4): p. 635-652.
256. Rout, M.P., G. Blobel, and J.D. Aitchison, A Distinct Nuclear Import Pathway Used by Ribosomal Proteins. *Cell*, 1997. 89(5): p. 715-725.
257. Rowe, C.L., et al., Nuclear Trafficking of the Rabies Virus Interferon Antagonist P-Protein Is Regulated by an Importin-Binding Nuclear Localization Sequence in the C-Terminal Domain. *PLOS ONE*, 2016. 11(3): p. e0150477.
258. Ruigrok, R.W., T. Crepin, and D. Kolakofsky, Nucleoproteins and nucleocapsids of negative-strand RNA viruses. *Curr Opin Microbiol*, 2011. 14(4): p. 504-10.
259. Ryu, W.-S., Chapter 14 - Rhabdovirus, in *Molecular Virology of Human Pathogenic Viruses*, W.-S. Ryu, Editor. 2017, Academic Press: Boston. p. 187-194.
260. Sánchez, F., et al., Viral Strain-Specific Differential Alterations in Arabidopsis Developmental Patterns. *Molecular Plant-Microbe Interactions*, 2015. 28(12): p. 1304-1315.
261. Sanderfoot, A.A., D.J. Ingham, and S.G. Lazarowitz, A viral movement protein as a nuclear shuttle. The geminivirus BR1 movement protein contains domains essential for interaction with BL1 and nuclear localization. *Plant Physiol*, 1996. 110(1): p. 23-33.
262. Scheckel, C. and R.B. Darnell, Microexons--tiny but mighty. *Embo j*, 2015. 34(3): p. 273-4.
263. Seewald, M.J., et al., Biochemical characterization of the Ran-RanBP1-RanGAP system: are RanBP proteins and the acidic tail of RanGAP required for the Ran-RanGAP GTPase reaction? *Mol Cell Biol*, 2003. 23(22): p. 8124-36.

264. Sen, A., N. Sen, and E.R. Mackow, The Formation of Viroplasm-Like Structures by the Rotavirus NSP5 Protein Is Calcium Regulated and Directed by a C-Terminal Helical Domain. *Journal of Virology*, 2007. 81(21): p. 11758-11767.
265. Shargil, D., et al., Development of a fluorescent in situ hybridization (FISH) technique for visualizing CGMMV in plant tissues. *Journal of Virological Methods*, 2015. 223: p. 55-60.
266. Shen, H.B. and K.C. Chou, Virus-PLoc: a fusion classifier for predicting the subcellular localization of viral proteins within host and virus-infected cells. *Biopolymers*, 2007. 85(3): p. 233-40.
267. Simons, K. and H. Garoff, The Budding Mechanisms of Enveloped Animal Viruses. *Journal of General Virology*, 1980. 50(1): p. 1-21.
268. Smith, A., A. Brownawell, and I.G. Macara, Nuclear import of Ran is mediated by the transport factor NTF2. *Curr Biol*, 1998. 8(25): p. 1403-6.
269. Solon, J., et al., Membrane deformations induced by the matrix protein of vesicular stomatitis virus in a minimal system. *Journal of General Virology*, 2005. 86(12): p. 3357-3363.
270. Soniat, M. and Yuh M. Chook, Karyopherin- β 2 Recognition of a PY-NLS Variant that Lacks the Proline-Tyrosine Motif. *Structure*, 2016. 24(10): p. 1802-1809.
271. Stade, K., et al., Exportin 1 (Crm1p) is an essential nuclear export factor. *Cell*, 1997. 90(6): p. 1041-50.
272. Strassburg, M.A., et al., Influenza in the elderly: report of an outbreak and a review of vaccine effectiveness reports. *Vaccine*, 1986. 4(1): p. 38-44.
273. Subramani, C., et al., Host-Virus Protein Interaction Network Reveals the Involvement of Multiple Host Processes in the Life Cycle of Hepatitis E Virus. *mSystems*, 2018. 3(1): p. e00135-17.
274. Suhy, D.A., T.H. Giddings, and K. Kirkegaard, Remodeling the Endoplasmic Reticulum by Poliovirus Infection and by Individual Viral Proteins: an Autophagy-Like Origin for Virus-Induced Vesicles. *Journal of Virology*, 2000. 74(19): p. 8953.
275. Sun, K., et al., Rapid Construction of Complex Plant RNA Virus Infectious cDNA Clones for Agroinfection Using a Yeast-E. coli-Agrobacterium Shuttle Vector. *Viruses*, 2017. 9(11): p. 332.
276. Sun, K., et al., Matrix-glycoprotein interactions required for budding of a plant nucleorhabdovirus and induction of inner nuclear membrane invagination. *Molecular Plant Pathology*, 2018. 19(10): p. 2288-2301.
277. Sun, X., et al., Role of clathrin-mediated endocytosis during vesicular stomatitis virus entry into host cells. *Virology*, 2005. 338(1): p. 53-60.
278. Takizawa, C.G., K. Weis, and D.O. Morgan, Ran-independent nuclear import of cyclin B1-Cdc2 by importin β . *Proceedings of the National Academy of Sciences of the United States of America*, 1999. 96(14): p. 7938-7943.
279. Tamura, K. and I. Hara-Nishimura, The molecular architecture of the plant nuclear pore complex. *Journal of Experimental Botany*, 2013. 64(4): p. 823-832.
280. Tang, H.C., Y.J. Lin, and J.C. Horng, Modulating the folding stability and ligand binding affinity of Pin1 WW domain by proline ring puckering. *Proteins*, 2014. 82(1): p. 67-76.

281. Tanno, F., et al., Complete nucleotide sequence of Northern cereal mosaic virus and its genome organization. *Arch Virol*, 2000. 145(7): p. 1373-84.
282. Tierney, M.B.a.L., K.H. , An Introduction to Reverse Genetic Tools for Investigating Gene Function. *The Plant Health Instructor.*, 2005.
283. Tilton, R.F., J.C. Dewan, and G.A. Petsko, Effects of temperature on protein structure and dynamics: x-ray crystallographic studies of the protein ribonuclease-A at nine different temperatures from 98 to 320K. *Biochemistry*, 1992. 31(9): p. 2469-2481.
284. Timney, B.L., et al., Simple rules for passive diffusion through the nuclear pore complex. *The Journal of Cell Biology*, 2016.
285. Tsai, C.W., et al., Complete genome sequence and in planta subcellular localization of maize fine streak virus proteins. *J Virol*, 2005. 79(9): p. 5304-14.
286. Verdaguer, N., D. Ferrero, and M.R.N. Murthy, Viruses and viral proteins. *IUCrJ*, 2014. 1(Pt 6): p. 492-504.
287. Villarreal, L.P., Persistence pays: how viruses promote host group survival. *Current Opinion in Microbiology*, 2009. 12(4): p. 467-472.
288. Vincent, M.J., A.S. Martin, and R.W. Compans, Function of the KKXX motif in endoplasmic reticulum retrieval of a transmembrane protein depends on the length and structure of the cytoplasmic domain. *J Biol Chem*, 1998. 273(2): p. 950-6.
289. Vzorov, A.N., K.M. Gernert, and R.W. Compans, Multiple domains of the SIV Env protein determine virus replication efficiency and neutralization sensitivity. *Virology*, 2005. 332(1): p. 89-101.
290. Walker, P.J., et al., ICTV Virus Taxonomy Profile: Rhabdoviridae. *J Gen Virol*, 2018. 99(4): p. 447-448.
291. Walker, P.J., et al., Rhabdovirus accessory genes. *Virus Research*, 2011. 162(1): p. 110-125.
292. Walker, P.J., et al., Evolution of Genome Size and Complexity in the Rhabdoviridae. *PLOS Pathogens*, 2015. 11(2): p. e1004664.
293. Walker, P.J. and K. Kongsuwan, Deduced structural model for animal rhabdovirus glycoproteins. *J Gen Virol*, 1999. 80 (Pt 5): p. 1211-20.
294. Walpita, P. and R. Flick, Reverse genetics of negative-stranded RNA viruses: A global perspective. *FEMS Microbiology Letters*, 2005. 244(1): p. 9-18.
295. Wang, H., et al., Development of leafhopper cell culture to trace the early infection process of a nucleorhabdovirus, rice yellow stunt virus, in insect vector cells. *Virology Journal*, 2018. 15(1): p. 72.
296. Wang, L.Y., et al., Multiple domains of the tobacco mosaic virus p126 protein can independently suppress local and systemic RNA silencing. *Mol Plant Microbe Interact*, 2012. 25(5): p. 648-57.
297. Wang, Q., et al., Rescue of a Plant Negative-Strand RNA Virus from Cloned cDNA: Insights into Enveloped Plant Virus Movement and Morphogenesis. *PLoS Pathog*, 2015. 11(10): p. e1005223.

298. Wang, R. and M.G. Brattain, The maximal size of protein to diffuse through the nuclear pore is larger than 60kDa. *FEBS Lett*, 2007. 581(17): p. 3164-70.
299. Ward, B.M. and S.G. Lazarowitz, Nuclear export in plants. Use of geminivirus movement proteins for a cell-based export assay. *The Plant Cell*, 1999. 11(7): p. 1267-1276.
300. Wasag, P. and R. Lenartowski, Nuclear matrix - structure, function and pathogenesis. *Postepy Hig Med Dosw (Online)*, 2016. 70(0): p. 1206-1219.
301. Weber, P.H. and J.J. Bujarski, Multiple functions of capsid proteins in (+) stranded RNA viruses during plant-virus interactions. *Virus Res*, 2015. 196: p. 140-9.
302. Weiss, R.A. and P.L.P. Bennett, Assembly of membrane glycoproteins studied by phenotypic mixing between mutants of vesicular stomatitis virus and retroviruses. *Virology*, 1980. 100(2): p. 252-274.
303. Weninger, A., A. Glieder, and T. Vogl, A toolbox of endogenous and heterologous nuclear localization sequences for the methylotrophic yeast *Pichia pastoris*. *FEMS Yeast Research*, 2015. 15(7): p. fov082.
304. Wentz, S.R. and M.P. Rout, The nuclear pore complex and nuclear transport. *Cold Spring Harb Perspect Biol*, 2010. 2(10): p. a000562.
305. Wheeler, D.L., et al., Database resources of the National Center for Biotechnology Information. *Nucleic Acids Res*, 2007. 35(Database issue): p. D5-12.
306. Whelan, S.P.J. and G.W. Wertz, Regulation of RNA Synthesis by the Genomic Termini of Vesicular Stomatitis Virus: Identification of Distinct Sequences Essential for Transcription but Not Replication. *Journal of Virology*, 1999. 73(1): p. 297.
307. Whelan, S.P.J. and G.W. Wertz, Transcription and replication initiate at separate sites on the vesicular stomatitis virus genome. *Proceedings of the National Academy of Sciences*, 2002. 99(14): p. 9178.
308. Whittaker, G.R. and A. Helenius, Nuclear Import and Export of Viruses and Virus Genomes. *Virology*, 1998. 246(1): p. 1-23.
309. Wintermantel, W.M. and G.C. Wisler, Vector Specificity, Host Range, and Genetic Diversity of Tomato chlorosis virus. *Plant Disease*, 2006. 90(6): p. 814-819.
310. Wu, J.Y. and T. Maniatis, Specific interactions between proteins implicated in splice site selection and regulated alternative splicing. *Cell*, 1993. 75(6): p. 1061-1070.
311. Wu, X., et al., Both Viral Transcription and Replication Are Reduced when the Rabies Virus Nucleoprotein Is Not Phosphorylated. *Journal of Virology*, 2002. 76(9): p. 4153-4161.
312. Xu, D., N.V. Grishin, and Y.M. Chook, NESdb: a database of NES-containing CRM1 cargoes. *Mol Biol Cell*, 2012. 23(18): p. 3673-6.
313. Xu, Y., K.S. Colletti, and G.S. Pari, Human Cytomegalovirus UL84 Localizes to the Cell Nucleus via a Nuclear Localization Signal and Is a Component of Viral Replication Compartments. *Journal of Virology*, 2002. 76(17): p. 8931.
314. Yan, T., et al., Characterization of the complete genome of Barley yellow striate mosaic virus reveals a nested gene encoding a small hydrophobic protein. *Virology*, 2015. 478: p. 112-22.

315. Yang, J., et al., Phosphorylation of Rabies Virus Nucleoprotein Regulates Viral RNA Transcription and Replication by Modulating Leader RNA Encapsidation. *Journal of Virology*, 1999. 73(2): p. 1661-1664.
316. Ye, Q., R.M. Krug, and Y.J. Tao, The mechanism by which influenza A virus nucleoprotein forms oligomers and binds RNA. *Nature*, 2006. 444: p. 1078.
317. Ye, Z., et al., Membrane-binding domains and cytopathogenesis of the matrix protein of vesicular stomatitis virus. *J Virol*, 1994. 68(11): p. 7386-96.
318. Yun, S.-I., et al., Development and Application of a Reverse Genetics System for Japanese Encephalitis Virus. *Journal of Virology*, 2003. 77(11): p. 6450-6465.
319. Zarrinpar, A., R.P. Bhattacharyya, and W.A. Lim, The structure and function of proline recognition domains. *Sci STKE*, 2003. 2003(179): p. Re8.

VITA

A. Name: Chanyong Jang

B. Place of birth: Korea, South

C. Education:

1. Ph. D candidate, plant pathology
August 2012 – present
University of Kentucky, Lexington, KY (USA); GPA 3.902/4.0
2. Master of agricultural science, Plant pathology
March 2010 – February 2012
Chungnam National University, Daejeon (South Korea); GPA 4.45/4.5
3. Bachelor of Science, Agronomy & Chemistry (Double major)
March 2001- February 2010 (2003-2005: Military service)
Chungnam National University, Daejeon (South Korea); GPA 3.88/4/5
4. Certificate course in next generation sequencing analysis
University of Kentucky NGS workshop 2014

D. Publications and presentations in professional meeting:

1. Publications

Anderson, G., **Jang, C.**, Wang, R, Goodin, M. M. (2018) Mapping the nuclear localization signal in the matrix protein of potato yellow dwarf virus. J Gen Virol. 99:743-752, doi: 10.1099/jgv.0.001051

Jang, C., Wang, R, Wells, J., Leon, F., Farman, M., Hammond, J., Goodin, M. M. (2017) Genome sequence variation in the *constricta* strain dramatically alters the protein interaction and localization map of Potato yellow dwarf virus. J Gen Virol.;98(6):1526-1536. PubMed PMID: 28635588

Lim, H., Nam, J., Seo, E., Vaira, A., Bae, H., **Jang, C.**, Lee, C., Kim, H., Roh, M., and Hammond, J (2014). The coat protein of Alternanthera mosaic virus is the elicitor of a temperature-sensitive systemic necrosis in *Nicotiana benthamiana*, and interacts with a host boron transporter protein. Virology. 2014 Mar; 452-453:264-78. Doi:10.1016/j.virol.2014.01.021

Jang, C., Seo E., Nam, J., Bae, H., Gim, Y., Kim, H., Cho, I., Lee, J., Bauchan, G., Hammond, J., Lim, H. (2013). Insight into Alternanthera mosaic virus TGB3 Functions: Interactions with *Nicotiana benthamiana* PsbO correlate with Chloroplast Vesiculation and Veinal Necrosis Caused by TGB3 over expression. Frontier in Plant Science. Doi: 10.3389/fpls.2013.00005

Lim, H., **Jang, C.**, Kim, H., Kim, J., Lee, C., Ju, H., Domier., L (2011). Soybean mosaic virus infection and helper component-protease enhance accumulation of Bean Pod mottle virus-specific siRNAs. Plant Pathol. J. 27 (4): 315-323, pISSN 1598-2254

2. Presentations in professional meeting

1. 14th Southeastern Regional virology conference 2016

Title: The genome and proteins of Constricta yellow dwarf virus (Oral presentation)

2. The American phytopathological society annual meeting 2017

Title: Effect of sequence variation in the Constricta strain on the protein localization and interaction of Potato yellow dwarf virus (Poster presentation)

3. American society for virology conference 2018

Title: Functional domains in the matrix protein of potato yellow dwarf virus implication for cell-to-cell movement (Poster presentation)

E. Professional position held

1. Teaching assistant (University of Kentucky): Jan 2016 – Dec 2016

F. Scholastic and professional honors

1. Awarded full tuition scholarship by the graduate school, University of Kentucky, Lexington, KY

2. Awarded Teaching assistantship at the department of plant pathology, University of Kentucky, Lexington, KY

3. Bio Medical Human Resources Honors Fellowship for distinctive graduate students, Chungnam National University, Spring 2011

4. Bio-Peace Center of Independent Study Fellowship for undergraduate student research, Chungnam National University, Spring 2008

5. Merit Scholarship for undergraduate students, Department of Applied Biology, Chungnam National University, Fall 2007

6. Encouragement Scholarship for undergraduate students, Department of Applied Biology, Chungnam National University, Spring 2006

7. Merit Scholarship for undergraduate students, Department of Applied Biology, Chungnam National University, Fall 2002

8. Encouragement Scholarship for undergraduate students, Department of Applied Biology, Chungnam National University, Spring 2002 spring

9. Best Poster Presentation, 2011 Annual Fall Meeting Organized by The Korean Society of Plant Pathology.